

A mineralogical and petrographical investigation of  
the upper zone of the Bushveld Complex,  
northwest of Potgietersrus

by

Christina Johanna Nienaber Roberts

Submitted in partial fulfilment of the requirements  
for the degree of  
MASTER OF SCIENCE  
in the Faculty of Science  
University of Pretoria

DATE March 1987

A mineralogical and petrographical investigation of  
the upper zone of the Bushveld Complex,  
northwest of Potgietersrus

by

Christina Johanna Nienaber Roberts

Supervisor: Prof. G. von Gruenewaldt.

Department: Geology.

Master of Science.

This study comprises a mineralogical and petrographical investigation of rocks from three boreholes northwest of Potgietersrus. The core from these boreholes contains rocks from the upper zone of the Bushveld Complex, which was subdivided into subzones on the basis of marker horizons and the entrance of certain cumulus minerals. The entire upper zone is not represented in the borehole core, with a gap between the two sets of core.

The olivine-free lithologies of the lower horizons consist of anorthosites, gabbros, gabbronorites and norites. Troctolites, olivine-gabbros and gabbronorites dominate the upper horizons, although anorthositic layers, norites and one lherzolite are also present. All these rock types vary from leucocratic to melanic. The magnetite content, likewise, varies considerably, with the rocks grading from magnetite-free through magnetite-rich to pure magnetitites.

Mineralogical investigations were restricted to those minerals that characteristically display compositional variation in layered intrusions, namely plagioclase, ortho- and clinopyroxene and olivine. Plots of these compositional trends against stratigraphic height were used, and compared with similar studies from other

areas of the Complex, in order to establish the stratigraphic position of borehole END12 within the upper portion in the upper zone. Indications are that the upper zone in the Potgietersrus area is a compacted version of that in the eastern Bushveld.

Plagioclase in the Potgietersrus area has a high Fe-Ti content, due to needle-like inclusions of titanomagnetite. The two-pyroxene minimum for the area is at  $\text{Ca}_{40}\text{Mg}_{34}\text{Fe}_{26}$  and  $\text{Mg}_{49}\text{Fe}_{51}$ , which is considerably lower, and the miscibility gap wider, than for the rest of the Bushveld. The clinopyroxenes display a trend of continuous Ca-depletion. Olivine compositions indicate that an olivine gap may not exist in this area.

These differences indicate that the Potgietersrus upper zone crystallized at lower  $a\text{SiO}_2$ , higher  $a\text{FeO}$  (lower  $f\text{O}_2$ ) and a lower temperature than the eastern Bushveld.

The apatite- and olivine-rich nature of certain of these magnetitite layers indicate that they may have formed through a process of liquid immiscibility.

'n Mineralogiese en petrografiese ondersoek van  
die bosone van die Bosveldkompleks,  
noordwes van Potgietersrus

deur

Christina Johanna Nienaber Roberts

Promotor: Prof. G. von Gruenewaldt.

Departement: Geologie.

Magister in Wis- en Natuurkunde.

Hierdie studie behels 'n mineralogiese en petrografiese ondersoek van gesteentes uit drie boorgate noordwes van Potgietersrus. Die kern van hierdie boorgate bevat gesteentes van die bosone van die Bosveldkompleks, en is in subsones onderverdeel op grond van merkerhorisone en die verskyning van sekere kumulus-minerale. Die bosone is nie in sy geheel in die boorgatkern aanwesig nie, en 'n gaping bestaan tussen die twee stelle kerne.

Die olivien-vrye litologieë van die laer horisone bestaan uit anortosiete, gabbro's, gabbronoriëte en noriëte. Troktoleïete, olivien-gabbro's en gabbronoriëte domineer die hoër horisone, hoewel anortositiese lae, noriëte en een lherzoliëte ook voorkom. Al hierdie gesteentetipes varieer van leukokraties tot melanies. Die magnetietkonsentrasie varieer ook aansienlik, met gesteentes wat gradeer van magnetietvry, deur magnetietryk, tot suiwer magnetitiëte.

Mineralogiese ondersoeke is tot daardie minerale beperk wat karakteristiek samestellingsvariasies in gelaagde intrusies vertoon, naamlik plagioklaas, orto- en klinopirokseene en olivien. Plotte van samestellingskurwes teen stratigrafiese hoogte is gebruik, en vergelyk met soortgelyke studies van ander dele van

die Kompleks, om die stratigrafiese posisie van boorgat END12 in die boonste gedeelte van die bosone te bepaal. Aanduidings bestaan dat die bosone in die Potgietersrus-gebied 'n gekompakteerde weergawe van dié in die oostelike Bosveld is.

Plagioklaas in die Potgietersrus-gesteentes het 'n hoër Fe-Ti inhoud as gevolg van naaldvormige insluitels van titanomagnetiet. Die twee-pirokseen-minimum vir die gebied is by  $\text{Ca}_{40}\text{Mg}_{34}\text{Fe}_{26}$  en  $\text{Mg}_{49}\text{Fe}_{51}$ , is heelwat laer, en die mengbaarheidsgaping groter, as vir die res van die Bosveld. Die klinopiroksene vertoon 'n kurwe van aanhoudende Ca-verarming. Olivien-samestellings dui daarop dat die olivien-gaping moontlik nie in hierdie gebied bestaan nie.

Hierdie verskille dui aan dat die Potgietersrus-bosone gekristalliseer het by laer  $a\text{SiO}_2$ , hoër  $a\text{FeO}$  (laer  $f\text{O}_2$ ) en 'n laer temperatuur as die oostelike Bosveld.

Die apatiet- en olivienryke geaardheid van sekere van die magnetietlae dui daarop dat hulle deur 'n proses van vloeistofontmenging kon ontstaan het.

## CONTENTS

	Page
1. INTRODUCTION .....	1
2. PREVIOUS WORK .....	4
2.1 PREVIOUS WORK IN THE AREA .....	4
2.2 PREVIOUS WORK ON THE UPPER ZONE .....	5
3. FIELD RELATIONS.....	6
3.1 BOREHOLE DESCRIPTIONS.....	6
3.1.1 Borehole M5 .....	8
3.1.2 Borehole M4 .....	9
3.1.3 Borehole END12 .....	10
3.1.3.1 Anorthosite unit .....	10
3.1.3.2 Melatroctolite unit A .....	10
3.1.3.3 Leucotroctolite unit A .....	10
3.1.3.4 Magnetitite-olivine gabbro unit A .....	11
3.1.3.5 Leucotroctolite unit B .....	11
3.1.3.6 Magnetitite-olivine gabbro unit B .....	11
3.1.3.7 Magnetite troctolite unit A .....	11
3.1.3.8 Melatroctolite unit B .....	11
3.1.3.9 Banded unit .....	12
3.1.3.10 Magnetite troctolite unit B .....	12
3.2 DISCUSSION.....	12
4. PETROGRAPHY.....	16
4.1 GRAINSIZE AND MODAL DETERMINATIONS.....	16
4.2 TEXTURES.....	20
4.2.1 Crystallization and accumulation textures.....	22
4.2.1.1 Anorthosite.....	22
4.2.1.2 Gabbro.....	24
4.2.1.3 Gabbronorite.....	25
4.2.1.4 Norite.....	28
4.2.1.5 Troctolite.....	30
4.2.1.6 Dunite.....	31
4.2.1.7 Plagioclase-bearing lherzolite.....	32
4.2.1.8 Magnetitite.....	32
4.2.2 Postcumulus textures.....	33
4.2.2.1 Annealing.....	33
4.2.2.2 Exsolution.....	34
4.2.2.3 Reaction textures.....	34
4.2.2.3.1 Symplectites.....	34
4.2.2.3.2 Monomineralic coronas.....	38
4.2.2.4 Deformation .....	39
4.2.2.4.1 Bent crystals .....	39
4.2.2.4.2 Interpenetration .....	40
4.2.2.4.3 Recrystallization .....	41
5. MINERALOGY .....	42
5.1 DESCRIPTIVE MINERALOGY .....	42
5.1.1 Plagioclase .....	42
5.1.2 Orthopyroxene .....	45
5.1.3 Clinopyroxene .....	46
5.1.4 Olivine .....	47
5.1.5 Biotite .....	48
5.1.6 Hornblende .....	48
5.1.7 Apatite .....	48
5.1.8 Magnetite .....	49
5.1.9 Ilmenite .....	49
5.2 MINERAL COMPOSITIONS.....	49
5.2.1 Plagioclase .....	51
5.2.1.1 Composition of needles .....	53
5.2.2 Orthopyroxene .....	55
5.2.3 Clinopyroxene .....	58
5.2.4 Coexisting clino- and orthopyroxenes .....	59
5.2.5 Olivine .....	65
5.2.6 Comparative trends in coexisting minerals.....	66

6.	LAYERING.....	70
7.	CONCLUSIONS.....	75
8.	ACKNOWLEDGEMENTS.....	78
9.	REFERENCES.....	79
10.	APPENDICES.....	90

## LIST OF FIGURES

FIGURE		Page
1	Geological map of part of the Potgietersrus limb of the Bushveld Complex, showing the location of boreholes in the upper zone .....	3
2	Small grains of cumulus titanomagnetite enclosed in silicate minerals, in olivine leucogabbronorite (END12/381m) .....	
3	Adjacent magnetite grains displaying necking where enclosed by intercumulus clinopyroxene in magnetite leucogabbro (M4/64,1m) .....	21
4	Olivine enclosed by titanomagnetite, displaying tripple junctions where in contact with other olivine grains in magnetite leucotroctolite (END12/396,2m) .....	21
5	Clusters of rounded optically continuous inverted pigeonite grains, intercumulus clinopyroxene and laths of plagioclase in gabbronorite (M5/60,4m) .....	21
6	Resorbed inverted pigeonite, enclosed by interstitial clinopyroxene, with rounded olivine and 'intercumulus' magnetite in magnetite olivine melagabbronorite (END12/582,1m) .....	21
7	Igneous lamination in anorthosite (M5/39,9m). Note wedge-shape twin lamellae, indicating post-depositional stress .....	21
8	Plagioclase displaying tripple junctions in anorthosite (M5/38,9m) .....	23
9	Intercumulus clinopyroxene poikilitically enclosing plagioclase laths in mottled anorthosite (M5/39,7m) ...	23
10	Cumulus plagioclase enclosed by intercumulus magnetite in magnetite anorthosite, a variety of mottled anorthosite (M5/154,0m) .....	23
11	Concentration of euhedral apatite in magnetite-rich areas (END12/71,6m). Note the six-sided inclusion in the apatite .....	23
12	Irregular grains of olivine and clinopyroxene and rounded apatite enclosed by annealed magnetite in olivine melagabbro (END12/184,4m). Note tripple junctions between olivine grains .....	23
13	Intercumulus clinopyroxene subophitically enclosing cumulus plagioclase laths in leucogabbronorite (M5/89,0) .	23
14	Cumulus twinned clinopyroxene enclosed by 'intercumulus' magnetite in magnetite leucogabbronorite (M4/92,0m) ...	27
15	Large intercumulus plagioclase grains ophitically enclosing rounded clinopyroxene and groups of optically continuous inverted pigeonite grains in melagabbronorite (M4/77,1m) .....	27
16	Reaction-olivine between inverted pigeonite and mag-	

	netite (M5/39,0m) .....	27
17	Orthopyroxene-titanomagnetite symplectite around olivine (M5/139,0m) .....	27
18	Clusters of optically continuous inverted pigeonite parallel to the igneous lamination in norite (M5/83,0m) .....	27
19	Coarse-grained olivine-plagioclase symplectite forming in leucotroctolite, where in contact with magnetite (END12/332,5m) .....	27
20	Rounded olivine and clinopyroxene, euhedral apatite and 'interstitial' titanomagnetite in plagioclase-bearing lherzolite (END12/521,2m) .....	35
21	Pyroxene-plagioclase symplectite radiating into plagioclase from titanomagnetite (M5/36,0m) .....	35
22	Monomineralic rim of orthopyroxene between magnetite and plagioclase (M5/31m) .....	35
23	Bent needle-like inclusions of titanomagnetite in strained plagioclase (M5/64,7m) .....	35
24	Serricite in dislocation traces in plagioclase. Note disruption of twin lamellae (M5/148,7m) .....	35
25	Possible evidence for grain-boundary recrystallization in olivine from melatroctolite (END12/579,1m) .....	35
26	Interstitial plagioclase in plagioclase-bearing dunite (END12/202,7m) .....	43
27	Exsolved needles of titanomagnetite in plagioclase (M5/148,7m) .....	43
28	Three sets of exsolution lamellae in inverted pigeonite (M5/182,0m) .....	43
29	Fine exsolution lamellae and titanomagnetite platelets in clinopyroxene (END12/172,2m) .....	43
30	Three sets of exsolution lamellae of inverted pigeonite in clinopyroxene (M5/72,5m) .....	43
31	Needles in olivine, thought to indicate incipient alteration (END12/365,8m) .....	43
32	Comparative plot of compositional variation of pyroxenes on the pyroxene quadrilateral .....	60
33	Comparative plot of compositional variation of pyroxene from different parts of the Bushveld Complex .....	62
34	Variation in the Fe/Mg ratio of ferromagnesian minerals from different parts of the Bushveld Complex .....	68

#### LIST OF FOLDERS

##### FOLDER

- 1 Detailed borehole log for M5, with modal analyses and sample points for microprobe analyses.
- 2 Detailed log for the main magnetite layer on Commandodrift compiled from borehole logs of M5 and M4.
- 3 Detailed borehole log for M4, with modal analyses and sample points for microprobe analyses.
- 4 Detailed borehole log for END12, with modal analyses and sample points for microprobe analyses.



- 5 Correlation between boreholes M5, M4 and END12 with the stratigraphy of the upper zone from various parts of the Bushveld Complex.
- 6 Compositional variation of plagioclase, pyroxene and olivine compared to similar data from other parts of the Bushveld Complex.

#### LIST OF TABLES

TABLE	Page
I Modified Streckeisen-based nomenclature .....	7
II Abbreviations used in cumulus nomenclature .....	7
III Standards used in microprobe analyses .....	50

#### LIST OF APPENDICES

APPENDIX	Page
1A Modal analyses on thin sections from borehole M5.....	90
1B Modal analyses on thin sections from borehole M4.....	91
1C Modal analyses on thin sections from borehole END12....	92
2 Plagioclase compositions obtained microscopically.....	94
3 Microprobe analyses of plagioclases.....	95
4 Microprobe analyses of orthopyroxenes.....	96
5 Microprobe analyses of clinopyroxenes.....	97
6 Microprobe analyses of olivines.....	98
7 Calculations used to obtain plotted mineral compositions.....	99
8 Comparative nomenclature.....	100

## 1. INTRODUCTION

This study comprises a mineralogical and petrographical investigation of core from three boreholes located northwest of Potgietersrus. The core consists of rocks from the upper zone of the Bushveld Complex, which is subdivided into subzones on the basis of marker horizons or the appearance of certain cumulus minerals (Von Gruenewaldt *et al.*, 1980). Although the SACS nomenclature (Von Gruenewaldt *et al.*, 1980) is acknowledged, the older, internationally accepted zonal nomenclature is adhered to in this study.

Owing to its economic significance (Willemse, 1969a; Von Gruenewaldt, 1977) and scientific interest in the mechanisms responsible for its formation, the Bushveld Complex has been the subject of a vast amount of research since it was first mentioned in the geological literature by Molengraaff (1898). During the past few decades many studies have been carried out on the upper zone (eg. Berning 1941; Boshoff, 1942; Molyneux, 1964; 1970b; 1974; Raal, 1965; Von Gruenewaldt, 1966; 1970; 1973a and b; Groeneveld, 1970; Buchanan, 1975; 1977; 1979; Reynolds, 1978b; 1985a; 1985b; Dehm, 1980; Henkel 1981). These investigations concentrated mainly on the eastern portion of the Complex, where exposures are reasonably good. The upper zone of the Potgietersrus compartment has not been studied intensively but Van der Merwe (1976) recently made a generalised, field-orientated study of the rocks of this zone. Lack of outcrop hampered his investigations and he consequently only obtained a limited amount of data on the upper zone.

Although sample material available from borehole core may be considered to be inadequate to reflect the geology of an area, in this case it does represent the only available means of obtaining a more detailed understanding of the upper zone in the Potgietersrus area. The material available for this study consists of core from boreholes M4 and M5, drilled by the South African Development Trust Corporation Ltd. on the farm Commandodrift

228 KR and borehole END12, drilled by Johannesburg Consolidated Investment Co. Ltd. on Elandsfontein 766 LR, north-northwest of Potgietersrus (Fig. 1). These farms fall in the area mapped by Van der Merwe (1978) and remapping was not considered necessary for this investigation.

At the start of the study it was believed that the material from these boreholes represented the larger part of the upper zone succession and that the magnetitite layers, present in all three holes, would facilitate correlation between the cores. A detailed study of the upper zone, comparable to that published on the eastern Bushveld (Von Gruenewaldt, 1973a), was attempted.

Petrographic and mineralogical studies, as well as modal analyses were undertaken on a total of 249 polished thin sections. The petrographic studies revealed different lithological successions for boreholes M4 and M5 compared to END12. The rock sequence intersected by the M boreholes can be correlated with parts of subzones A and B in the eastern Bushveld, whilst the succession intersected by the borehole on Elandsfontein is considered to correlate with parts of subzones C and D. No overlap appears to exist between the M and END boreholes and the middle part of the upper zone does not appear to be represented in the investigated sequence. Furthermore, it was also impossible to correlate borehole END12 with the stratigraphy described by Van der Merwe (1976; 1978), so that a detailed study of the compositional variation of the main cumulus minerals in the boreholes was imperative to determine the relative positions of the boreholes in the succession.

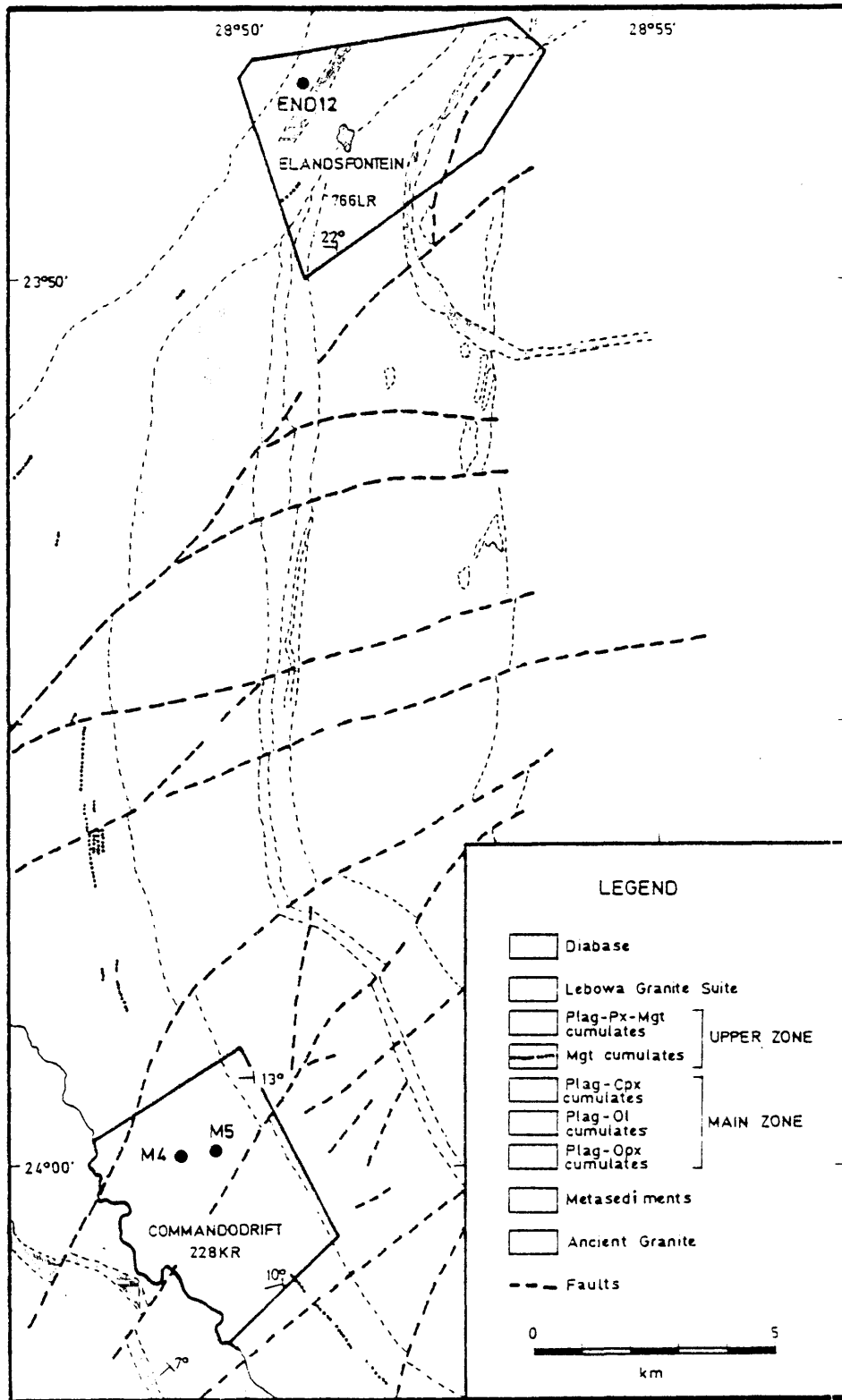


Figure 1. Geological map of part of the Potgietersrus limb of the Bushveld Complex (after Van der Merwe, 1978), showing the location of boreholes in the upper zone.

## 2. PREVIOUS WORK

### 2.1 PREVIOUS WORK IN THE AREA

The first description of rocks from the Bushveld Complex appears to be that of Molengraaff (1898). He included the area around Potgietersrus in his description and noted the similarity between gabbro in this area and that of the Pyramids north of Pretoria. He subsequently (1901) published a paper on the geology of Transvaal and described the 'Plutonic series of the Bushveld' as a group of intrusive and eruptive rocks younger than the Pretoria Series.

Kynaston and Mellor (1905) found alternating norite, pyroxenite and serpentinite in the vicinity of Potgietersrus to belong to the same 'basic zone' found elsewhere in the Transvaal between the red granite and Pretoria Series. From the close association of these basic rocks with the red granite, they concluded that they had the same origin.

Hall (1909) also reported on the geology to the east of Potgietersrus and found the noritic rocks petrographically uniform, although some banding was noted. He quoted a thickness of 3 960 m for the norite (Hall, 1932). The main and upper zones as well as the granitic rocks in the Potgietersrus compartment were studied by Berning (1941), who included the granitic rocks in the upper zone. He concluded that differentiation of these rocks was affected by successive influxes of more evolved magma, culminating in the residual granitic magma. Each batch of magma was thought to have differentiated further *in situ*.

Van der Merwe (1976) investigated the layered sequence of this area and pointed out the differences between the stratigraphy and thickness here and in the rest of the Bushveld Complex. In areas of good outcrops a noritic marginal zone was found to occur between the floor and the main mass of the intrusion. The lower zone is developed only as satellite bodies and as xenolithic inclusions in the main body. The critical zone has a limited

distribution and thickness in this area, and consists of norite, pyroxenite, anorthosite and chromitite layers. The main zone differs from that encountered elsewhere in the Bushveld, the main difference being the presence of the Platreef at the base of this zone and in that troctolite layers are developed.

Van der Merwe (1976) described the upper zone to be a 1 100 m thick succession of alternating layers of gabbro, magnetite gabbro, anorthosite, magnetite and olivine diorite. He observed 20 magnetite layers, with  $V_2O_5$  and  $TiO_2$  contents comparable to those noted from the eastern Bushveld Complex. He reported four reversals in the differentiation trend with stratigraphic height. These he interpreted as indications of influxes of new undifferentiated magma at various times.

## 2.2 PREVIOUS WORK ON THE UPPER ZONE

The informally accepted type locality of the upper zone occurs in the eastern Bushveld Complex, where the majority of studies on the upper zone have been undertaken. Molyneux (1964; 1970b; 1972) concentrated his investigations on the magnetite-rich horizons of the Magnet Heights area, while Von Gruenewaldt (1970; 1973a) studied the mineralogy and petrography of the silicate and sulphide minerals, as well as apatite in the Tauteshoogte area. On the basis of this work he was able to establish crystallization and differentiation trends in the basic rocks and could define indices by which to gauge the degree of crystallization and differentiation in these rocks (1973b).

### 3. FIELD RELATIONS

#### 3.1 BOREHOLE DESCRIPTIONS

Boreholes M5 and M4 were logged and then sampled at approximately 6 m intervals. Half-sections of core were generally available, except for magnetite layers or sulphide-bearing horizons, of which only quarter-core samples could be acquired. These two boreholes penetrate 184,46 and 184,61 m of upper zone rocks respectively (Folders 1 and 3). The Rustenburg Layered Sequence here dips southwest between 10 and 16 degrees, so that the overlap at the level of the main magnetite layer is about 60 m. A total stratigraphic thickness of about 305 m (Folder 5) was thus available for study.

JCI provided a log for borehole END12 and Dr. M. van der Merwe kindly sampled the core from this hole. The magnetite layers were sampled in less detail than was the case for M5 and M4. More detailed logging of END12 was attempted at a later stage, using the modal analyses done on the core samples. This borehole provided a 670,5 m section through the upper zone (Folder 4). The strata here dip at 15 degrees in a north north-westerly direction. Cawthorn and McCarthy (1980) considered one of the layers in this borehole to be the main magnetite layer. The available core was initially thought to represent virtually the entire upper zone.

All core-samples were point-counted and classified according to the method of Streckeisen (1974). The names thus obtained were used in the construction of the detailed logs shown in Folders 1, 3 and 4. This classification does not distinguish between cumulus and intercumulus material. Where cumulus terminology is used in textural descriptions, it is according to the non-genetic terminology suggested by Irvine (1982).

Since the classification of Streckeisen (1974, p. 780) only caters for a maximum of 5 per cent ore mineral and the rocks studied here contain up to 50 per cent magnetite in places, the classification

was modified to accommodate such high magnetite contents (Table I.)

TABLE I MODIFIED STRECKEISEN-BASED NOMENCLATURE\*

MODAL % MAGNETITE	TERMINOLOGY
90-100%	Magnetitite
50-90%	Plagioclase-clinopyroxene magnetitite
5-50%	Magnetite gabbro
0-5%	Gabbro

\* (Gabbro used as example)

Although this classification was found to be useful in the present study, it may lead to the anomalous situation that a magnetite leucogabbro may contain more dark minerals than a gabbro! For this reason, as well as to give an indication which minerals are cumulus, each rockname is followed by an acronym system (as suggested by Irvine, 1982, p. 136). According to this system, one letter abbreviations of the cumulus minerals are listed in order of decreasing abundance to describe each cumulate. The abbreviations used in this study are listed in Table II. These abbreviations also apply to the minerals in the microphotographs.

TABLE II ABBREVIATIONS USED IN CUMULUS NOMENCLATURE

a	apatite
c	clinopyroxene
i	inverted pigeonite
m	titanomagnetite
o	olivine
p	plagioclase
C	cumulate



A problem inherent to this system is, however, that it is not always easy to assess whether phases are cumulus (titanomagnetite, for example). In such cases the abbreviation is bracketed, e.g. (po(m)C) for a plagioclase olivine cumulate that contains titanomagnetite of uncertain cumulus or intercumulus origin.

Following Wager and Brown (1968, p. 30) and Molyneux (1970a, Fig. 18), the appearance or disappearance of cumulus minerals was used to define the various subzones. Olivine is used as an index mineral for subzone C and apatite for subzone D. The base of the main magnetite layer was used to indicate the subdivision between subzones A and B (Von Gruenewaldt, 1973a, p. 208).

### 3.1.1 Borehole M5

If the division between the main and upper zones is taken at the first appearance of magnetite (Molyneux, 1970b, p. 229), then it follows that all rocks intersected in this borehole are of the upper zone (Folder 1). Apart from the lowermost 20 m, the succession consists mainly of anorthosite (pC, pmC and piC), interlayered by gabbro, gabbro-norite and norite, including their leucocratic varieties. All these lithologies may contain varying amounts of magnetite. In some instances the anorthosite may be spotted or mottled. Magnetite (mC) layers occur mainly in the anorthositic layers, although exceptions exist, e.g. in the magnetite leucogabbro (pcC) and magnetite leucogabbro-norite (pciC) between 170 and 160 m depth.

Contacts between layers are generally gradational, with the exception of the bottom contact of magnetite layers which tend to be sharp, e.g. the main magnetite layer which overlies a sulphide-bearing anorthosite. The main magnetite layer (Folder 2) is subdivided into two principal parts by an approximately 1 m thick parting of magnetite anorthosite. The lower part, consisting essentially of pure magnetite and feldspathic magnetite (about 10-20% plagioclase), contains a few thin layers of magnetite anorthosite (pmC) and one of magnetite leuconorite (pmC) at 37,7m. The upper part consists predominantly of feldspathic magnetite (mC) with six thin layers of magnetite-rich anorthosite (pmC).

Contacts between these layers may be sharp or gradational. The upper contact of the main magnetitite layer is gradational into magnetite anorthosite (pC), which contains one thin magnetitite layer (mC).

### 3.1.2 Borehole M4

The bottom part of M4 (Folder 3), drilled approximately 1 km due west of M5, correlates well with the top of M5. Above the main magnetitite layer plagioclase becomes more abundant forming a 26 m thick sequence of magnetite anorthosites (pC, pmC), with two interlayered magnetitites at 152,1 and 145,7 m (61 cm and 92 cm thick, respectively). Both layers have sharp bottom contacts against magnetite anorthosite and grade upwards into the same rocktype. The magnetite content of the magnetite anorthosite beneath layer no. 2 is lower than the magnetite anorthosite overlying it.

Above 118 m depth anorthosite is less common and the majority of rocks in this borehole are leucogabbro (pcmiC, pmC and pC), gabbronorite (picC, pmicC, p(m)ciC and pciC) and leuconorite (pimC). Four layers of melagabbronorite (pcmiC, ciC, ci(p)C and cipC) occur between 112 and 76 m depth, alternating with leucogabbronorite layers. Magnetite-poor rocks are rare above 120 m.

Magnetitite (pmC, mC and mpC) layers are restricted to anorthosite and leucogabbronorite environments. Within layers their grain size and magnetite-content decrease upward. Between 28,1 and 27,9 m a coarse-grained feldspathic magnetitite containing visible sulphides was found.

Magnetitite layer no. 3 consists of alternating thin layers of magnetite anorthosite (pmC) and magnetitite. No. 4 has gradational bottom and top contacts with magnetite anorthosite and magnetite leucogabbro respectively, while both 5 and 6 exhibit sharp bottom and gradational top contacts with magnetite leucogabbro (pmC). Layer no. 7 has the same relationships as 5 and 6 but is itself layered, containing variable proportions of plagioclase in the

magnetitite. Layer no. 8, has a gradational contact with magnetite gabbronorite (pcmiC).

### 3.1.3 Borehole END12

Virtually all rocks in this borehole are olivine-bearing (Folder 4), hence no correlation between this and either borehole M5 or M4 is possible. Less information is available on the nature of contact-relationships between layers than in the case of the other boreholes. However, the contacts between silicate-layers are often gradational, while contacts of the magnetitite layers are more commonly sharp.

#### 3.1.3.1 Anorthosite unit

Below 600 m all the rocks are leucocratic and contain the only major anorthosite (pC and p(m)C) layer in this borehole. This anorthosite has a spotted appearance towards the top.

#### 3.1.3.2 Melatroctolite unit A

The anorthosite unit is overlain at ±600 m by a unit of magnetite melatroctolite (om(p)C), magnetite olivine melagabbronorite (moc(p)C) and melagabbronorite (ipmcC) that contains two magnetitite layers (mC and moC) both with sharp lower and upper contacts. Locally these magnetitites consist solely of magnetite and sulphide. A metamorphosed sedimentary inclusion occurs at the top of this unit.

#### 3.1.3.3 Leucotroctolite unit A

The unit above 553 m is troctolitic, contains four magnetitite (mC and mpoC) layers and displays an increase in plagioclase toward the top of subzone C.

#### 3.1.3.4 Magnetitite - olivine gabbro unit A

A magnetite lherzolite (omacC), containing the first cumulus apatite in the sequence marks the beginning of subzone D. The following 80 m of core contains eight magnetitite (moaC) layers, occurring in rocks containing olivine in such quantities that certain layers may be classed as dunites (moaC and omaC). Olivine and apatite are also developed within the magnetitite layers.

#### 3.1.3.5 Leucotroctolite unit B

The next unit (from 437 m to 320 m), consists mainly of magnetite troctolite (po(m)C and o(p)maC), magnetite leucotroctolite (p(m)C, pomC, pC) and leucotroctolite (poC and poamC), whilst other olivine-bearing rocks, such as olivine leucogabbronorite (po(m)C), magnetite olivine gabbro (poaC), magnetite dunite, and magnetite olivine leucogabbro (pomC), are subordinate. Olivine-free melagabbro (cpC), magnetite leucogabbro (po(a)C) and seven magnetitite (mpC) layers are also present.

#### 3.1.3.6 Magnetitite - olivine gabbro unit B

At 317 m depth the silicate-layers contain more clinopyroxene and up to the fracture zone between 280 and 290 m magnetite olivine gabbro (pomaC, pomacC, poamcC, paomcC and pomaC) is the dominant rock type. Four magnetitite layers occur in this unit.

#### 3.1.3.7 Magnetite troctolite unit A

Above the fracture zone magnetite troctolite (omaC, pomaC and (m)poaC) is the dominant rock type.

#### 3.1.3.8 Melatroctolite unit B

From 205 m to 180 m layers of magnetite dunite (omapC, omaC), magnetite melatroctolite (om(p)aC) and magnetite olivine melagabbro (o(m)caC) dominate.

### 3.1.3.9 Banded unit

Up to the contact with the dolerite sill an alternating sequence of more dunitic (omapC and omaC) and leucocratic rocks is found to contain two magnetite layers and a sedimentary inclusion.

### 3.1.3.10 Magnetite troctolite unit B

Core from the uppermost portion of the borehole consists of magnetite troctolite (po(m)aC and pomaC) and magnetite leucotroctolite (pomaC and poaC), with one magnetite layer.

## 3.2 DISCUSSION

Lithological logging of boreholes M5 and M4 has demonstrated the successions here to consist of predominantly olivine-free, anorthositic and gabbroic rocks that include the main magnetite layer. In contrast, virtually all rocks from the Elandsfontein borehole are olivine-bearing, suggesting that a higher stratigraphic position was penetrated in this borehole. Apatite is generally only present in the uppermost part of the upper zone (Daly, 1928, p. 738; Boshoff, 1942, p. 28; Wager and Brown, 1968, p. 380). Consequently the presence of apatite about 150 m from the bottom of END12 and its absence in the M-boreholes also corroborates the higher stratigraphic position of the former. In addition, no layers were found in END12 and in the M-boreholes that could be correlated, so that it is concluded that the middle part of the upper zone succession is not represented. No roof rocks are intersected by borehole END12.

The results of an attempted correlation between the succession in the boreholes and that established in various parts of the Bushveld Complex are shown in Folder 5.

Boreholes M5 and M4 (column 4) can be correlated reasonably well with subzone A and the lower part of subzone B elsewhere in the

Complex on the basis of the gabbro-noritic and anorthositic layers and the main magnetite layer.

The following distinct differences between the successions recorded by Van der Merwe (1976) and in the M boreholes are noteworthy, although the difference may be due to the fact that Van der Merwe's succession is based solely on outcrops, which are known to be very restricted over the upper zone in the Potgietersrus area.

- a.) According to Van der Merwe (1978, p. 36), the lowermost magnetite layer is 7 cm thick and overlain by 20 m of anorthosite. In the M5/M4 sequence the same layer is split into a multitude of thin layers and interlayered with magnetite leucogabbro, magnetite leuconorite, anorthosite and magnetite anorthosite.
- b.) Van der Merwe (1978, p. 36) reported the main magnetite layer to be generally 2 m thick, but that variations at different localities exist. On Commandodrift the main magnetite layer is a 6 m thick composite unit of mostly magnetite and several partings of anorthositic material, some of which contain 50 per cent magnetite.
- c.) Van der Merwe does not describe the upper layers 1 and 2, which are present in borehole M4 in virtually the same position as they are found in the eastern Transvaal (Folder 5).
- d.) Eight magnetite layers are developed in borehole M4 at a level that corresponds to layers no. 3 - 6 in the typical section of Van der Merwe (1978).

If these layers are indeed the same and magnetite 9 and 10 in M4 correspond to layers 9 and 10 of Van der Merwe, as Folder 5 would suggest, then the upper portion of borehole M4 must contain rocks belonging to subzone C. However, Van der Merwe (1978) takes the top of subzone B at the appearance of an anorthosite which forms the base of a magnetite layer containing 0,6 per cent  $V_2O_5$ .

Since magnetitites have not been analysed during the present investigation, the appearance of mineral phases is considered a more useful criterion on which to base subdivisions. Therefore, a subdivision using the appearance of a cumulus mineral, e.g. olivine at the base of subzone C is preferred. As no olivine was observed in M4, the entire borehole, above the main magnetitite layer, is considered to represent part of subzone B.

There is no specific marker horizon between subzones C and D to use as starting-point for attempted correlation of the END succession with data from other authors. Although different criteria can be used for the subdivision between these two subzones, both the presence of plagioclase with compositions below  $An_{50}$  (Van der Merwe, 1978, p. 40) and the appearance of cumulus apatite (present study) appear to occur at the same stratigraphic level (Von Gruenewaldt, 1973a, p. 210). A plot attempting correlation of the stratigraphy using these criteria shows that no correlation between the succession of Van der Merwe (1978) and END12 exists.

Van der Merwe (1978, p. 37) found the anorthosite layers to be useful in mapping subzone C, but these can not be correlated with the anorthosite layers in borehole END12. Neither the position nor the thickness of the magnetitite layers are useful either. Furthermore, according to Van der Merwe (1978, p. 75), olivine is present only in the upper 300 m of the upper zone, whereas the entire 670 m of END12 is olivine-bearing. According to Van der Merwe (1978, p. 75), apatite is present throughout the upper zone but in borehole END12 it was only observed from 521,2 m upwards.

It could be argued that the presence of a fracture zone about 300 m from the top of borehole END12 resulted in a duplication of the olivine-bearing succession and in that way account for the discrepancy between the END12 succession and Van der Merwe's columnar section. The layers in END12, however, display no repetition and the olivine-bearing succession intersected below the fracture zone is about 80 m thicker than the thickness of olivine-bearing rocks described by Van der Merwe (1978, p. 34). This indicates that no duplication has taken place. A further indication that processes other than faulting are responsible for

the observed differences in the successions is the presence of olivine-apatite-magnetite layers more similar to those in the Villa Nora area (Grobler and Whitfield, 1970) and in the Bierkraal (BK1) borehole (Reynolds, 1985b, p. 1028).

If the boundary between subzones C and D in END12 is used as a datum level and correlated with the C-D boundary in Van der Merwe's section, then it is evident that the total thickness of the upper zone must be more than the 1 100 m shown by Van der Merwe (1978). The difference in thickness is even more evident if it is borne in mind that about another 150 - 200 m of layered rocks occur above the collar of END12 (Hulbert, pers. com., 1983).

The stratigraphy of the Bushveld Complex remains remarkably constant over long distances, but differences between areas as far apart as Potgietersrus and Tauteshoogte should be expected because lateral facies changes are known to exist in other parts of the Complex (Von Gruenewaldt, 1973a). One distinct difference from the eastern Bushveld is the presence of apatite-magnetite-olivine-cumulates in END12. Similar units are described from upper parts of the Bierkraal succession (Reynolds, 1985b, p. 1028), which also supports the inferred position of END12 in the upper zone.

From the foregoing it is evident that the true stratigraphic position of borehole END12 in the upper zone could not be established solely on lithological grounds and hence the compositional variation of cumulus minerals had to be determined for correlation purposes. Since similar data are available for the upper zone in other areas of the Bushveld Complex, it was hoped that such information would shed more light on the stratigraphic height of this borehole.



#### 4. PETROGRAPHY

Polished thin sections were made from all the borehole cores at an average interval of 7,2 m. The top 70 m of M5 was sampled at smaller intervals in order to allow a more detailed investigation of the main magnetitite layer. In all, 249 thin sections were investigated.

##### 4.1 GRAIN-SIZE AND MODAL DETERMINATIONS

An indication of the grain-size of the rocks was obtained by determining the I.C. numbers (Chayes, 1956, p. 27). Because of the difficulties in distinguishing the boundaries between ore grains in transmitted light, the accuracy of I.C. numbers in the case of ore-rich rock-types is questionable. Magnetitites have, as a result, not been analysed in this manner.

For the silicate-rich rock-types the I.C. number is on average 69. The rocks from subzones A and B (Appendix 1A and 1B) are generally coarser-grained than those from END12 (Appendix 1C), yielding average I.C. numbers of 51 and 85 respectively. The former figure compares well with that given by Von Gruenewaldt (1973a, p. 223) for the eastern Bushveld.

Van der Merwe (1978, p. 86) found that the grain-size of anorthosites increase with height, but seldom to exceed 2 mm. The anorthosites in the M-borehole are considerably coarser-grained than those in END12, showing that this conclusion of Van der Merwe (1978) is not generally valid. The coarsest anorthosite found is in subzone A in which the plagioclase laths exceed 17 mm. Raal (1965, p. 20) found similar coarse-grained plagioclase in saussuritized anorthosites and recorded lengths of 15 mm. A decrease in grain-size of the anorthosites upward in the succession is noted, similar to the upward fining of plagioclase noted by Tyson and Chang (1984, p. 25) in the Duluth Complex.

The I.C. numbers were used to establish the number of points needed to obtain statistically sound modal analyses. Use was made of a Swift Point Counter and between 1017 and 2958 points, spaced 0,3 mm apart across the layering, were counted per thin section. Where layers were too thin, a compromise between statistical soundness and the necessity for data had to be made. Data are presented in Appendix 1.

The modal compositions were determined in order to classify the rock-types, to detect mineralogical trends between various layers and to facilitate comparison with studies by others on the upper zone. In addition, an attempt was made to determine whether compositional and textural variations correspond to variations in the modal abundances.

Von Gruenewaldt (1971, p. 154) observed that the upper zone in the Tauteshoogte area contains several thick accumulations of plagioclase-rich rocks, followed by plagioclase-poor rocks (less than 50 volume per cent). This does not apply to subzone A in the Potgietersrus limb, where samples with less than 50 per cent plagioclase are generally absent. In subzone B, on the other hand, such a trend seems to be present, e.g. the 40 m thick anorthosite which is followed at about 118 m in M4 by alternating mela- and leucogabbroic rocks, with the former containing between 17,3 and 27,5 per cent plagioclase. Gabbroic rocks with less than 50 per cent plagioclase are absent in subzone C and subzone D contains no thick anorthosites. The leucotroctolitic units are usually followed by mafic units, but the reverse is also found.

Van der Merwe (1978, p. 75) reported average orthopyroxene concentrations between 2 and 5 per cent, increasing to a maximum of 16 per cent in subzone B. Up to 37,6 per cent orthopyroxene was found in some of the rocks from the boreholes studied. According to Groeneveld (1970, p. 39) the upper zone generally contains less orthopyroxene than the main zone. This was suggested by Von Gruenewaldt (1973a, p. 223) to be the consequence of the presence of magnetite in the upper zone rocks. Buchanan (1975, p. 343) found an inverse relationship between magnetite and orthopyroxene. Although this appears to hold for some of the specimens studied, exceptions were again noted.

Cumulus inverted pigeonite crystals coexist with cumulus olivine in subzone C intersected in END12, but the former is virtually absent in subzone D.

Clinopyroxene is, next to plagioclase, the most widely distributed mineral in the sequence, but olivine is present in greater volumes in subzones C and D, which was also observed by Von Gruenewaldt (1973a, p. 223) for the upper zone rocks in the eastern Bushveld. He also found that clinopyroxene exceeds orthopyroxene by a few modal per cent. The values in Appendix 1 shows that the opposite is generally true for subzones A and B in the Potgietersrus limb. The highest value for clinopyroxene is 60,0 per cent, in sample M4/77,0m from subzone B. This melagabbronorite (ciC) can possibly be correlated with the feldspatic pyroxenite which Von Gruenewaldt (1973a, p. 210) and Molyneux (1974, p. 334) described from this subzone in the Tauteshoogte and the Magnet Heights areas, respectively.

Cumulus olivine (3,7%) is present in a magnetite leuconorite (pmoC) about 100 m below the main magnetite layer, at a level equivalent to that described for olivine-bearing rocks from the Magnet Heights area by Molyneux (1974, p. 334). Olivine is also present as a thin film of symplectite at the base of the main magnetite layer, similar to the olivine described by Willemsse (1969b, p. 202) from symplectitic textures in the same position in the Magnet Heights area.

Subzone B is entirely olivine-free, but rocks in subzone C (borehole END12) contain an average of 18,2 per cent olivine. Apart from the anorthositic rocks, no olivine-poor rocks such as found in the Tauteshoogte and the Magnet Heights areas (Von Gruenewaldt, 1973a, p. 210) are developed.

Except for some magnetites and the melagabbro (opC) at 400,5 m depth, all the rocks in subzone D are olivine-bearing. The average modal content is 28,6 per cent, with a maximum of 80,6 per cent in a plagioclase-bearing magnetite dunite (omaC). The decrease in olivine content near the roof, as was described by Von Gruenewaldt (1973a, p. 211), could not be confirmed, since the borehole does

not include this part of the succession. The absence of olivine in rocks close to the magnetitite layers in the Tauteshoogte area does not apply in the Potgietersrus area. In subzone C olivine-plagioclase-magnetitites (mpoC) and olivine-magnetitites (moC) are interlayered with troctolites, whilst olivine-apatite-magnetitites (moaC) are found in subzone D. Magnetitite layers also occur interlayered with troctolite, magnetite-olivine gabbro, and olivine gabbro-norite. In both the Magnet Heights and Potgietersrus areas, the olivine displays phase layering and alternates with orthopyroxene (Molyneux, 1970a, p. 38).

Apatite is absent below subzone D and only sporadic intercumulus grains are found in subzones A and B. At 521,2 m in END12 apatite increases to 11,8 volume per cent and then fluctuates between 0 and 24,5 per cent up to 289,5 m in subzone D, from where it remains constant at about 6,2 per cent, which is fairly close to the 6 per cent maximum found by Van der Merwe (1978, p. 75). The rapid drop in apatite content close to the roof, as described from Tauteshoogte (Von Gruenewaldt, 1973a, p. 223) was again not observed.

In the eastern Bushveld, cumulus apatite is always associated with olivine-rich rocks (Von Gruenewaldt, 1973a, p. 223). Since no olivine- and magnetite-bearing rocks occur in that area, this infers that magnetite-bearing rocks contain no apatite. In the Potgietersrus area, however, the highest apatite content (24,5 per cent) occurs in a rock containing approximately 16 per cent magnetite, with 20,3 per cent olivine (paomcC). The second highest apatite content of 21 per cent is in a magnetite dunite (moaC) containing 44,3 per cent magnetite.

The distribution of apatite in the Potgietersrus area, thus appears to be analogous to that in the lenticular Villa Nora olivine-apatite magnetitites (Grobler and Whitfield, 1970, p. 219). Three zones of similar apatite- and oxide-rich rocks are also described from upper zone lithologies in the Bierkraal area (Reynolds, 1985b, p. 1028).

For the purpose of classification the opaque minerals were counted as magnetite, but also includes sulphides and ilmenite. The ratio of magnetite to sulphide is generally so large that the contribution of sulphides was ignored. Below the main magnetite layer the content of opaque minerals is low (2 per cent), compared to the rest of the upper zone, as was also observed by Von Gruenewaldt (1973a, p. 223), whilst the rocks overlying the main magnetite layer are richer in opaques than at Tauteshoogte. As noted in the eastern Bushveld, the magnetite-content is not influenced by the rock-types in the upper zone above the main magnetite layer. The melagabbroic rocks of M4 (cipC, ci(p)C, ciC and pcmiC), some of the leucotroctolites (p(o)C, poC, poamC) and the olivine gabbroic rocks of END12 (p(o)ac) are, however, exceptions in that they contain little magnetite.

#### 4.2 TEXTURES

All the rocks investigated are holocrystalline and medium- to coarse-grained, with only a few of relatively fine grain-size. Although the textures are generally characteristic of particular rock-types and are therefore described accordingly, some general features resulting from mineral proportions are first dealt with in this subsection. A distinction has, furthermore, been made between textures resulting from crystallization and crystal accumulation and those that formed by reaction during the postcumulus stage.

The proportion of opaques present in the rock-types influences textures and mineral habit. In the magnetite-poor rocks, the opaque oxides often have a cumulus habit and small crystal size, as grains occur enclosed in larger silicate grains (Fig. 2, p. 21). An increase in the modal magnetite content may result in necking where grains are in mutual contact (Fig. 3, p. 21). Where opaque oxide aggregates occur in interstitial areas, they appear to take on an intercumulus appearance. In reflected light, however, the magnetite often consists of polygonal grains showing triple-point junctions, especially when present in large concentrations. Grain-size of the opaques appear to increase from small, when cumulus, to large, in polygonal aggregates.

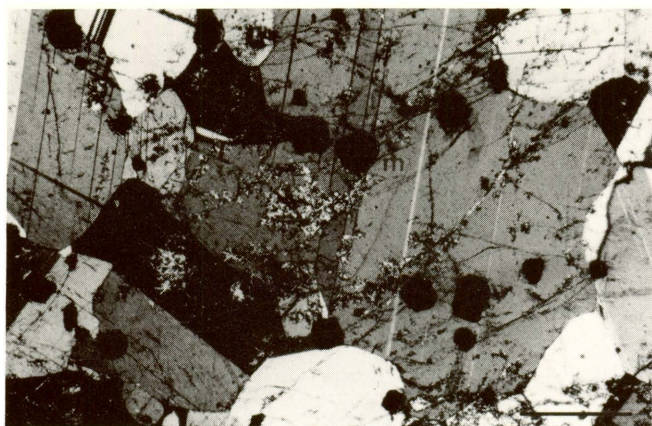


Fig. 2 Small grains of cumulus titanomagnetite (m) enclosed in silicate minerals in olivine leucogabbro-norite (END12/381m). Bar scale 1,0mm. Crossed nicols.

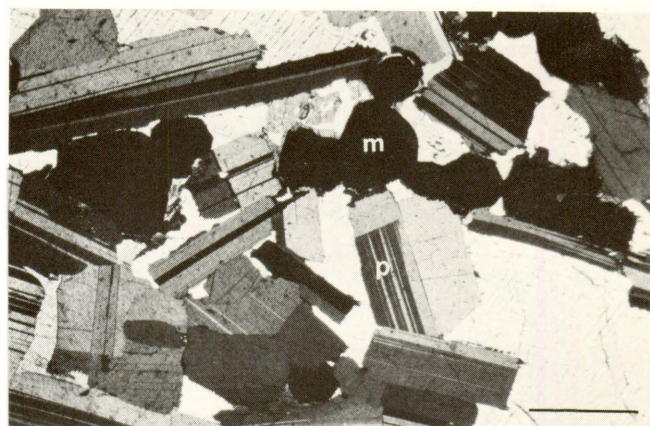


Fig. 3 Adjacent magnetite grains (m) displaying necking where enclosed by intercumulus clinopyroxene (c) in magnetite leucogabbro (M4/64,1m). Bar scale 1,0mm. Crossed nicols.

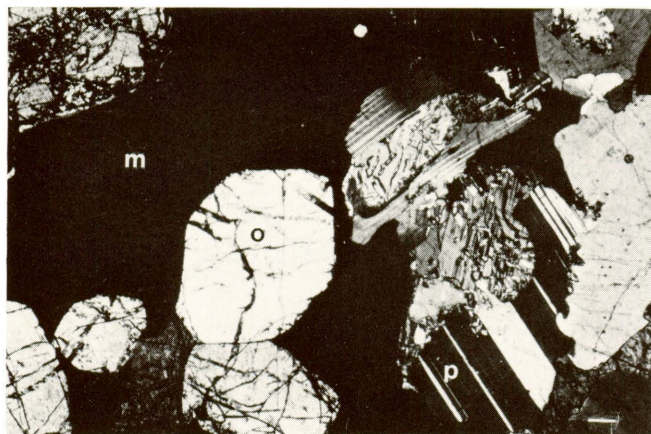


Fig. 4 Olivine (o) enclosed by titanomagnetite (m), displaying triple junctions where in contact with other olivine grains in magnetite leucotroctolite (END 12/396m). Bar scale 1,0mm. Crossed nicols.

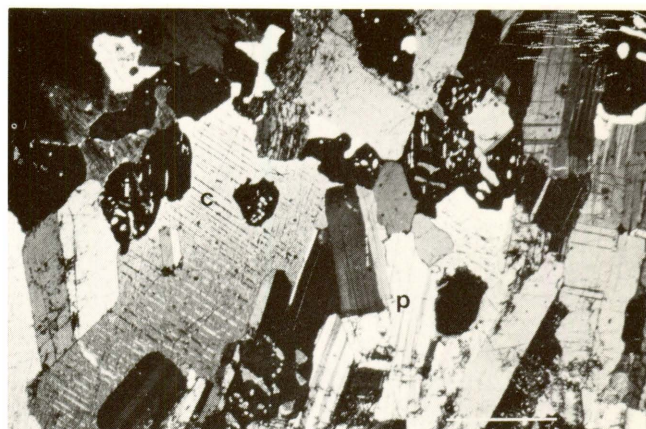


Fig. 5 Clusters of rounded optically continuous inverted pigeonite grains (i), intercumulus clinopyroxene (c) and laths of plagioclase (p) in gabbro-norite (M5/60,4m). Bar scale 1,0mm. Crossed nicols.

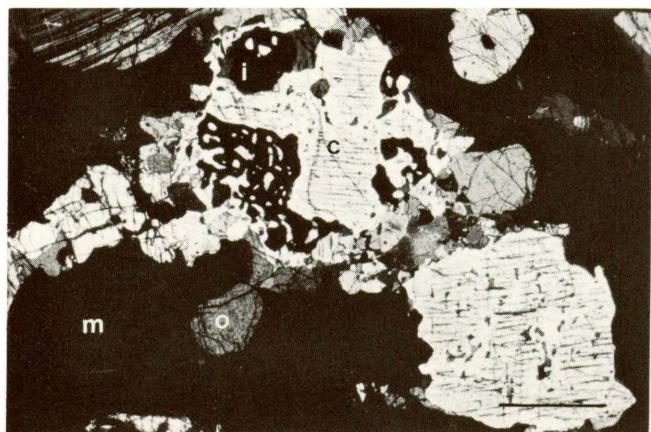


Fig. 6 Resorbed inverted pigeonite (i), enclosed by interstitial clinopyroxene (c), with rounded olivine and 'intercumulus' magnetite in magnetite olivine melagabbro-norite (END12/582,1m). Bar scale 1,0mm. Crossed nicols.

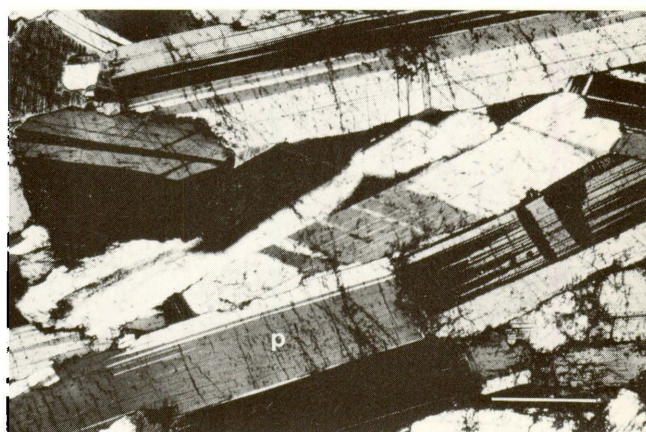


Fig. 7 Igneous lamination in anorthosite (M5/39,9m). Note wedge-shape twin lamellae, indicating post-depositional stress. Bar scale 1,0mm. Crossed nicols.

Olivine is likewise cumulus where enclosed by other minerals (e.g. magnetite), tending to tripple-point junctions where it is in contact with other olivine grains, especially higher up in the succession (Fig. 4, p. 21). In rock-types with abundant cumulus inverted pigeonite, this mineral occurs as groups of optically continuous grains showing the same textures as those in the eastern lobe of the Bushveld Complex (Von Gruenewaldt, 1971, p. 70-71; and Fig. 5, p. 21). Where these are enclosed in interstitial clinopyroxene, the latter is itself optically continuous with one set of exsolution lamellae of the inverted pigeonite (Fig. 6, p. 21).

#### 4.2.1 Crystallization and accumulation textures

##### 4.2.1.1 Anorthosite

The anorthosite (pC, and occasionally piC or pmC) is generally coarse-grained and the euhedral to subhedral lath-like nature of the plagioclase grains imparts an igneous lamination to these rocks (Fig. 7, p. 21). Interstitial, anhedral grains are present between the laths, but some layers display grains with tripple junctions (Fig. 8, p. 23). Small amounts of interstitial clinopyroxene, magnetite or quartz may be present and these are optically continuous over large areas, despite being detached in two dimensions. Orthopyroxene is cumulus where present.

The spotted and mottled anorthosites contain larger amounts of interstitial material (Fig. 9, p. 23). They are rather inhomogeneous and their modal composition may consequently range from leucogabbro (piC, pmC, pC) to leuconorite (piC or pC).

Magnetite anorthosite (pC, pmC or pmaoC; Fig. 10, p. 23), a variety of spotted anorthosite in which magnetite is the dominant 'dark mineral', is also present. Orthopyroxene occurs interstitially in the magnetite anorthosite, whereas it is more cumulus in the magnetite-free varieties. Mottled anorthosite is named after the intercumulus 'clumps' (Goode, 1977, p. 215) of pyroxene (or magnetite) that poikilitically enclose plagioclase (Fig. 9, p. 23). In mottled anorthosites cumulus plagioclase and

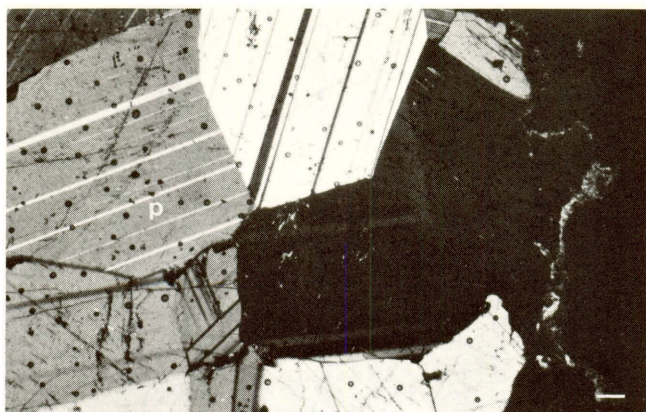


Fig. 8 Plagioclase (p) displaying tripple junctions in anorthosite (M5/38,9m). Bar scale 0,1mm. Crossed nicols.

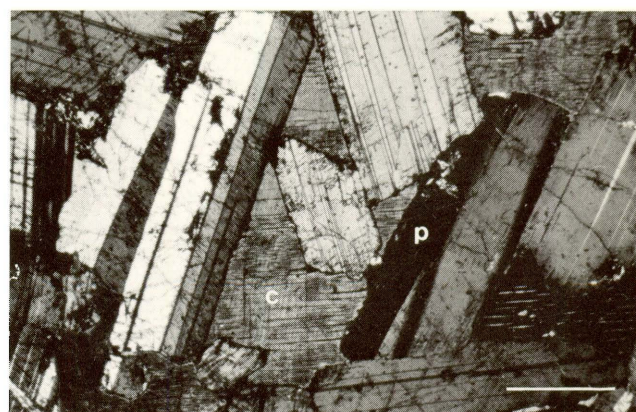


Fig. 9 Intercumulus clinopyroxene (c), poikilitically enclosed plagioclase laths (p) in mottled anorthosite (M5/39,7m). Bar scale 1,0mm. Crossed nicols.

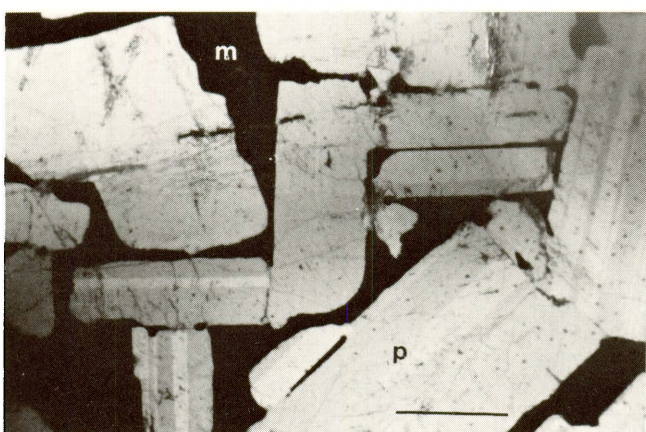


Fig. 10 Cumulus plagioclase (p), enclosed in intercumulus magnetite (m) in magnetite anorthosite, a variety of mottled anorthosite (M5/154,0m). Bar scale 1,0mm. Plain polarized light.

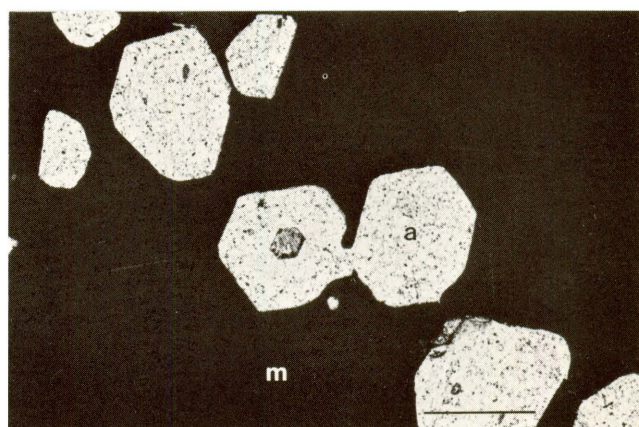


Fig. 11 Concentration of euhedral apatite (a) in magnetite-rich areas (m) (END12/71,6m). Note the six-sided inclusion in the apatite. Bar scale 0,1mm. Plain polarized light.

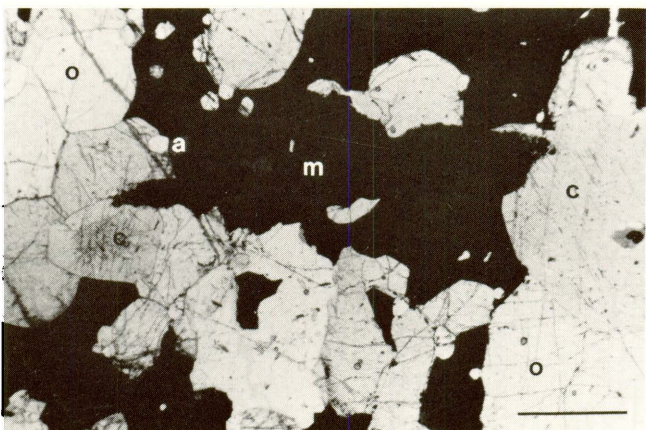


Fig. 12 Irregular grains of olivine (o) and clinopyroxene (c) and rounded apatite (a) enclosed by annealed magnetite in olivine melagabbro (END12/184,4m). Note tripple junctions between olivine grains. Bar scale 1,0mm. Plain polarized light.

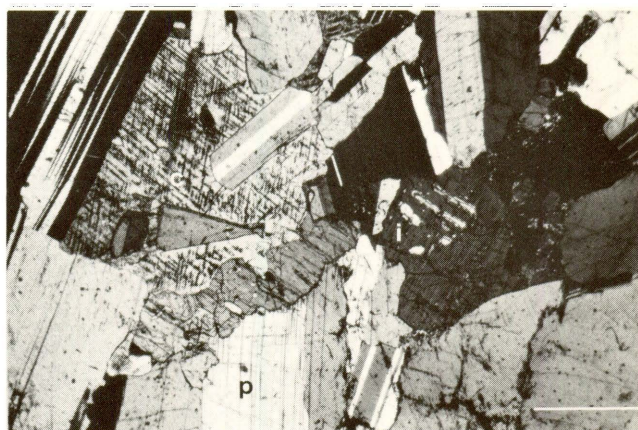


Fig. 13 Intercumulus clinopyroxene (c) subophitically enclosing cumulus plagioclase laths (p) in leucogabbro (M5/89,0m). Bar scale 1,0mm. Crossed nicols.



magnetite are poikilitically enclosed by large unzoned clinopyroxene crystals.

The anorthosites are invariably saussuritized, even when adjacent rock-types are unaltered. According to Raal (1965, p. 19) this preferential alteration of the anorthosites indicates plagioclase is unstable during deuteric alteration.

#### 4.2.1.2 Gabbro

True gabbro, according to the Streckeisen definition, is absent in the sequence studied, and all the gabbroic rocks are either leuco-, mela-, or olivine gabbro, with or without magnetite. Leucogabbros (piC, pC or pmC) are present in M5 and END12. They consist of large semi-parallel laths of plagioclase together with smaller anhedral plagioclase, interstitial clinopyroxene and, less commonly, orthopyroxene.

The orthopyroxene in gabbroic rocks of borehole M5 is cumulus, whilst interstitial quartz was also observed in places. Irregularly shaped olivine grains were observed in the uppermost sample of this rock-type in borehole M5.

The leucogabbro contains magnetite as small, euhedral to rounded grains which are enclosed in clinopyroxene (Fig. 3, p. 21). The plagioclase is subophitically enclosed by optically continuous intercumulus clinopyroxene which is sometimes seen to enclose relicts of optically continuous inverted pigeonite.

Despite magnetite being present in larger amounts and as cumulus crystals, the texture of magnetite leucogabbro (pcC, pcmiC, pmC or pC), is similar to that of the leucogabbros, except for the tendency of clinopyroxene to be cumulus.

True melagabbro (cpC) occurs at 400,5 m depth in END12, between magnetite leucotroctolite layers. This rock is medium-grained and consists of semi-parallel, subhedral laths of plagioclase and subhedral grains of clinopyroxene. The clinopyroxene encloses

relicts of inverted pigeonite, whilst flakes of uralite indicate incipient alteration.

The olivine gabbro (opaC) of borehole END12 consists of large plagioclase laths in sub-parallel orientation, rounded olivine, intercumulus clinopyroxene and euhedral magnetite and apatite grains.

Texturally the magnetite olivine gabbro (opmaC, pomacC, pomaC or paomcC) is similar to the olivine gabbro, although the pyroxene may be more rounded. The olivine occurs as subhedral to rounded cumulus grains. Large euhedral apatite grains are found in all these rocks, often concentrated in the opaque interstitial areas (Fig. 11, p. 23).

The magnetite olivine leucogabbro (pomcaC, pmocC, pomC, poamcC, p(o)maC, pmC) displays similar textures to the leucogabbro, but in addition, displays igneous lamination. Olivines tend to be rounded to irregular in shape, whereas clinopyroxene is interstitial.

Olivine melagabbro occurs at two horizons in END12 and is magnetite-rich (>15 %) in both cases (o(m)caC, opcmaC). It consists of a mozaic of irregular grains of olivine and clinopyroxene interspersed by lath-like plagioclases and 'interstitial' (annealed) opaque oxides (Fig. 12, p. 23). Apatite is also present in the interstitial areas.

The sample from higher in the succession has the typical sugary texture, with tripple junctions between the olivine grains, found in dunites.

#### 4.2.1.3 Gabbronorite

The gabbronorites vary in texture and composition and occur lower down in the sequence than the gabbros. Melagabbronorite and olivine gabbronorite are the most common varieties. Normal gabbronorite (piC) is limited to two horizons in the sequence (M5/65,8 m and M5/60,4 m). They vary in grain-size but are texturally similar to the gabbros. Cumulus inverted pigeonite

occurs as groups, while clinopyroxene is interstitial, often enclosing the latter (Fig. 5, p. 21). Smaller, rounded titanomagnetite grains are present between the main minerals.

Two magnetite gabbronorite layers are present in the lower part of the succession (pimcC and pcmiC). These vary in grain-size and their texture differs from that of the other gabbronorites in that the clusters of inverted pigeonite consist of fewer grains.

Leucogabbronorite (pimC or piC) is well represented in the lower part of the succession. It has a restricted grain-size range and is texturally similar to the gabbronorite. Where the plagioclase grains are smaller and more lath-like, they are in places subophitically enclosed by clinopyroxene (Fig. 13, p. 23). Where magnetite is present, it encloses clinopyroxene, which is then rounded and has a cumulus habit (Fig. 14, p. 27).

Two layers of melagabbronorite and one of magnetite melagabbronorite (cipC) are intersected in borehole M4. The lower of the melagabbronorite layers (ci(p)C) contains relatively fewer laths of plagioclase in semi-parallel orientation, since they are mostly sub-ophitically enclosed by clusters of inverted pigeonite. Euhedral grains of twinned clinopyroxene occur. Few opaque minerals are present. The other melagabbronorite layer (ciC) contains a few large, optically continuous, plagioclase grains, which ophitically enclose smaller, rounded pyroxenes (Fig. 15, p. 27). Small grains of euhedral to rounded opaque oxides are disseminated through the rock.

The magnetite melagabbronorite is texturally similar to the melagabbronorite, but is finer-grained. The clinopyroxene is larger and more stubby in habit, while the inverted pigeonite appears to be more euhedral. Olivine is present in small amounts, forming a reaction rim along orthopyroxene-magnetite boundaries (Fig. 16, p. 27).

Olivine gabbronorite also has leuco- and mela-varieties, with or without magnetite, but is restricted to the END borehole. The olivine gabbronorite horizon at a depth of 320,0 m in END12 has large subhedral laths of plagioclase, that are in places

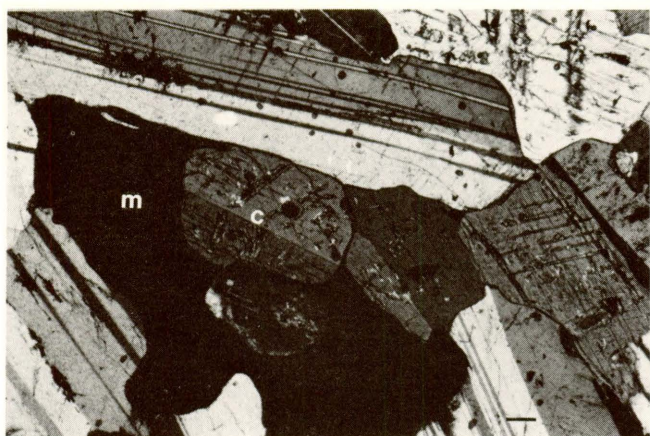


Fig. 14 Cumulus twinned clinopyroxene (c) enclosed by 'intercumulus' magnetite (m) in magnetite leucogabbronorite (M4/92,0m). Bar scale 0,1mm. Crossed nicols.

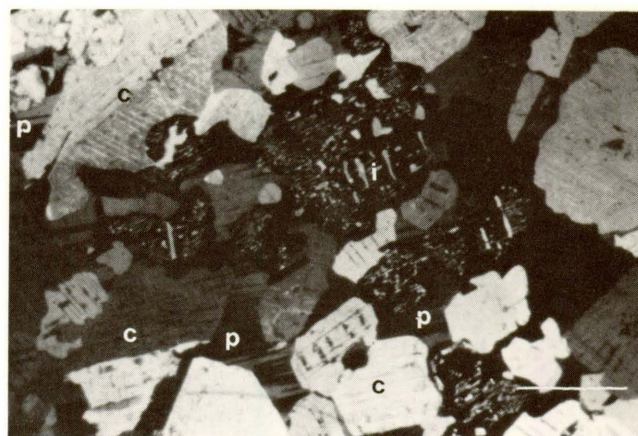


Fig. 15 Large intercumulus plagioclase grains (p) optically enclosing rounded clinopyroxene (c) and groups of optically continuous inverted pigeonite grains (i) in melagabbronorite (M4/77,1m). Bar scale 1,0mm. Crossed nicols.

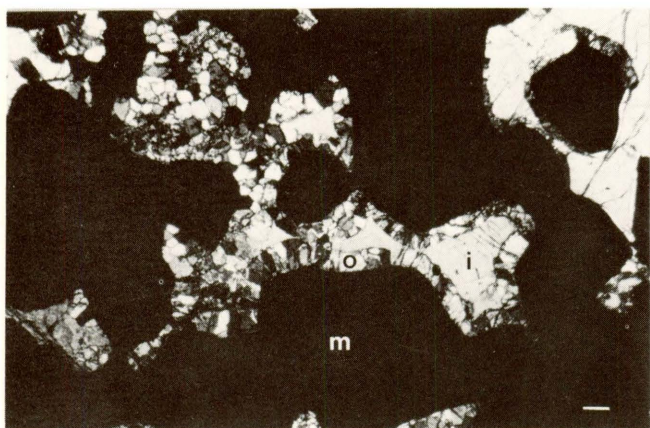


Fig. 16 Reaction-olivine (o) between inverted pigeonite (i) and magnetite (m) (M5/39,0m). Bar scale 0,1mm. Crossed nicols.



Fig. 17 Orthopyroxene-titanomagnetite symplectite (i,m) around olivine (o) (M5/139,0m). Bar scale 1,0mm. Plain polarized light.



Fig. 18 Clusters of optically continuous inverted pigeonite (i) parallel to the igneous lamination (arrow) in norite (M5/83,0m). Bar scale 1,0mm. Crossed nicols.

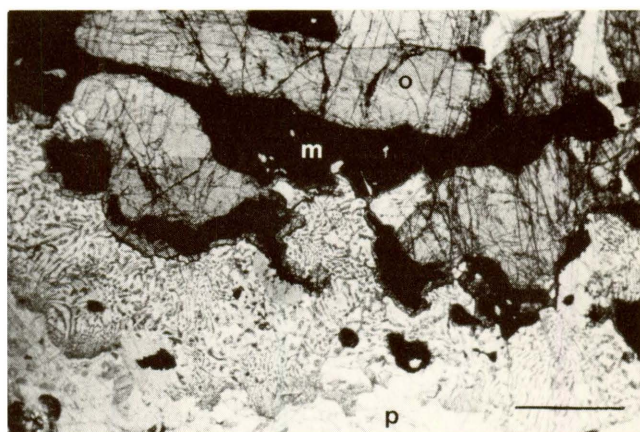


Fig. 19 Coarse-grained olivine-plagioclase symplectite forming in leucotroctolite, where in contact with magnetite (END12/332,5m). Bar scale 1,0mm. Plain polarized light.

sub-ophitically enclosed by rounded olivine. Olivine is resorbed where it is surrounded by symplectitic orthopyroxene-titanomagnetite intergrowths (similar to that in Fig. 17, p. 27). Exsolution-free orthopyroxene grains are also present. Interstitial to all the other minerals are large clinopyroxene grains. Apatite occurs as large euhedral crystals. Secondary biotite replaces the interstitial clinopyroxene. Opaque oxides are disseminated as irregular masses between the other minerals. The magnetite olivine gabbro-norite (pocmaC) displays a similar texture to the olivine gabbro-norite.

All the olivine leucogabbro-norite layers contain more than 5 per cent magnetite (pc(mo)iC, pcm(oi)C, pc(m)C, p(o)m(i)C, pC or pmoC) and all occur below 580 m depth in END12. Texturally they are similar to the normal olivine gabbro-norite. The magnetite olivine leucogabbro-norite is fairly coarse-grained, consists of sub-parallel laths of plagioclase, displays irregular grain boundaries, and contains large, rounded olivine grains. The olivine is surrounded by iron oxides and by interstitial grains of ortho- and clinopyroxene. The grain-size of the magnetite olivine leucogabbro-norite decreases upward in the sequence. Texturally these rocks are similar to the olivine leucogabbro-norites, with the exception that clinopyroxene may occur as cumulus grains. The orthopyroxene clusters contain fewer than usual grains per cluster.

One olivine melagabbro-norite unit (moc(p)C) is developed at END12/582,1m and no magnetite-free variety of this rock-type is present in the sequence. Plagioclase is more equant in shape than in the leucocratic varieties and tends to occur interstitially. Inverted pigeonite occurs as irregular grains, generally enclosed in large clinopyroxene grains (Fig. 6, p. 21). Olivine is relatively coarse-grained.

#### 4.2.1.4 Norite

Noritic rocks are rare compared to gabbroic and gabbro-noritic equivalents. The only norite layers include a normal norite at 83,0 m in M5 and the magnetite norite at 116,2 m depth in M4. The

former (piC) consists of subhedral, as well as more equidimensional plagioclase grains, with strings of inverted pigeonite which are arranged parallel to the igneous lamination (Fig. 18, p. 27). Few intercumulus grains of clinopyroxene and 'interstitial' opaque oxide grains are present.

The magnetite norite (piC) is medium-grained and consists of large, semi-parallel plagioclase laths, subophitically enclosed by inverted pigeonite. The latter occurs as large clusters. A few small, irregular patches of clinopyroxene are present and are optically continuous with the larger bleb-like exsolutions in the inverted pigeonite. The opaque oxides fill the spaces between the other minerals.

Leuconorite is more abundant than norite and contains less magnetite. It occurs in boreholes M5 and M4 and a magnetite-bearing variety forms two units in the lower parts of M5 and END12. These rocks have variable grain-sizes. Texturally the leuconorite (pimC, pC or piC) is similar to the norite described above. The exception is a fine-grained leuconorite which contains irregular masses of rounded grains of inverted pigeonite. The plagioclase between the inverted pigeonite grains is anhedral and displays triple junctions. Small, euhedral grains of opaque oxides are disseminated in the plagioclase. Clinopyroxene is a rare constituent.

The texture described for the norite is also present in the magnetite leuconorites (pmoC, pmC or piC), one of which contains irregular grains of olivine, mantled by a reaction rim of orthopyroxene-magnetite symplectite (Fig. 17, p. 27). This is the only olivine-bearing rock in the M-boreholes. Inverted pigeonite is interstitial to the large plagioclase laths and to irregularly shaped, annealed magnetite grains. Evidence of reaction is seen where titanomagnetite in contact with orthopyroxene is rimmed by olivine.

The magnetite olivine leuconorite (10,6% olivine) layer at 638,6 m in END12 (pmiC) is texturally unique. Plagioclase is present mostly as squat to equidimensional grains, showing straight boundaries and triple-point junctions. Small, rounded plagioclase

grains are optically enclosed in some of the inverted pigeonite grains. The latter also occurs as small, rounded, grains disseminated through the plagioclase 'matrix'. Clusters of larger inverted pigeonite grains enclose magnetite-, plagioclase- and serpentinized olivine grains.

#### 4.2.1.5 Troctolite

These rocks are found only in the upper subzones of the Potgietersrus limb. Magnetite troctolite consists essentially of plagioclase laths and rounded olivine grains. Small magnetite grains and euhedral grains of apatite are present, together with interstitial clinopyroxene, between the main constituents. Orthopyroxene is seldom present. Sample END12/552,0m (pomC) differs texturally in that it is fine-grained. Irregularly shaped olivines are present in a matrix of plagioclase, showing triple junctions and containing scattered euhedral magnetite grains.

Textural variations are present, in END12/275,8m (omaC), where the plagioclase occurs as anhedral grains with cumulus magnetite grains and apatite, while in other samples (END12/204,2m (m)poaC and END12/71,6m po(m)aC), apatite is associated with the opaque oxides, yielding a sieve-texture, similar to Figure 11 (p. 23).

Both leucotroctolite (p(o)C, poC or poamC) and its magnetite-bearing equivalent differ little in grain-size from the normal troctolite, but display a more prominent igneous lamination. Olivine is surrounded by interstitial inverted pigeonite but symplectite is absent. An interesting feature is the contact of the leucotroctolite with the underlying magnetite layer at 332,5 m. This contact consists of coarse olivine-plagioclase symplectite (Fig. 19, p. 27), which appears to have grown from the magnetite outwards into the adjacent plagioclase. The olivine in the magnetite is elongated, almost lath-shaped and twinned. Interstitial plagioclase is present between these olivine grains.

In the magnetite leucotroctolite (pmC, p(o), p(m)oC, p(m)C, pomC, pC, pmcC, pomacC, pmaC, pomaC, poaC) the olivine, when not

enclosed in magnetite, is interstitial and less rounded. Plagioclase is both lath-shaped and anhedral, in places appearing interstitial to the laths. Apatite is not always euhedral and also occurs as irregular blebs. The opaque oxides may be rimmed by hornblende (END12/460,2m).

All 5 layers of melatroctolite are magnetite-rich (om(p)C, moC, omaC, o(m)aC, om(p)aC) and vary in grain-size. Semi-orientated laths of plagioclase in these rocks have sutured boundaries and are often bent. Interstitial plagioclase is also present between the eu- to subhedral olivine grains. Although pyroxene is completely absent in some samples, resorbed inverted pigeonite grains (END12/579,1m) or large interstitial clinopyroxene grains may be present. Neither ever constitute more than 1 per cent of the rock. Apatite is present in all samples and may constitute up to 8 per cent of the rocks.

Rutherford and Hermes (1984, p. 844) describe a magnetite melatroctolite from Cumberland, Rhode Island and remarked on the scarcity of this rock-type. Only one other such occurrence has been described, from Taberg in Sweden (Singewald, 1913). Unfortunately it could not be established whether the latter is a layered intrusion.

#### 4.2.1.6 Dunite

All the dunite layers are restricted to END12 and are magnetite-rich (moaC, omaC). A plagioclase-bearing type (omapC, omaC) is also recognized. Both types are generally medium- to fine-grained, with a distinctive texture of cumulus olivine in a 'matrix' of magnetite. Euhedral apatite occurs in the magnetite. In the plagioclase-bearing type anhedral plagioclase between magnetite is often rimmed by biotite. Rare clinopyroxene of similar size and habit as plagioclase is present.



#### 4.2.1.7 Plagioclase-bearing lherzolite

Only one layer of lherzolite (omacC) occurs in borehole END12. This rock is fine-grained, and consists of rounded olivine and clinopyroxene in a 'matrix' of titanomagnetite (Fig. 20, p. 35), that contains inclusions of euhedral apatite. Interstitial plagioclase grains are rarely observed between the other mineral phases.

#### 4.2.1.8 Magnetitite

Magnetitite by definition, consists of at least 90 per cent magnetite. Such pure magnetitites are not common in this area, but where they do occur, consist of coarse-grained interlocking polygonal crystals of magnetite. Silicates occur in the roughly triangular areas between these grains. In subzones A and B this is mainly plagioclase or clinopyroxene while in subzones C and D olivine may also occur in this position. Certain magnetitite layers in subzone D are, however, unique in that they also contain cumulus olivine and apatite.

As the proportion of magnetite decreases so does the grain-size, resulting in the textural changes described at the beginning of this chapter (p. 20). The magnetitites that occur in subzones A and B of the Potgietersrus area are similar to those described from the eastern Bushveld, in that they are associated with plagioclase-rich silicate rocks. In this type of magnetitite (mpC, mC, pmC) plagioclase, inverted pigeonite and clinopyroxene may occur between the magnetite grains.

Some of the magnetitite layers of the END borehole are strikingly different, in that they contain abundant euhedral olivine and apatite (moC, mC, mpoC, moaC). Both of these minerals are absent from the M-boreholes. This type of magnetitite may, according to Reynolds (1985b, p. 1036) be termed nelsonite. In these rocks polygonal aggregates have only been noted locally, due to the abundance of apatite, which complicates the textural relationships.

## 4.2.2 Postcumulus textures

### 4.2.2.1 Annealing

The development of polygonal grains is fairly common in the monomineralic rocks (Fig. 8, p. 23). It was also described by Reynolds (1985b) from the Bierkraal magnetitites and by Rutherford and Hermes (1984, p. 849) from a magnetite melatroctolite from the Rhode Island Complex.

Similar polygonal textures also commonly occur in annealed metals (Stanton, 1972, p. 285-302). The triple-point junctions between magnetite grains in magnetitites may therefore be indicative that solid state readjustment has taken place. Voll (1960: quoted by Reynolds, 1985a, p. 1100) concluded that annealing of crystals under the influence of interfacial free energy was responsible for these textures. During annealing, the interprecipitate liquid is gradually expelled, leaving an end product that is an aggregate of polygonal grains with interfacial angles of 120 degrees (Vernon, 1970: quoted by Reynolds, 1985a, p. 1100). No additional material is required during this process.

Annealing takes place at temperatures below the melting points of the materials involved. In plutonic rocks annealing would be initiated as soon as point contact has been established between grains of the same composition (Fig. 4, p. 21). This process was also favoured by Hulbert and Von Gruenewaldt (1985) to explain the textures in the Bushveld chromitites.

Three stages are recognised in this process (Reynolds, 1985b, p. 1101-1102):

1. Necking between individual grains (Fig. 3, p. 21).
2. Individual grains start to lose their identity and pore space is reduced (Fig. 16, p. 27).
3. Further grain growth results in pores being 'pinched off' and the liquid thus entrapped crystallizes.

#### 4.2.2.2 Exsolution

Whereas annealing is the expression of processes at work during high subsolidus temperatures, exsolution features generally form during lower subsolidus temperatures. These features are dealt with in the sections on mineralogy.

#### 4.2.2.3 Reaction Textures

During the late magmatic stage disequilibrium and deuteric processes result in the reaction features described below.

##### 4.2.2.3.1 Symplectites

a) Pyroxene-plagioclase symplectites between plagioclase and titanomagnetite:

In the leucocratic rocks of subzones A and B, vermicular growths radiate from the opaque oxide - plagioclase grain boundaries into the plagioclase grains (Fig. 21, p. 35). The inter-vermicular feldspar appears to be stressed, showing distortion of the twin lamellae. The fineness of these textures precludes optical identification of the constituents. Von Gruenewaldt (1971, p. 146), suggested that the high relief and low birefringence vermicules may be orthopyroxene, but X-ray diffraction studies indicated them to be clinopyroxene (Hiemstra and Liebenberg, 1964, p. 11), possibly hedenbergite. Both types may exist.

Several variations of these symplectites were observed in thin section. The magnetite may be surrounded by an inner zone of biotite flakes, followed by biotite 'needles', radiating into the symplectite. Any one or all of these zones may be present, but according to Von Gruenewaldt (1971, p. 146), the needle-like inner rim is rarely present on its own. Raal (1965, p. 23) also describes several variations, including the presence of chlorite. From the samples investigated, the latter is seen to be a replacement product of biotite.

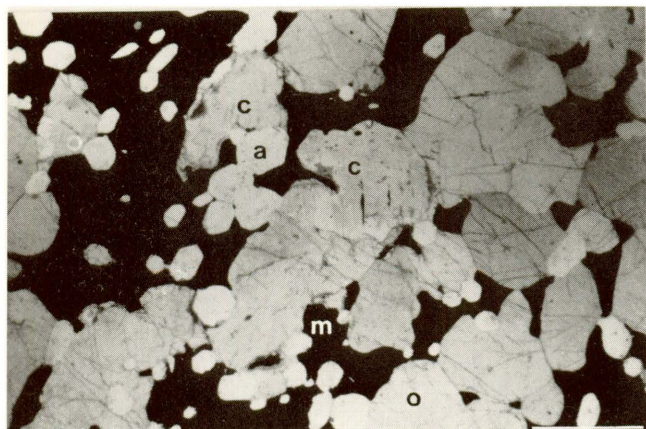


Fig. 20 Rounded olivine (o) and clinopyroxene (c), euhedral apatite (a) and 'interstitial' titanomagnetite (m) in plagioclase-bearing Iherzolite (END12/521,2m). Bar scale 1,0mm. Plain polarized light.

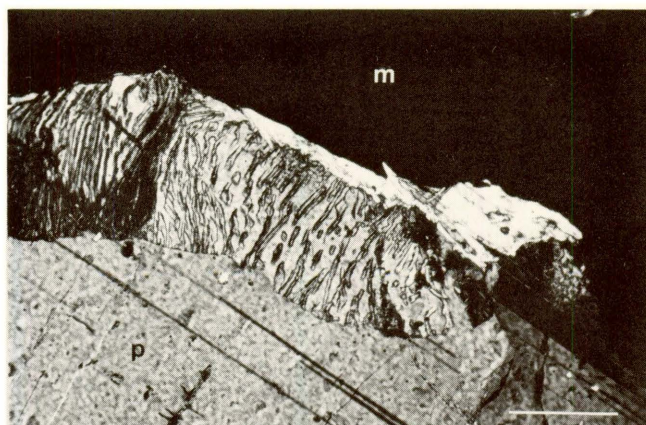


Fig. 21 Pyroxene-plagioclase symplectite radiating into plagioclase (p) from titanomagnetite (m) (M5/36,0m). Bar scale 0,1mm. Crossed nicols.

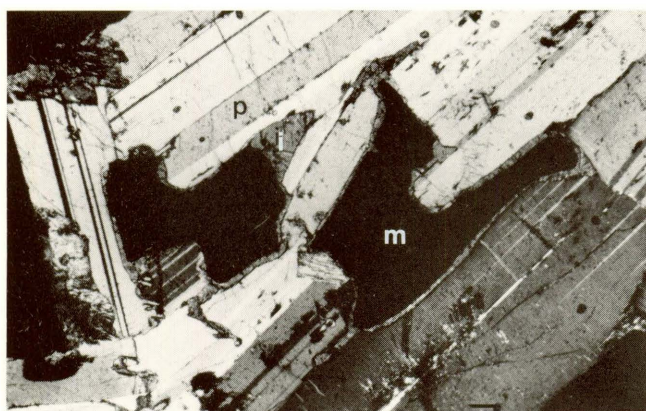


Fig. 22 Monomineralic rim of orthopyroxene (i) between magnetite (m) and plagioclase (p) (M5/31,0m). Bar scale 0,1mm. Crossed nicols.

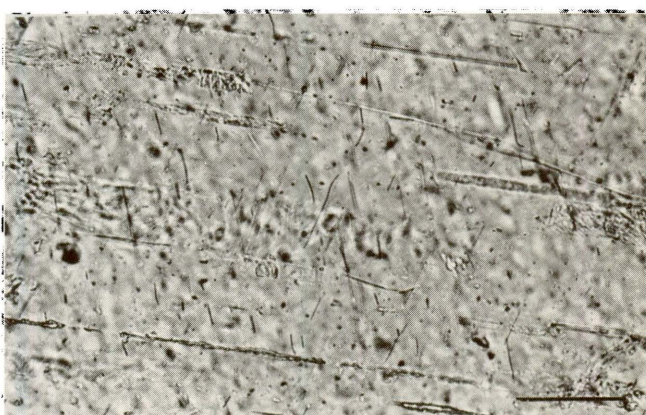


Fig. 23 Bent needle-like inclusions of titanomagnetite in strained plagioclase (M5/64,7m). Bar scale 0,1mm. Plain polarized light.

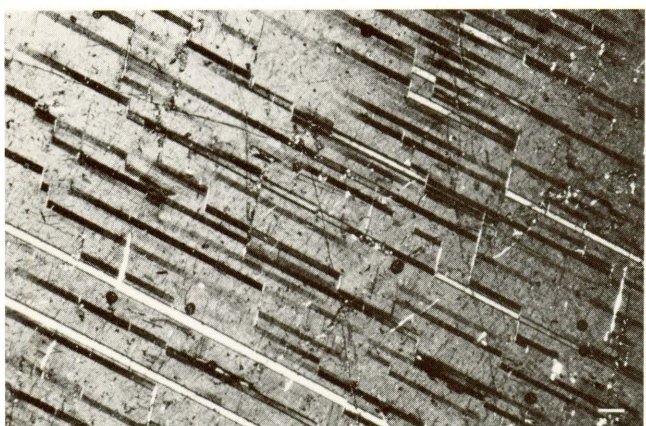


Fig. 24 Serricite in dislocations in plagioclase. Note disruption of twin lamellae (M5/148,7m). Bar scale 0,1mm. Crossed nicols.

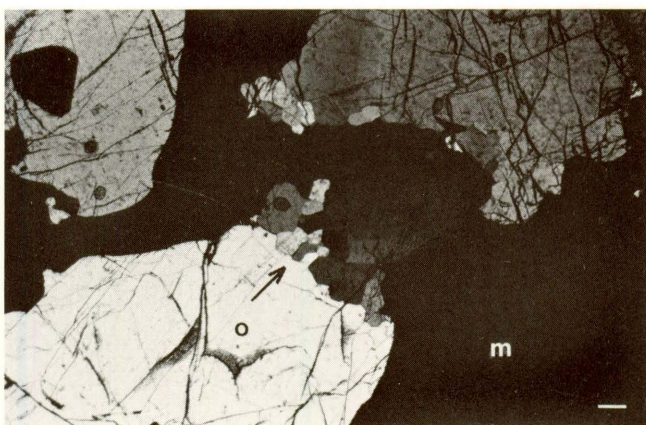


Fig. 25 Possible evidence for grain boundary recrystallization in olivine (o) from melatroctolite (END12/579,1m). Bar scale 0,1mm. Crossed nicols.

Higher up in the sequence the vermicules are coarser and consist of olivine (END12/598,9m), as also described by Reynolds (1985a, p. 1038). In some samples the olivine is not vermicular but optically continuous with smaller, interstitial grains.

According to Von Gruenewaldt (1971, p. 147), previous studies ascribed plagioclase-pyroxene symplectites to later metamorphism of the gabbroic and anorthositic rocks in which they occur but later researchers favour Buddington's (1939, p. 235) view that they result from discontinuous reaction between cumulus crystals and intercumulus liquid. This view is also held in the present study.

#### b) Orthopyroxene-titanomagnetite symplectite

This type of symplectite is best developed in the olivine-bearing norite in borehole M5 (Fig. 17, p. 27). The olivine is surrounded by a zone of orthopyroxene-titanomagnetite intergrowth, with the titanomagnetite being coarse and bleb-like close to the olivine but finer and elongated towards the periphery. The magnetite vermicules contain exsolutions of ilmenite, similar to the cumulus grains, while small granular ilmenites are also present. This zone is rimmed by a uniform, exsolution-free orthopyroxene, followed by a zone of inverted pigeonite.

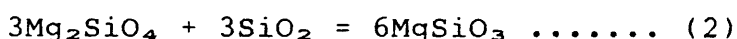
Orthopyroxene-titanomagnetite symplectites similar to those observed in the present investigation are common and have been described from elsewhere in the Bushveld Complex (Von Gruenewaldt, 1971, p. 147) and from various localities around the world, e.g. Kalka intrusion (Goode, 1974, p. 500); Skaergaard (Haselton and Nash, 1975, p. 290); Dutchmans Creek gabbroic intrusion (McSween and Nystrom, 1979, p. 540), and Wateranga layered mafic intrusion (Ambler and Ashley, 1977, p. 163-172).

Orthopyroxene-titanomagnetite symplectite occurs mainly around less fayalitic olivines (Deer *et al.*, 1963, 2, p. 27). The excellent development of this texture in subzone A (M5), involving olivine with composition  $Fa_{45}$ , and its absence in the higher

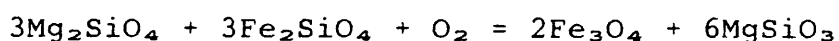
horizons of END12 confirms this conclusion. Forsteritic olivines, however, do not display this type of corona (Goode, 1974, p. 500).

The origin of these symplectites has also been ascribed to metamorphism (Goode, 1974, p. 500), or oxidation in the late magmatic environment (Carstens, 1957: quoted in Ambler and Ashley, 1977, p. 107). Haggerty and Barker (1967, p. 234) proposed that the orthopyroxene-magnetite symplectites may have formed by both processes, with differences characterizing each. The breakdown of olivine is more complex in the metamorphic symplectites, with addition or removal of Mg, Al, Ca or Fe taking place. In the magmatic environment they form solely from the breakdown of olivine during oxidation.

According to Goode (1974, p. 500), the fayalite molecule breaks down during subsolidus oxidation of the olivine, and the forsterite molecule reacts with the liberated SiO<sub>2</sub> to yield magnetite and orthopyroxene according to the first two reactions:



So that with the oxidation of olivine Fa<sub>50</sub>:



The orthopyroxene is thus more Mg-rich than the original olivine. Probe data obtained during the present study indicate an olivine composition of Fa<sub>45</sub> (37,45 wt% Fe), rimmed by orthopyroxene (in orthopyroxene-titanomagnetite symplectite) of composition Fs<sub>42</sub> (25,83 wt% Fe). The orthopyroxenes surrounding the more Fe-rich olivines (Fa<sub>72</sub>) are not symplectically intergrown with titanomagnetite and contain no exsolution lamellae. This texture supports the contention of Deer *et al.* (1963, 2, p. 27), that orthopyroxene-magnetite symplectites do not form from very Fe-rich olivine.

#### 4.2.2.3.2 Monomineralic coronas

##### a.) Olivine between inverted pigeonite and titanomagnetite

Rims of small olivine grains are often developed between cumulus titanomagnetite and inverted pigeonite. The olivine displays triple junctions (Fig. 16, p. 27) between successive rims of olivine grains which seem to have replaced the inverted pigeonite. Serpentinization of this olivine may occur. The formation of olivine between orthopyroxene and magnetite was also described by Willemse (1969b, p. 200), at the base of the main magnetite layer and by Reynolds (1985a, p. 1029) from the lower part of subzone D in the Bierkraal core.

Olivine of this form was found in the present study to be less Fe-rich ( $Fa_{37}$ ; 31,71 wt% Fe) than the inferred composition of cumulus olivines for that level in the intrusion. Since this rim olivine only develops where magnetite is in contact with inverted pigeonite, and the olivine contains more Fe than the 25 weight per cent Fe in the orthopyroxene at this level in the intrusion, a reaction relationship involving undersaturated interstitial liquids is inferred. Molyneux (1974, p. 366) and Reynolds (1985b, p. 1029) also found that the olivine in magnetites is markedly richer in Mg than in the associated silicate-rich rocks.

##### b.) Orthopyroxene rimming ore

In some thin sections irregular rims of orthopyroxene were observed where magnetite-grains are in contact with plagioclase (Fig. 22, p. 35). These continue as bleb-like vermicules along the plagioclase boundaries. They are coarser-grained than the symplectic orthopyroxene described earlier and may contain clinopyroxene exsolution lamellae.

It appears that the orthopyroxene rims between magnetite and plagioclase formed due to a reaction-relationship between the magnetite and plagioclase. The only manner in which this could take place is in the presence of reducing interstitial liquids so that FeO from the magnetite,  $SiO_2$  from the plagioclase and MgO

from the liquid can form the pyroxene. Plagioclase, by implication must then become more calcic.

c) Hornblende rimming ore

A brown pleochroic mineral rarely surrounds titanomagnetite (END12/460,2m). It differs from the biotite-rims in that it is not flaky, but forms a continuous rim without any associated symplectite. This mineral was optically identified as hornblende.

d) Biotite rimming ore

The biotite coronas around magnetite were described earlier as a variation of the symplectites which occur between magnetite and plagioclase. Their presence suggests the involvement of hydrous interstitial liquids.

e) Inverted pigeonite rimming olivine

In some leucotroctolites, interstitial inverted pigeonites enclose olivine, as was the case with the orthopyroxene symplectites, but without any symplectite formation.

#### 4.2.2.4 Deformation

##### 4.2.2.4.1 Bent crystals

a.) Plagioclase

Deformation textures include bent plagioclase laths, as indicated by deformed and wedge-shaped twin lamellae becoming thicker and more numerous at the centre of grains (Fig. 7, p. 21). These features are described by Smith (1974, p. 348) as a consequence of nucleation in the solid state at stressed positions and "growing into a grain by a series of spear head dislocations".



Von Gruenewaldt (1971, p. 95) considers them as being indicative of post-depositional deformation, whilst Wager, Brown and Wadsworth (1960, p. 76) concluded that the equilibration of cumulus crystals at lower temperatures would cause shearing stress on the crystal mush. Such dynamic metamorphism could take place in thick piles of rapidly accumulated primary minerals, due to the excess weight of the overlying column of crystals and liquid.

Bending on a micro-scale is shown by the distortion of ore needles in plagioclase (Fig. 23, p. 35).

Some of the larger plagioclase grains show step-like dislocations of individual albite twin lamellae (Fig. 24, p. 35), that compare well with the mechanical twinning introduced by uniaxial compression (Smith, 1974, p. 355), and resemble growth twins in many respects. Flakes of sericite or biotite are often present in these dislocations.

#### b.) Olivine

The undulose extinction observed in olivine may have been caused by the same metamorphic stresses which affected the plagioclase. Kink banding, which also results from stress deformation was noted in some sections. Raal (1965, p. 24) suggested that this feature is due to translation gliding under the influence of pressure.

#### 4.2.2.4.2 Interpenetration

A further feature interpreted as the result of deformation is interpenetration (Raal, 1965, p. 24-25), i.e. where plagioclase grains protrude into adjacent plagioclase grains. Variations of this texture were also described by Von Gruenewaldt (1971, p. 98). The similarity between Figure 47A of Von Gruenewaldt (1971, p. 99) and that of Vance (1969, Fig. 5b, p. 9), however, opens the question whether interpenetration is not a consequence of synneusis. Synneusis involves the union of two crystals in twin relations, but deviations by several degrees may take place, and even random orientation is not excluded. Continued crystallization

after synneusis results in interpenetrating crystals. Magmatic turbulence is a major factor in the differential movement of crystals when synneusis takes place (Vance, 1969, p. 26), but the movement must cause contact between many crystals, though not fusion of them. Such momentum could be attained once turbulent magma stops moving. Conditions favourable for synneusis could thus be related to separate episodes of active movement in the magma chamber, such as emplacement, injection of a new magma-pulse, or vigorous convection. Vance (1969, p. 27), notes that textural evidence indicates that synneusis is favoured by a high ratio of melt to crystals in the early stages of crystallization since the increasing viscosity of the magma would restrict movement and hence synneusis.

#### 4.2.2.4.3 Recrystallization

Strain shadows are fairly common in plagioclase and olivine crystals but sutured boundaries less so. Evidence of recrystallization along grain boundaries is scarce, but has been noted on plagioclase and olivine grains (Fig. 25, p. 35).

## 5. MINERALOGY

### 5.1 DESCRIPTIVE MINERALOGY

#### 5.1.1 Plagioclase

Plagioclase occurs throughout the sequence, being absent only in some monomineralic magnetite and dunite layers. It generally occurs as large euhedral to subhedral lath-shaped grains, orientated parallel to the layering (Fig. 7, p. 21). Anhedral plagioclase occurs interstitially to the laths in the leucocratic rocks and interstitial to the mafic minerals in certain dunite layers at the top of the sequence (Fig. 26, p. 43).

Twinning of plagioclases in plutonic rocks is, according to Smith (1974, p. 343), the result of nucleation errors in the liquid. Erratic features and a high frequency of twinning characterize primary growth from a liquid. This is in agreement with the situation noted in these rocks. Zoning is noted, but not pronounced in the sections studied and was not investigated.

Opaque needles of various lengths are contained in the plagioclases. The most pronounced development of these is in the unusually large plagioclase grains found especially in magnetite-poor layers (Fig. 27, p. 43) of boreholes M5 and M4. In the more lath-like grains the needles are larger and more numerous in the cores of the plagioclase grains, decreasing in both size and density toward the rims. Clear rims, as described by Tyson and Chang (1984, p. 26) who suggested that the zoned distribution of needles in the cores of plagioclase grains may indicate a decrease in needle-forming components as crystallization progressed, is not obvious. According to Von Gruenewaldt (1971, p. 104) the distribution of the needles may delineate the outline of the original cumulus grains. The irregular, interstitial plagioclase grains display an even distribution of these needles, although both size and density are less than in the central portions of cumulus grains.

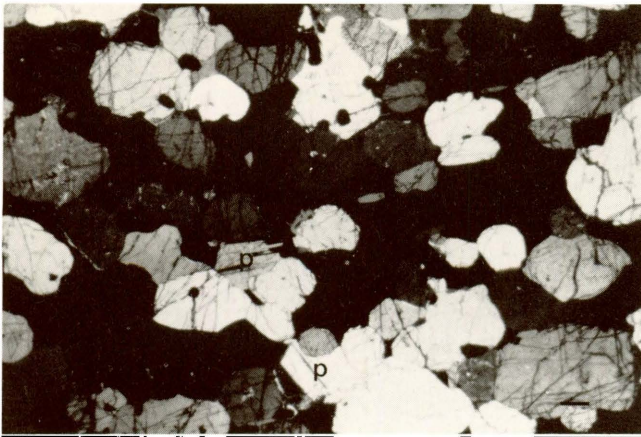


Fig. 26 Interstitial plagioclase (p) in plagioclase-bearing dunite (END12/202,7m). Bar scale 0,1mm. Crossed nicols.

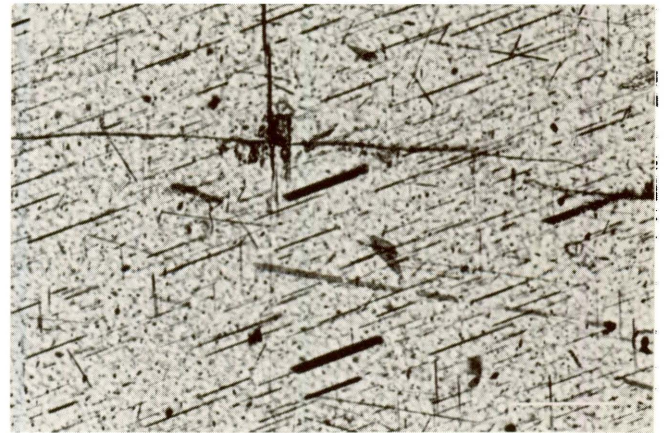


Fig. 27 Exsolved needles of titanomagnetite in plagioclase (M5/148,7m). Bar scale 0,1mm. Plain polarized light.

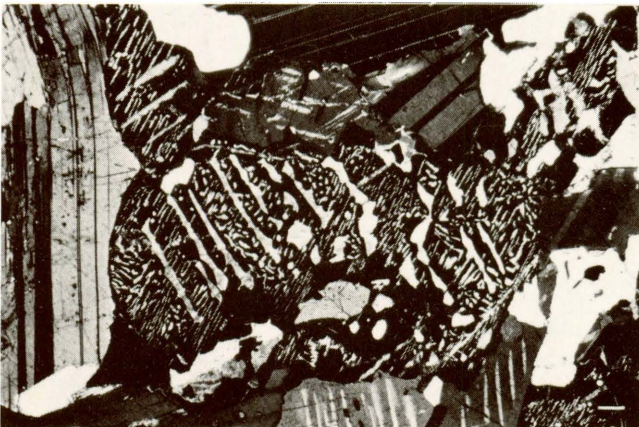


Fig. 28 Three sets of exsolution lamellae in inverted pigeonite (M5/182m). Bar scale 0,1mm. Crossed nicols.

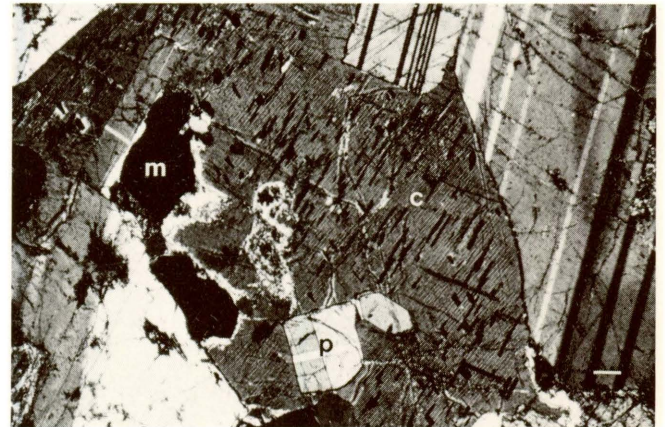


Fig. 29 Fine exsolution lamellae and titanomagnetite platlets in clinopyroxene (END12/172,2m). Bar scale 0,1mm. Crossed nicols.

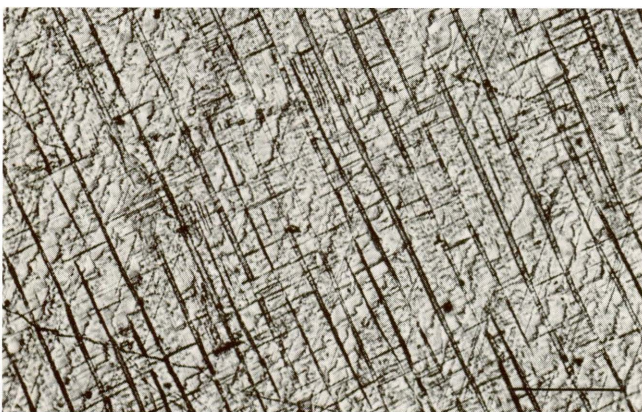


Fig. 30 Three sets of exsolution lamellae of inverted pigeonite in clinopyroxene (M5/172,5m). Bar scale 0,1mm. Plain polarized light.

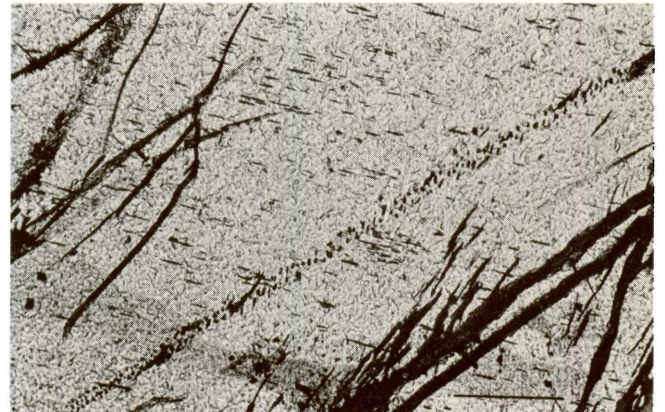


Fig. 31 Needles in olivine, thought to indicate incipient alteration (END12/365,8m). Bar scale 0,1mm. Plain polarized light.

Similar needles were found by Von Gruenewaldt (1971, p. 104) in plagioclase from subzones A, B and C but in subzone D of the upper zone in the Tauteshoogte area they were absent. Similar needles have also been reported 300 m above the appearance of cumulus magnetite in the Magnet Heights area by Molyneux (1974, p. 335). 'Black gabbros' in the main zone result from a high concentration of needles in the plagioclase (Groeneveld, 1970, p. 39).

Opaque needles have been recorded in plagioclases of the Skaergaard (Wager and Mitchell, 1951, p. 204), Duluth (Taylor, 1964, p. 25; Tyson and Chang, 1984, p. 26) and Dutchmans Creek (McSween and Nystrom, 1979, p. 537) gabbroic intrusions, from the Lambertville Diabase sill (Hargraves and Young, 1969, p. 1170), and even from Lunar plagioclases (Mao and Bell, 1972, p. 664).

The needles are oriented in five directions in the host plagioclases (Nienaber-Roberts, in press). According to Groeneveld (1970, p. 39) the directions in which the needles occur in the 'black granites' are not related to a cleavage direction, but are parallel to the c-axis. Hargraves and Young (1969, p. 1170) note that they are only visible in some directions.

Beside opaque needles, honey-coloured inclusions of sphene were also noted. Fine-grained spherules of opaque oxides are ubiquitous in the plagioclases examined. Similar spherules were mentioned by Von Gruenewaldt (1971, p. 104). He also described minute biotite flakes in the cleavage planes of plagioclase crystals and ascribes their origin to late stage exsolution of K from the plagioclase due to decreasing temperatures. These flakes may be similar to the sericite noted along dislocations in plagioclase grains (Fig. 24, p. 35).

The plagioclase is to varying degrees altered to saussurite and chloritic aggregates. Alteration commences along cracks and cleavage planes. The plagioclase in anorthosites is preferentially altered.

### 5.1.2 Orthopyroxene

Although orthopyroxene was reported by Molyneux (1970a, p. 41) from the lowermost portion of the upper zone, below the lowest magnetitite layer and a localized sample above the main magnetitite layer (Molyneux, 1974, p. 336), primary orthopyroxene was not observed in the succession studied. Only inverted pigeonite is present.

The inverted pigeonite occurs in optically continuous clusters showing two or three sets of clinopyroxene exsolution lamellae: (Figs. 5, p. 21; 18, p. 27 and 28, p. 43), a pre-inversion set of broad lamellae, now oriented at random in the clusters and one or two post-inversion sets (one of which is very thin, straight and parallel to (010) of the inverted pigeonite). The third set is more bleb-like and does not clearly display a crystallographic orientation (Fig. 28, p. 43). Higher up in the succession the grains may have a more interstitial habit and may even optically enclose plagioclase.

Above approximately 410 m in END12 the orthopyroxenes do not exhibit much exsolution (similar to sample UC361-475, described by Buchanan, 1972, p. 36). These grains generally have higher interference colours and tend to surround olivine. This orthopyroxene is, however not symplectitically intergrown with titanomagnetite as is the case in M5/139m and END12/160,6m. According to Buchanan (1972, p. 36) the lack of lamellae may be due to the pigeonite being calcium-poor since the low An composition of the plagioclase in UC361-475, together with the large amounts of modal apatite suggests to him that the Ca in the magma may have been taken up preferentially by the apatite. Neither the lamellae-poor orthopyroxene nor the plagioclase analysed during the present investigation display obvious Ca-deficiency, nor do the rocks contain exceptionally high apatite-contents. Perhaps this orthopyroxene is intercumulus and crystallized from the intercumulus liquid directly, or formed by reaction between olivine and interstitial liquid. If the crystallization (or reaction) temperature was below the inversion temperature, an orthorhombic pyroxene would crystallize.

The orthopyroxene progressively alters to produce uralite.

### 5.1.3 Clinopyroxene

Although small cumulus clinopyroxene grains may be found in the melanic rocks (Fig. 15, p. 27), more commonly the clinopyroxene occurs as large interstitial grains that subophitically enclose the other minerals (Figs. 3 and 5, p. 21; 9 and 13, p. 23).

Clinopyroxene ubiquitously exhibits fine exsolution lamellae (Fig. 29, p. 43), which occur at an angle to the cleavage and impart a schiller-like appearance to these grains.

The exsolution textures displayed by the clinopyroxenes form, according to Deer *et al.* (1963, 2, p. 130), when augite crystallizes above the pigeonite-orthopyroxene inversion temperature and exsolves pigeonite parallel to {001}. Below the inversion temperature the augite may invert to orthopyroxene forming a second set of exsolution lamellae parallel to the {100} plane of the clinopyroxene.

In some samples clinopyroxenes are seen to contain a third set of even finer exsolution lamellae, which are not quite parallel to the lamellae of the thicker set (Fig. 30, p. 43). Samples containing these, invariably display tapered and bent lamellae, similar to those described by Deer *et al.* (1963, 2, p. 15) and also noted in some orthopyroxenes. This feature causes a patchy extinction. Bent and tapered exsolution lamellae are, according to Robinson *et al.* (1977, p. 858), a cooling phenomena. They suggest that 'phase boundaries', in existence during the formation of exsolution lamellae, become semi- or incoherent, since the lattice parameters of clino- and orthopyroxenes change at different rates during cooling. In response, changes in the phase boundary orientation may be initiated in order to accommodate further longitudinal growth, thus forming the curved ends to exsolution lamellae observed. If the growth of exsolution lamellae is impeded, growth is stopped and nucleation at new phase boundaries takes place in the interlamellar areas. These lamellae will have a

slightly different orientation to the earlier set to produce the third set of thin exsolution lamellae referred to above.

Twinning of the clinopyroxenes is rare, but in sample M5/182,0m repetitive twinning is observed.

Schiller exsolution are common in clinopyroxene throughout the sequence, but increase considerably in both size and amount as the clinopyroxene becomes more iron-rich (Fig. 29, p. 43).

Clinopyroxene alters to uraalite, usually starting along cleavage planes and grain boundaries. Pseudomorphous replacement by hornblende was observed in sample END12/609,6m.

#### 5.1.4 Olivine

Throughout the succession of END12 olivine occurs mainly as subhedral to rounded cumulus grains enclosed by other silicates or opaque oxides. When surrounded by orthopyroxene-titanomagnetite-symplectite (Fig. 17, p. 28) olivine grains have irregular (resorbed) shapes. Olivine rarely occurs interstitial to other minerals, which it then subophitically encloses. Grain boundaries between olivine grains usually show triple-point contacts. Granoblastic olivine (Fig. 26, p. 43) and reaction rims of olivine (Fig. 16, p. 27) were observed in different thin sections.

Twinning is present in isolated cases, but kink-bands were encountered in several samples.

Olivine alters mainly pseudomorphously to iddingsite and serpentine products. Brownish needles observed in the olivine under high magnification (Fig. 31, p. 43) are thought to indicate incipient alteration to iddingsite. It also occurs as brown fibres along the rims of olivine grains, but is optically continuous with the relict olivine. Chlorite also replaces olivine and usually forms along irregular fractures in the olivine.



### 5.1.5 Biotite

In the lower part of the succession biotite is present mainly as part of the symplectite that forms between the titanomagnetite and plagioclase, or as alteration product of the ferromagnesian minerals. Higher up, in END12, it occurs as large interstitial plates and is evidently a primary magmatic mineral. It alters mainly to chlorite.

### 5.1.6 Hornblende

Hornblende occurs as an alteration product (of pyroxene), in the lower two subzones but appears to be a primary mineral in the upper parts of subzone D.

### 5.1.7 Apatite

Apatite occurs in substantial quantities in the upper 523 m of the succession. In the silicate rocks it is present as small subhedral crystals between the larger silicate minerals. Where found in opaque oxide-rich areas, the apatite is euhedral, coarser grained and tends to be evenly distributed throughout the oxides (Fig. 11, p. 23) resulting in net textures. Similar modes of occurrence were noted in the Bierkraal core by Reynolds (1985b, p. 1028).

Green and brown six-sided flakes, similar to those described by Von Gruenewaldt (1971, p. 112) have been observed as inclusions in apatite (Fig. 11, p. 23). Some inclusions are partly green and partly brown. Von Gruenewaldt (1971, p. 112) suggested an epitaxial relationship between the apatite and biotite inclusions therein. Reynolds (1985b, p. 1036) describes small rounded chlorite inclusions from Bierkraal apatites. It now appears that these are melt inclusions that crystallized to a glass and later devitrified. Roeder (1984, p. 348) described instances where the crystallization of minerals from such melt inclusions could be determined.

### 5.1.8 Magnetite

Resorption of magnetite was noted in some sections and reaction textures in others. Reaction with plagioclase during the subsolidus stage resulted in the formation of pyroxene-plagioclase or olivine-plagioclase symplectites.

Alteration to hematite was only found in samples from the upper parts of the boreholes, where surface oxidation took place. All transitional stages of preferential alteration of the magnetite component from fresh titanomagnetite to unaltered skeletons of the original ilmenite lamellae (Ramdohr, 1969, p. 901) are present. Biotite and chlorite (Reynolds, 1985b, p. 1036) may form in the interlamellar areas of these skeletal grains. Exsolution of ilmenite and ulvöspinel are present in magnetite, displaying all the textural varieties described by Molyneux (1970b) and Reynolds (1985a).

### 5.1.9 Ilmenite

Discrete grains of ilmenite occur but this mineral is generally less abundant than the ilmenite lamellae associated with the titanomagnetites.

## 5.2 MINERAL COMPOSITIONS

An approximate differentiation trend for the sequence studied, was initially constructed on the basis of optical determination (extinction angle measurements) of the An-content of the plagioclase. This was used to select 30 plagioclase grains for electron microprobe analysis to confirm the compositional variations deduced from the optical study. Analyses were also done on selected orthopyroxene, clinopyroxene and olivine grains in the samples.

Cumulus minerals were analysed using a Jeol JXA-50A electron probe X-ray microanalyser, connected to an online Digital PDP 8/M microprocessor at the Geological Survey of South Africa. In all

cases it was attempted to select homogeneous, alteration-free grains. These were microphotographed and the thin sections coated with a 250 Å carbon-coating to render them conducting.

Average settings at which the microprobe operated were 15 kV excitation voltage and  $255 \times 10^{-8}$  A beam current. The standards used in the microprobe analyses of all minerals in this study (Table III) are the routine standards used at the Geological Survey of South Africa for microprobe analyses.

TABLE III STANDARDS USED IN MICROPROBE ANALYSES

ELEMENT	STANDARD	CONCENTRATION OF OXIDES
Si	Wollastonite	50,27
Al	Corundum (synth.)	100,00
Mg	Periclase	98,20
Mn	Pyrolusite	10,86
Fe	Hematite	89,98
Ti	Rutile	94,52
Cr	Chromite	43,90
Ni	Trevorite	24,21
Ca	Wollastonite	47,61
Na	Albite	10,26
K	Sanidine	14,89

Duplicate analyses were made on some grains, and a few grains reanalysed at Rhodes University in order to check results. X-ray counts obtained on the samples were converted to concentrations using the correction factors of Bence and Albee (1968), and structural formulae, and atomic percentages were then calculated for each mineral using the method of Deer *et al.* (1963). It was subsequently found that, due to the abundance of exsolution lamellae, the spot-analyses of pyroxenes were not representative of bulk composition. Therefore several grains were reanalysed on the Jeol superprobe at the University of Pretoria, using a 20 µm beam diameter to obtain analyses on 30 spots per grain. Averages

of these analyses were thought to represent bulk compositions more closely. Analytical results and the structural formulae are presented in Appendices 2-6 and summarized on Folder 6.

### 5.2.1 Plagioclase

The optical and analytical data are presented in Appendices 2 and 3. The anorthite contents of the plagioclases were determined with a universal stage, initially using Eulerian angles, according to the method described by Burri *et al.* (1967) and later extinction angles, as described by Kerr (1959, p. 257-260) and Tröger (1959, p. 127-131). The plagioclase variation-trend (Folder 6) is based on both sets of data, but where the optical results differed by more than 7 mol% An from the microprobe results, the former have been omitted.

In plotting Folder 6, for boreholes M5 and M4, the main magnetite layer was used as a datum line, and the depth below the surface was used for borehole END12. The variation in the plagioclase compositions after Von Gruenewaldt (1973a, Fig. 16) and Van der Merwe (1978, Table 6) is also depicted in this diagram. The An-content decreases across the total succession of the upper zone from An<sub>62</sub> near the base of the zone, to An<sub>47</sub> near the top of END12, but fluctuates in between.

The An-content decreases after the first appearance of apatite. This may be due to the fact that apatite and plagioclase crystallized simultaneously and competed for Ca<sup>2+</sup> in the magma (Von Gruenewaldt, 1973a, p. 210). The gradual decrease in An-content observed in the eastern Bushveld after this point, is not present in borehole END12. Since the apatite content fluctuates considerably and may even be absent in certain layers after this point, a fluctuating supply of Ca available for incorporation in the plagioclases is indicated. This may explain the erratic trend displayed in this part of the sequence, although a correlation exists between An-content of less than 50 and the apatite content in the rocks. An exception exists in sample END12/300,2m, in that An<sub>52,3</sub> was determined for a plagioclase from

a magnetite olivine leucogabbro containing 11,8 per cent apatite. No explanation is found for this discrepancy.

Comparative data from the upper zone in the Potgietersrus limb is scarce, and only three analyses are available (Van der Merwe, 1978, Table 6, p. 87). All three of these are from the upper portion of the upper zone (upper subzone C and lower and upper subzone D) and are clearly inadequate to establish the stratigraphic position of END12. A correlation was, therefore, attempted using the data for the upper zone in the Tauteshoogte area (Von Gruenewaldt, 1973a, Fig. 16).

Folder 6 shows that, the trends in An-content with stratigraphic height for subzones A, B and C are similar for the eastern Bushveld (Von Gruenewaldt, 1973a, Fig. 16) and the Potgietersrus area. In contrast to the eastern Bushveld, where rocks of subzone D are dioritic because of the presence of plagioclase with a composition of less than  $An_{50}$ , such rocks are not well developed in END12.

Von Gruenewaldt (1971, p. 92) ascribes the difference in An-content between his microscopical and chemical data to the possibility that the analysed mineral separates had a higher bulk An-content because of reverse zoning of the plagioclase. The average compositions obtained optically during this study and those calculated from microprobe analyses indicate that, despite the odd discrepancies, the average difference is only 1,45 mol% An.

From the An-trend on Folder 6 it is concluded that:

- a) The entire subzone A is present and that it may even be slightly thicker than in the eastern Bushveld.
- b) Only the lowermost 150 m of subzone B is present in borehole M4.
- c) The upper 150 m of subzone C is present in END12.
- d) If the upper zone in the Potgietersrus limb is of comparable thickness to that in the Tauteshoogte area, about 900 m is absent between the M and END boreholes.

- e) The position of the roof relative to the top of the boreholes is uncertain.

The amount of  $K_2O$  present in the plagioclases is small and fluctuates between 0,3 and 0,9 wt. per cent. This is similar to the Skaergaard intrusion where the  $K_2O$  content of plagioclase is also low and displays very little change with fractionation (Wager and Mitchell, 1951, p. 147).

#### 5.2.1.1 Composition of needles

Plagioclase analyses obtained during the present investigation show relatively high FeO-contents, when compared with values for plagioclases of similar An-content (Deer *et al.*, 1963, 4, p. 116). Snyder (1959, p. 249) found a slight increase of Fe in plagioclase with anorthite content. This is also true for the present study with the plagioclases of the lowermost two boreholes ( $An_{60}$ ), containing 0,3-0,5 wt. per cent FeO, in contrast to the differentiated plagioclases of END12 ( $An_{50}$ ) which contain 0,2 wt. per cent FeO. The microscopical studies show that the highest FeO content of the plagioclase is caused by the presence of tiny opaque needles, which decrease in size and abundance with fractionation.

Von Gruenewaldt (1971, p. 104) also ascribed the high iron content in the plagioclases which he studied to the presence of the submicroscopic needles of magnetite. Hatch *et al.* (1972, p. 74), also ascribed schillerization of plagioclase to be due to oriented rod-like inclusions of iron ore.

The present study indicates that these needle-like inclusions in the plagioclases can also be held responsible for the  $TiO_2$  concentration, which is likewise relatively high. EDS-work on the terminations of needles protruding from plagioclase from sample M5/148,7m show the presence in some needles not only of Fe, but Ti as well, while others contain only Fe (Nienaber-Roberts, 1985).

Since all the cumulus Fe-oxides in the succession, as well as the platelets that occur as inclusions in the coprecipitating

clinopyroxene, consist of titanomagnetite, a similar composition is inferred for the needles in the plagioclase. As ilmenite and ulvöspinel are present as exsolutions, both in the cumulus titanomagnetite and in the platelets, similar exsolutions are thought to be responsible for the higher Ti values referred to above. Some needles in M5/148,7m display alteration skeletons similar to that described for the cumulus titanomagnetites (Section 5.1.8, p. 49).

According to Mao and Bell (1972, p. 664), these needles may be either exsolution products, or a consequence of simultaneous epitaxial growth during crystallization. An exsolution origin is favoured by this author. Hatch *et al.* (1972, p. 74) also favour exsolution and point out that schiller exsolutions disappear during heating, indicating that the needle-substance enters into solid solution in the feldspar, as was also recorded by Anderson (1915, p. 351: quoted in Moorhouse, 1959, p. 53), who achieved homogenization at 1235°C. Armbrustmacher and Banks (1974, p. 661) studied iron-rich plagioclases and also suggested that the Fe, originally present in solid solution in plagioclase, was later exsolved.

According to Wager and Mitchell (1951, p. 146) and Snyder (1959, p. 249)  $\text{Fe}^{3+}$  can replace up to about 0,5 per cent of the Al in the structure of plagioclase.  $\text{Fe}^{2+}$  on the other hand, replaces  $\text{Ca}^{2+}$  (Deer *et al.*, 1963, v.4), or  $\text{Na}^+$  (Wager and Mitchell, 1951, p. 146). The latter authors (*ibid*, p. 204) showed that the  $\text{Fe}_2\text{O}_3$  : FeO ratio in plagioclase from the Skaergaard is roughly similar to that in magnetite.

The question is, however, whether the amount of needles present in the plagioclases studied by these researchers is similar to that commonly observed in the Bushveld. If less, it must be asked whether it is possible to accommodate the large quantity of needles in solid solution at high temperature. Since microprobe analyses obtained during the present study indicate Fe-values well below the limit for replacement of Al advocated by Wager and Mitchell (*ibid.*), exsolution seems a distinct possibility.

Studies on the Fe-content of plagioclase by Sen (1960; quoted by Smith, 1974, p. 108) showed that the amount of Fe that can be accommodated in solid solution in plagioclase increases with increasing temperature, which is in accordance with the conclusions of Ribbe and Smith (1966) and data from the present investigation that the average Fe-content increases with the An-content.

Although Deer, *et al.* (1977, p. 332), state that only traces of Ti may be present in the plagioclase feldspar structure, Ribbe and Smith (1966) found that up to 0,06% could occur in labradorites and bytownites. According to Snyder (1959, p. 262),  $Ti^{4+}$  does not replace  $Si^{4+}$  in silicate minerals because of the difference in ionic radius. On the basis of ionic radius and electron-negativity  $Ti^{4+}$  could, however, substitute for  $Fe^{3+}$ . The analyses on the plagioclase of the upper zone (Appendix 3) contain between 0,14 and 0,19 wt. per cent  $TiO_2$ , which is considerably lower than the FeO content, suggesting that the needles may in fact, be titanomagnetite and that both  $Fe^{3+}$  and  $Ti^{4+}$  probably substitute for  $Al^{3+}$  in the plagioclase structure at high temperatures.

### 5.2.2 Orthopyroxene

To establish compositional trends, 21 orthopyroxene grains were initially selected for microprobe analysis. Since cumulus orthopyroxene is not abundant in the upper portion of the succession, only 7 of the analyses reported in Appendix 4 are of cumulus grains. All these analyses were obtained by using a focussed electron beam. Due to the presence of clinopyroxene exsolution lamellae of various sizes, it proved impossible to obtain a representative analysis of the entire orthopyroxene grain or even of the orthopyroxene host (excluding the exsolution lamellae) by probing only one spot. In addition three clinopyroxene lamellae, which were large enough, were analysed to compare their composition with the respective associated intercumulus clinopyroxene.

In an attempt to establish their bulk compositions, four orthopyroxenes were re-analysed with a 20  $\mu m$  beam. The results are



compared with the spot-analyses by distinguishing between bulk and spot (matrix) analyses on Folder 6. A further distinction has been made on this figure between analyses on cumulus and intercumulus grains. Below the main magnetite layer the inverted pigeonite has an average composition of  $Fs_{40}$ . Above this layer the composition fluctuates rapidly between  $Fs_{39}$  and  $Fs_{50}$ . About 25 m below the top of subzone C, the  $Fs$ -content increases to  $Fs_{52}$  and then reaches a maximum of  $Fs_{61}$  in the last layer containing intercumulus orthopyroxene. The last cumulus orthopyroxene to crystallize has a composition of  $Fs_{51}$ , compared to  $Fs_{60}$  in the eastern Bushveld, which would indicate a lower  $aSiO_2$  for the Potgietersrus limb (Campbell and Nolan, 1974, p. 210). As it is to be expected, the bulk compositions are slightly less  $Fs$ -rich than the matrix analyses. Buchanan (1972, p. 32) found the intercumulus orthopyroxene to be up to 10 mol. per cent enriched in the  $Fs$  molecule compared with cumulus orthopyroxene in associated rocks. This is, however, not very obvious from the data on Potgietersrus.

The analyses of Van der Merwe (1978, Table 7) from subzones A and B, show the same compositional range as those obtained in the present investigation. The variation trend for his analyses shows a slight upward decrease in  $Fs$ -content, which is also evident from the analysis of boreholes M5 and M4. No analyses of Van der Merwe are available from the upper part of the upper zone.

The analyses presented by Von Gruenewaldt (1973a, Fig. 16) for the Tauteshoogte area from subzones A, lower B and upper C, agree well with the observed trend. Since the data for the eastern Bushveld was obtained optically, it would obviate possible errors due to Ca-rich exsolution lamellae. Datapoints from the present investigation may have suffered in this respect, in that the orthopyroxene host would give higher  $Fe$ -values than bulk analyses.

Orthopyroxenes with values of  $Fs_{>50}$  in the eastern Bushveld occur at the top of subzone D, i.e. at higher levels than in Potgietersrus, suggesting that subzone D in the Potgietersrus area is a compacted version of that in the eastern Bushveld. The trend of olivine compositions displays a similar situation. If the upper zone in the Potgietersrus area is reduced in thickness, compared

to the eastern Bushveld, cooling may have been more rapid in this area. This may, according to Buchanan (1972, p. 58), be responsible for such differences in trends displayed between the two areas.

Campbell and Borley (1974, p. 281) found that most of the Al in the pyroxenes from the Jimberlana Intrusion substitutes for tetrahedral  $\text{Si}^{4+}$  and that charge balance requires  $\text{Cr}^{3+}$ ,  $\text{Ti}^{4+}$ ,  $\text{Fe}^{3+}$  or  $\text{Al}^{3+}$  to enter the octahedral sites. The orthopyroxene studied contains up to 1,06 per cent  $\text{Al}_2\text{O}_3$ , which decreases with fractionation. This was also observed by Atkins (1969, p. 233) in the Bushveld Complex.

The  $\text{Ti}^{4+}$  content of orthopyroxene shows a positive correlation with the  $\text{Cr}^{3+}$  and  $\text{Al}^{3+}$  contents, which suggests that titanium substitutes in octahedral sites (Campbell and Borley, 1974, p. 281). According to Verhoogen (1962, p. 212) substitution of titanium for Si, is favoured by a low silica activity and high temperature. The low Ti-content of the orthopyroxenes from the upper zone of the Potgietersrus Compartment (less than 0,41 wt. per cent  $\text{TiO}_2$ ) would therefore seem to suggest slightly higher silica activities and a lower magma temperature than for the eastern Bushveld. Atkins (1969, p. 233) found Ti to increase with an increase in the Fe-content of orthopyroxene in the Bushveld. From Appendix 4 this trend is, however, not apparent in the Potgietersrus area.

Although not smooth, MnO in orthopyroxenes shows a slight increase from 0,34 to 0,95 wt. per cent with fractionation (Appendix 4). Brown and Vincent (1963, p. 179) report similar values for Skaergaard, whilst a more distinct increase was observed in the Dufek intrusion by Himmelberg and Ford (1976, p. 232).  $\text{Mn}^{2+}$  replaces  $\text{Fe}^{2+}$  in the octahedral sites and is therefore dependent on the charge balance in the pyroxene lattice (Campbell and Borley, 1974, p. 281). The substitution of  $\text{Mn}^{2+}$  for  $\text{Fe}^{2+}$ , which has a similar size, rather than for the larger  $\text{Mg}^{2+}$  atom, led to the inclusion of  $\text{Mn}^{2+}$  in the calculation of Fs-contents of the pyroxenes.

### 5.2.3 Clinopyroxene

The clinopyroxenes ubiquitously contain fine and closely-spaced exsolution lamellae of orthopyroxene. Buchanan (1979, p. 338) suggested that due to the fineness of these lamellae, a focussed beam may be used for microprobe analyses. The exsolved needles of titanomagnetite in the clinopyroxene were, however, avoided, since problems were encountered in structural formula calculations, where these were included. Analyses presented will, therefore, be less Fs-rich than the true composition of the clinopyroxene at its time of crystallization. 'Bulk analyses' (host plus lamellae) were obtained on 4 cumulus and 2 intercumulus clinopyroxene grains. Three clinopyroxene lamellae in inverted pigeonite were also analysed (Appendix 5).

Despite a slight decrease in Fs-content upward in the M boreholes, the overall trend for the succession displays an increase (from  $Fs_{31}$  to  $Fs_{51}$ ) with height (Folder 6). The last cumulus clinopyroxene to crystallize has an Fs-content of 58. As was the case with plagioclase and orthopyroxene, slight fluctuations occur on the boundary between subzones C and D.

As noted by Fleet (1974, p. 251-257) in a study on coexisting Ca-rich and Ca-poor pyroxenes, Fe preferentially partitions into the orthopyroxenes. This figure also shows a scatter in the compositions of the clinopyroxene which may reflect a combination of the effects of different environment (e.g. cumulus or intercumulus) and the exsolution lamellae on the analyses.

Only one Fs-value each is available from Van der Merwe's (1978, Table 8) data for subzones A and B. These values are more iron-rich than the present data for the same stratigraphic position. Two values are available for subzone C from his work. The one from lower in this subzone compares well with the trend, while the other is much more iron-rich.

Bushveld clinopyroxenes contain more aluminium than orthopyroxenes (Atkins, 1969, p. 233), with higher values recorded in pyroxenes containing large amounts of  $Ti^{4+}$  and  $Fe^{3+}$  (Deer et al., 1963, 2, p. 113). Kushiro (1960, p. 552) found that clinopyroxenes from

tholeiitic rocks contain less Al than alkaline rocks, and that it decreases during fractionation in layered intrusions. A steady decrease in this constituent with increasing fractionation is not immediately apparent from values reported in Appendix 5, although the bulk compositions do suggest such a trend, with values decreasing from 0,071 to 0,052 cations.

This Al-fractionation trend results from the decrease of the molecular concentration of  $Al_2O_3$  in the magma with fractionation, with a resultant decrease in substitution of Al into the tetrahedral position (Kushiro, 1960, p. 553). According to Kushiro (*ibid.*, p. 552) the effect of pressure may be negligible, although the Al-content may be temperature dependant. Le Bas (1962, p. 280), however, states that any temperature effect on the Al-content of pyroxenes seems small for the clinopyroxenes and that the  $O_2$  partial pressure does not seem to effect the Al-relations of clinopyroxenes.

The MnO content of clinopyroxene is fairly low (average 0,21%) but can be an important constituent in ferroaugites (Deer *et al.*, 1963, 2, p. 113). MnO substitutes preferentially in Ca-poor pyroxenes (Atkins, 1969, p. 233), but increases with fractionation in all the pyroxenes of the Bushveld Complex. The analyses presented show an increase from 0,2 to 0,4 wt. per cent in the M-boreholes and from 0,4 to 0,7 wt. per cent in END12. MnO correlates positively with FeO indicating that the MnO/FeO ratio remains relatively constant. This was also noted by Snyder (1959, p. 252) and Wager and Mitchell (1951, p. 151).

#### 5.2.4 Coexisting clino- and orthopyroxenes

In Figure 32 the analyses of the coexisting clino- and orthopyroxenes have been plotted in the conventional pyroxene quadrilateral, in which the mineral compositions are expressed as atomic percentages of Ca, Mg, and Fe ( $Fe^{2+} + Fe^{3+} + Mn$ ). A distinction has, once again, been made between spot and bulk analyses, as well as between intercumulus and cumulus pyroxenes.

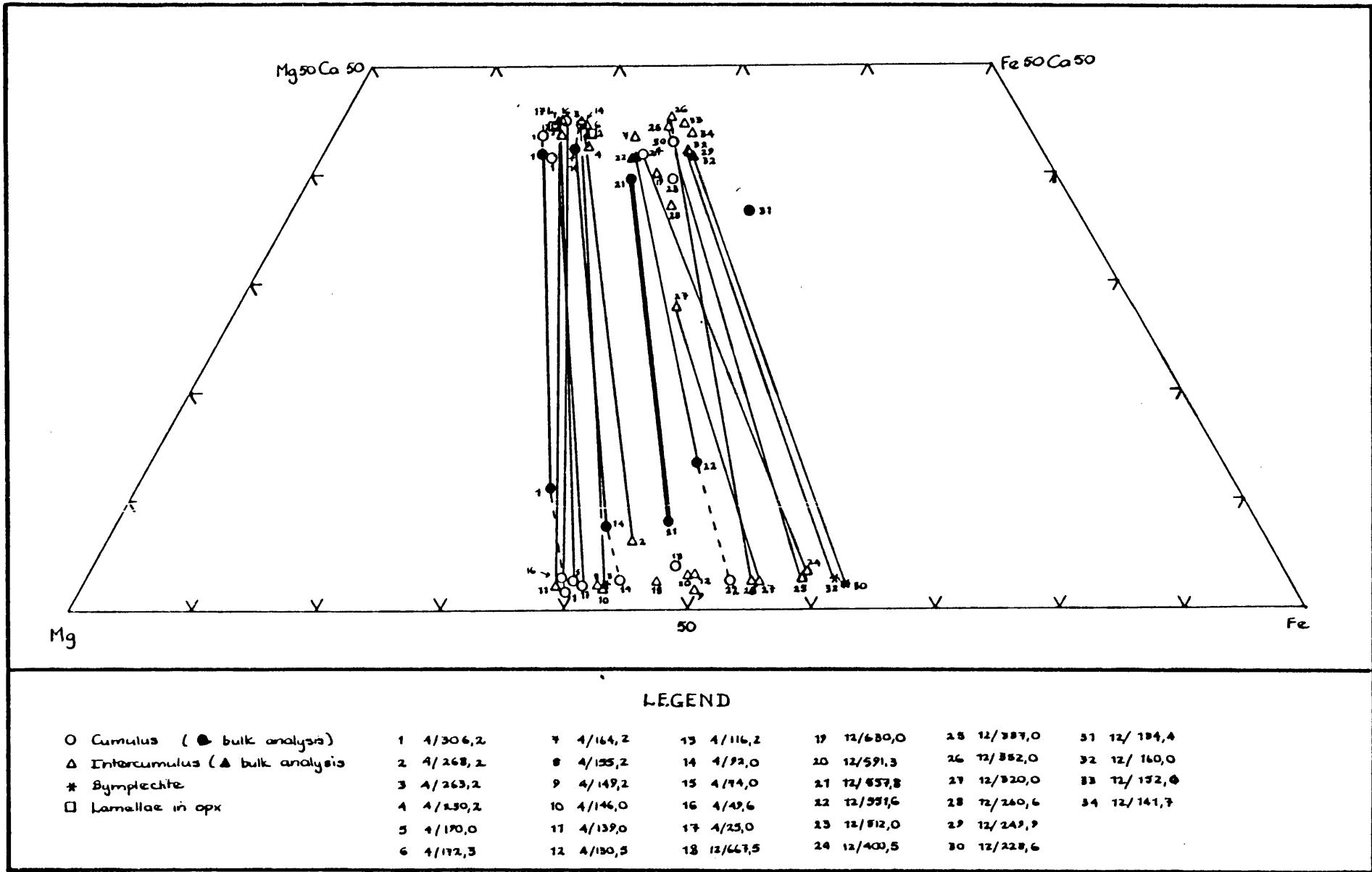


Figure 32. Compositional variation of pyroxenes on the pyroxene quadrilateral.

It is immediately obvious that the spot analyses are more Ca-rich for the clinopyroxenes and more Ca-poor for the orthopyroxenes, compared to bulk compositions. For this reason Hulbert (1983, Figs. 18 and 19) found it desirable to plot bulk compositions separately.

Boyd and Brown (1969, p. 85) studied compositional relationships between pyroxene hosts and exsolution lamellae from a Bushveld gabbro and found that lamellae in an augite host had a similar composition as an inverted pigeonite host in the same rock, and *vice versa*. Plotting the compositions on the pyroxene quadrilateral they also found that a tie-line established between the host- and their lamellae-compositions have "slopes comparable with those established by bulk analyses of other augite-inverted pigeonite pairs" (p. 86).

Hulbert (1983, p. 68) found that in the southern part of the Potgietersrus area the orientation of the tie-lines generally suggested equilibrium conditions, regardless of whether both phases were cumulus or one cumulus and the other intercumulus. Therefore, trends on Figure 33 are based on all bulk compositions, cumulus as well as intercumulus. This figure shows that the clinopyroxenes increase in Fe with fractionation, with Ca remaining fairly constant in the M boreholes. In END12 this trend continues.

A comparative plot of data from this investigation with similar data from elsewhere in the Bushveld Complex (Fig. 33) indicates that, although the clinopyroxenes from the Bethal area are less calcic, the trend is similar to that observed from data in the present investigation. It is of interest here that both Markgraaf (1976) and Atkins (1969) used mineral separates for their analyses and hence included the orthopyroxene lamellae (containing less Ca). Both Van der Merwe (1976) and Buchanan (1979) used an electron microprobe and hence excluded at least some lamellae. This may explain the relatively lower Ca-contents of the last two studies.

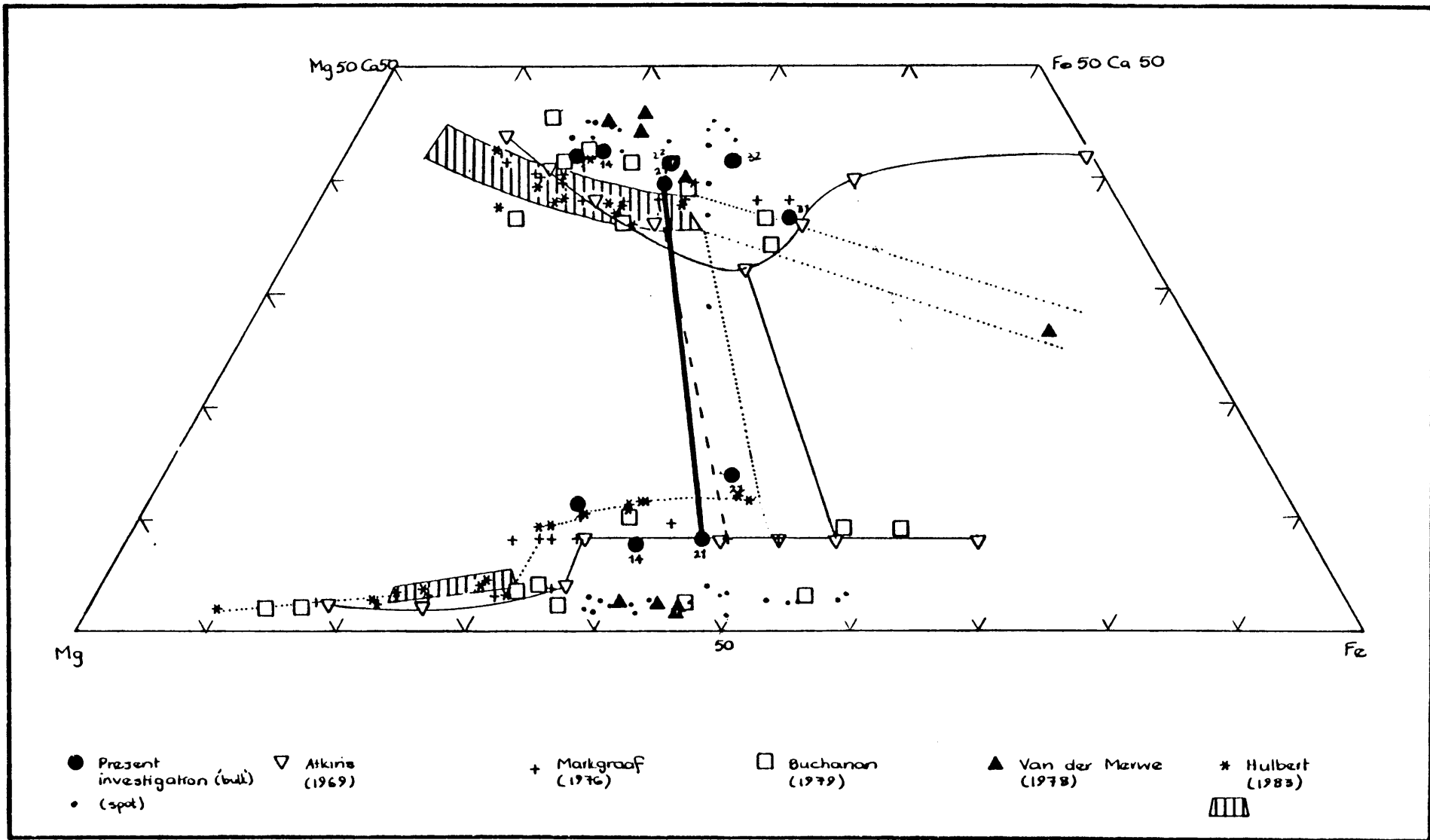


Figure 33. Comparative plot of compositional variation of pyroxenes from different parts of the Bushveld Complex.

From Figure 33 it is also apparent that the orthopyroxene compositions determined by Van der Merwe (1978) by electron microprobe contain less Ca than analysed mineral separates (Atkins, 1969 and Markgraaf, 1976). This is due to the fact that the clinopyroxene lamellae are discriminated against in the electron microprobe analyses, but not in separates.

When the trends obtained in Figure 32 are compared to similar trends from elsewhere in the upper zone (Fig. 33), the clinopyroxene trend based on data of Van der Merwe (1978) from the Potgietersrus limb corresponds to the observed trend of Ca-depletion, as described by Hulbert (1983, p. 70). This is different to the more common Ca-enrichment trend shown in the more Fe-rich clinopyroxenes elsewhere in the Bushveld Complex (Atkins, 1969).

Another distinct difference between the trends shown by pyroxenes from the eastern Bushveld and the Potgietersrus area is that the two-pyroxene minimum is reached at a much more magnesian composition in the latter area. In fact, it seems to be the case even at a more magnesian composition than previously thought (Hulbert, 1983, Fig. 19), in the northern part of the area at least. The last pyroxene pair in equilibrium have compositions of  $\text{Ca}_{40}\text{Mg}_{34}\text{Fe}_{26}$  and  $\text{Mg}_{49}\text{Fe}_{51}$ , compared to those of the eastern Bushveld with  $\text{Ca}_{33}\text{Mg}_{31}\text{Fe}_{36}$  and  $\text{Mg}_{40}\text{Fe}_{60}$  (Atkins, 1969, p. 340).

Available analytical data on the pyroxenite marker (Marais, 1977, p. 28) indicates lateral variation in the width of the pyroxene solvus in the eastern Bushveld, with the miscibility gap between the coexisting pyroxene pairs increasing in a southerly direction. This indicates that the pyroxene solidus intersected the solvus at a lower temperature in the Tonteldoos (southern) area.

It appears from Figure 33 that this miscibility gap is wider for the Potgietersrus area than for the eastern Bushveld, implying that the pyroxenes of the same composition crystallized at lower temperatures in the Potgietersrus area. Hulbert (1983, p. 70) favours a higher prevailing pressure in the Potgietersrus area to produce this difference, due to the pressure sensitivity of the solid solution between  $\text{MgSiO}_3$  and  $(\text{CaMg})\text{SiO}_3$ .



Hulbert (1983) has shown that a significantly higher mean  $KD_{Mg-Fe}^{Opx-Cpx}$  for the Grasvalley area compared to other parts of the Bushveld suggests that the pyroxenes of similar composition equilibrated at higher temperatures in the Potgietersrus area. A temperature of 1022 °C is calculated by him for the basal portion of the upper zone in the Potgietersrus area.

A comparative plot of the pyroxene trends for the Potgietersrus limb with that of other layered intrusions (Hulbert, 1983, p. 71) shows it to correspond most closely to that of the Dufek intrusion (Himmelberg and Ford, 1975), including the composition of the transition from orthopyroxene to pigeonite. The difference in trends between the Potgietersrus (and Dufek) and the eastern Bushveld (and Skaergaard) is explained by Hulbert (ibid, p. 72) as follows:

Since the plagioclase in the Potgietersrus area is more Ca-rich than in other intrusions at similar levels, it appears that the Ca-content of the clinopyroxene was controlled by the Ca-content of the coprecipitating plagioclase. In the upper portions of the upper zone the latter is in turn controlled by the precipitation of apatite (Von Gruenewaldt, 1971, p. 93). Whole-rock analyses of upper zone rocks in the Potgietersrus area contain less P<sub>2</sub>O<sub>5</sub> than equivalent rocks from the Skaergaard Intrusion and eastern Bushveld Complex, which is interpreted as indicating that less apatite crystallized from the Potgietersrus magma, leaving the residual liquids less depleted in Ca.

The present study does not indicate the plagioclase to be more Ca-rich than in the eastern Bushveld. Furthermore, apatite is abundant in certain layers intersected by END12. No alternative explanation can at this stage be put forward for the trend of continued Ca-depletion observed in the clinopyroxenes of the Potgietersrus limb.

### 5.2.5 Olivine

Twenty-one olivines were analysed (Appendix 6) and their Fa values plotted against height in the upper zone (Folder 6). In the boreholes studied the increase is from Fa<sub>45,1</sub> (M5/139m) to Fa<sub>84,1</sub> (END12/33,5m). The Fa-trend shown in Folder 6 fluctuates at several horizons. Molyneux (1974, p. 336) found olivine (Fa<sub>40</sub>) in the troctolite 30 m below the main magnetitite layer to coexist with plagioclase of An<sub>60</sub>. This troctolite layer is absent in the boreholes but reaction olivine (Fa<sub>37</sub>) described in Section 4.2.2.3.2 occurs in rocks with the same anorthite content.

The two analyses presented by Van der Merwe (1978) for the Potgietersrus limb, (one of which is by Gasparrini) appear to be very Fe-rich in relation to the stratigraphic position indicated on Folder 6. This may be interpreted either as a more rapid increase in iron-content of the olivines in the Potgietersrus limb compared to that in the eastern Bushveld Complex, which may suggest a reduced thickness of subzone D in the study area, or that the analyses of Van der Merwe are from more differentiated rocks, higher up in the stratigraphy of the upper zone, above the top of END12.

According to Wager and Brown (1968, p. 388) fractionation in the Bushveld magma resulted in virtually pure fayalitic olivine at the top of the succession. The fact that Fa<sub>100</sub> was not recorded in the samples studied corroborates the earlier conclusion that the END-borehole did not penetrate the top-most part of the succession.

A crystallization gap in the Fa-content of the olivines from the Bushveld intrusion, occurs between Fa<sub>14</sub> and Fa<sub>51</sub> in the eastern and between Fa<sub>32</sub> and Fa<sub>51</sub> in the western Bushveld (Wager and Brown, 1968, p. 388). The olivine from sample M5/139m in the bottom-most horizons of borehole M5 has a Fa-value of 45, indicating that this break might not necessarily exist in the Potgietersrus limb. Van der Merwe (1978) records a troctolite in the main zone, the olivines of which have a composition Fa<sub>31</sub>. This presence may support the suggestion that the gap is absent. Since the olivine gap is expanded by raising the pressure of

crystallization (Campbell and Nolan, 1974, p. 211), its absence may imply that the Potgietersrus limb crystallized at lower pressures than the eastern Bushveld, which is contrary to Hulbert's (1983, p. 70) suggestion based on the pyroxene miscibility gap. A second parameter which may influence olivine crystallization is the  $a_{\text{FeO}}$ . Campbell and Nolan (*ibid.*) indicate that an increase in the  $a_{\text{FeO}}$  of a magma would favour the crystallization of olivine over orthopyroxene. As the  $a_{\text{FeO}}$  is increased by a decrease in the  $f_{\text{O}_2}$  of a magma (Campbell and Nolan, *ibid.*), a lower  $f_{\text{O}_2}$  is implied for the Potgietersrus limb, compared to the eastern Bushveld. From inferred liquid compositions Hulbert calculated an  $f_{\text{O}_2}$  of  $10^{-11}$  to  $10^{-9}$  atm. in the upper zone of the Potgietersrus limb.

The MnO values reported in Appendix 6, indicate that an increase MnO in olivine takes place with stratigraphic height. The lowermost sample contains 0,26 wt. per cent, and values increase to 1,17 wt. per cent at the top. MnO behaves similarly in the olivines of the Bierkraal borehole (Reynolds, 1985b, p. 1040) and the Duluth Complex (Snyder, 1959, p. 252). Wager and Mitchell (1951, p. 152) also found MnO enrichment with fractionation in the olivines from the Skaergaard Intrusion. An increase the MnO content is also observed with fractionation in the Fongen-Hyllingen layered basic complex in Norway (Wilson, *et al.*, 1981, p. 597).

#### 5.2.6 Comparative trends in coexisting minerals

Normally differentiated tholeiitic rocks display increasing Fe in orthopyroxenes and olivines with decrease in Ca-content of plagioclase toward the roof (Buchanan, 1972, p. 56). In order to compare the degree of fractionation of orthopyroxene (olivine) and plagioclase in the same rock, the  $\text{Fe}/(\text{Fe}+\text{Mg})$  atomic ratios of the cumulus ferromagnesian minerals have been plotted against the atomic per cent Na in plagioclase for the same rock (Fig. 34).

Iron-enrichment with differentiation of plagioclase is evident for both the ferro-magnesian minerals. The olivine analysis of Van

der Merwe (1978), agrees with the trend established for the Potgietersrus area.

Data from the eastern Bushveld Complex (Molyneux, 1974 and Von Gruenewaldt, 1973a) display less pronounced iron enrichment in the mafic minerals than the Potgietersrus limb for corresponding sodium values; with enrichment in the Magnet Heights being slightly less than that from Tauteshoogte. Orthopyroxene in the Bethal area contains the least iron for any given Ab-value in the coexisting plagioclase (Buchanan, 1979).

Buchanan (1975, p. 345-346) argues that during high oxygen fugacities ferrous iron is oxidized to magnetite, leaving the magma poorer in the ferrous iron required for the formation of ferromagnesian minerals, thereby resulting in an increase in magnesian content of the orthopyroxene and olivine. By implication rocks of the Bethal area crystallized under higher oxygen fugacities than those of the eastern Bushveld. If this is extrapolated to the Potgietersrus limb, the exceptionally high Fe-values of the ferromagnesian minerals could indicate that the Potgietersrus rocks crystallized under lower oxygen fugacities than the remainder of the Bushveld Complex. This agrees with earlier deductions made from the possible absence of an olivine gap in the Potgietersrus area.

Marais (1977, p. 35) argues that a lateral temperature gradient could be a more feasible explanation to account for the iron-enrichment of orthopyroxene in a southerly direction, in the eastern Bushveld, and that pyroxene seems to be more sensitive to changes in temperature than the coexisting plagioclase. This argument is in agreement with the variation of the size of the pyroxene miscibility gap. From this it follows that an Fe-enrichment in the Potgietersrus pyroxenes, could be the result of a lower crystallization temperature.

In the Skaergaard intrusion olivine appears to re-enter the crystallization sequence later in the differentiation history than the Bushveld Complex (Wager and Brown, 1968). According to Campbell and Nolan (1974, p. 210), a lower temperature would raise the En-value at which the orthopyroxene would be replaced by

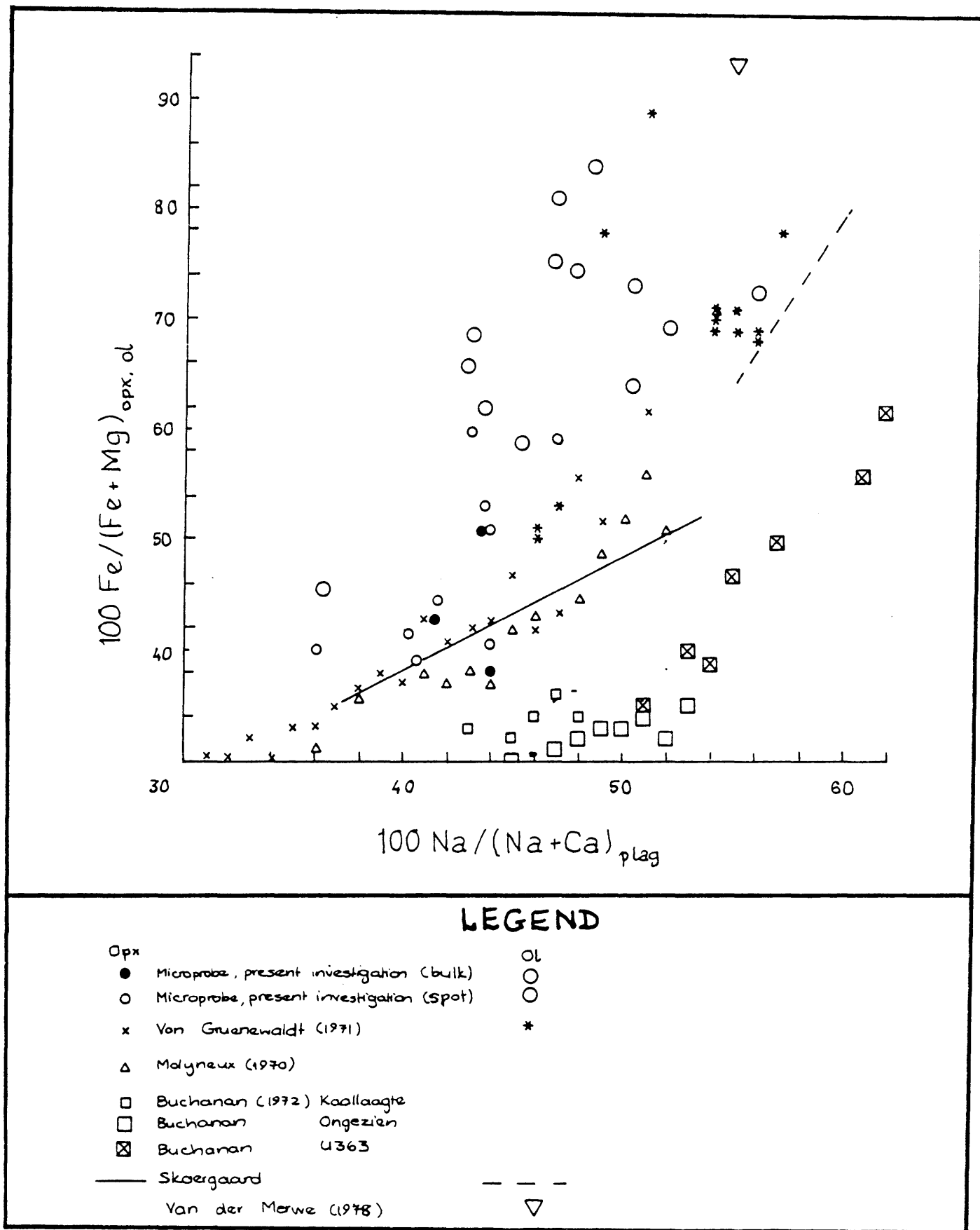


Figure 34. Variation in the Fe/Mg ratio of ferromagnesian minerals from different parts of the Bushveld Complex.

olivine as the primary ferromagnesian mineral. By implication, crystallization temperatures for the upper zone magma were lower in the Bushveld than in the Skaergaard intrusion. This corroborates the earlier deductions that in the Potgietersrus area the upper zone magma crystallized at lower temperatures than in the eastern Bushveld.

According to Lindsley and Munoz (1969, p. 316) the Bushveld crystallized Ca-poor pyroxene with a higher Fe/Mg ratio than the Skaergaard because the  $a\text{SiO}_2$  was higher in the Bushveld magma. They also point out that a higher  $a\text{SiO}_2$  would favour the crystallization of orthopyroxene over Fe-olivine, (thus increasing the crystallization gap for olivine which is contrary to what is suggested from Fig. 34, for the Potgietersrus area). It is therefore deducted from this figure that the lack of a crystallization gap for olivine indicates that the Potgietersrus upper zone crystallized at a lower  $a\text{SiO}_2$ . A lower  $a\text{SiO}_2$  may also be due to a lower crystallization temperature (Campbell and Nolan, 1974, p. 210).

The Fe/Mg ratio of the orthopyroxene for Potgietersrus is lower than for the eastern Bushveld, suggesting a lower  $a\text{SiO}_2$ . This would favour the crystallization of olivine over orthopyroxene, thereby possibly explaining the reason for the apparent lack of an olivine gap in this area.

## 6. LAYERING

In an attempt to explain the diversity of igneous rocks, Bowen (1928: Brown, 1979, p. 9) considered the most important igneous process to be that of magmatic differentiation during cooling. If the crystals are prevented from complete reaction with the liquid fractional crystallization occurs, resulting in the gradual change in composition of the residual liquids.

Sorting of the crystals was, according to Bowen, likely to be the second most important igneous process. Darwin (1844: Campbell, 1978, p. 311) first advocated the hypothesis that crystal settling might be responsible for layering in igneous rocks. Bowen referred to the resultant crystal fractions as accumulations (Brown, 1979, p. 11) and Wager *et al.* (1960) based their nomenclature for igneous cumulates on this concept.

Although there was, for some time at least, consensus of opinion that single grains are transported, opinions differed as to where the cumulus crystals nucleate and how they are transported to where they are now found.

During recent years several researchers began to doubt the theory of crystal settling (Campbell, 1978, p. 311; Irvine, 1979, p. 294; McBirney and Noyes, 1979, p. 490), since it does not adequately explain a number of features in layered intrusions. A major problem with this theory is that the plagioclase, that was thought to have settled to form the layers in which they are found, are less dense than the liquids from which they crystallized. Once this had been accepted, other indicators appeared against simple crystal settling. The paradox between the accumulation of fractionated minerals from the bottom up and the evidence against crystal settling led Irvine (1979, p. 294) to suggest two possibilities:

- a.) The fractionated crystals grew *in situ* on the floor of the intrusion

b.) Magmatic current flow could, in certain circumstances, cause downward transportation of crystals (even those that tend to float). For this second possibility he calls on convection.

*In situ* nucleation and growth of crystals on the floor was first proposed by Jackson (1961, p. 93). Bottom crystallization has since become a popular concept (McBirney and Noyes, 1979; Irvine, 1980b). With respect to the Bushveld Complex, Cawthorn *et al.* (1983) found that Cr showed rapid depletion with height within the main magnetite layer of the Bushveld Complex. This they interpreted as strong evidence that individual ore-rich layers formed through diffusion-controlled bottom crystallization from limited volumes of magma in convective cells at the base of the magma column.

After lengthy fractional crystallization (and the resultant enrichment of Fe, Ti and V in the differentiated liquids) *in situ* bottom crystallization of plagioclase would result in the formation of comparatively dense, Fe-rich liquids near plagioclase crystallization sites (Reynolds, 1985a, p. 1104-1105). Sparks and Huppert (1984, p. 300) point out that such a liquid would remain on the floor of the magma chamber and form a stagnant layer. Magnetite precipitation from this layer would be controlled by the  $\text{Fe}_2\text{O}_3$  : FeO ratio of the liquid (and therefore the  $f\text{O}_2$ ), and its crystallization would decrease the density of this stagnant layer. Continued magnetite crystallization could decrease the density of the stagnant layer sufficiently to allow mixing with the overlying magma, thereby terminating a crystallization cycle (Reynolds, 1985a, p. 1079). The ore-rich layers, therefore also form through *in situ* bottom growth (as previously suggested by McCarthy and Cawthorn, 1983, p. 516).

Although Du Toit (1918), amongst others, believed that titanomagnetites crystallized from Fe-Ti-liquids, the first mention of liquid immiscibility as a possible cause for certain igneous rocks was, according to Brown (1979, p. 9), by Bowen (1928). Osborne (1928, p. 921) also suggested accumulation of late-stage residual Fe-Ti liquid that was filter pressed from the surrounding partially consolidated rocks. Although early studies verified that fields of immiscibility exist in certain systems,



these were found "only in geologically unlikely compositions and at geologically unreasonable temperatures" (Brown, 1979, p. 15). Limited experimental evidence does support the existence of Fe-Ti oxide liquid immiscibility in phosphorous ferro-basaltic-dioritic systems (Naslund, 1976). Evidence is more profound that apatite-oxide rocks, such as those found in END12, are derived from immiscible liquids from magmas that underwent strong differentiation (Philpotts, 1967, p. 303). Philpotts postulated that Na-enrichment in the silicate magmas plays an important role in the formation of these immiscible liquids. Experimental work by Philpotts (1967, p. 313) indicated the existence of several immiscibility fields and led him to believe that a eutectic liquid of composition magnetite : apatite of 2 : 1 would form as an immiscible phase in silicate melts of dioritic composition. On examination of 32 natural oxide-apatite rocks from various localities, Kolker (1982, p. 1155) found evidence that this occurs in nature. McBirney (1975, p. 691) also found evidence in the Skaergaard intrusion that in its later stages the magma separated into two immiscible liquids, one rich in Fe and P and the other rich in silica and alkalis.

Therefore, the apatite-rich magnetitites are postulated by Reynolds (1985a, p. 1042-1044) to be due to the formation of immiscible liquids, high in Fe and P and low in Si, from an Fe-enriched residual magma (compositionally close to ferrodiorite) that formed during fractional crystallization. This liquid would be of higher density than the magma, resulting in droplets coalescing and moving toward the floor, where they settled or percolated into the interstitial areas below. Such a process is thought to be responsible for the formation of the magnetite melatroctolite, which displays textures similar to that of the oxide-apatite rocks reported by Reynolds. In the absence of evidence of liquid immiscibility in the Rhode Island magnetite melatroctolite, Rutherford and Hermes (1984, p. 85) consider their magnetite melatroctolite to have formed by simultaneous gravitational settling of olivine and titanomagnetite, while the plagioclase crystals did not sink and formed associated anorthositic gabbro. They therefore interpret this melatroctolite as an example of an adcumulate. In the present case, however, the fact that apatite is generally a major phase in the high Fe-Ti

oxide-rich rocks and because of the experimental evidence that  $P_2O_5$  partitions into the Fe-oxide-rich liquid during liquid immiscibility (Philpotts, 1967), such a process can not be ruled out for the origin of these apatite-rich rocks. The presence of Villa Nora- and Bierkraal-type olivine-apatite magnetitites suggest that liquid immiscibility occurred over wide areas in the Bushveld Complex during crystallization of the upper zone.

According to Campbell (1978, p. 320), *in situ* development of 'cumulates' may take place if the rate of diffusion is rapid compared to the rate of crystal growth. According to the terminology for cumulates (Wager *et al.*, 1960, p. 77), the monomineralic oxide layers may be classified as adcumulates that formed through processes of diffusion of magnetite molecules from a supernatant magma to the cumulus crystals, coupled with the 'squeezing out' of incompatible liquid by the growing crystals. Reynolds (1985a, p. 1101), however, shows that the impingement textures that would form through such a process are not present, but that the consistency of the interfacial angles between titanomagnetite grains (120 degrees) indicates post-crystallizational modification.

The granoblastic texture observed in the magnetitites develops during a solid state readjustment process at high subsolidus temperatures. Annealing of crystals under the influence of interfacial free energy is thought to be partially responsible for these textures (Reynolds, 1985a, p. 1100). Interstitial liquid would gradually be expelled during this process. Equilibrium was, however, not attained during this process, as a variation in grain size and curved grain boundaries are still present (Reynolds, 1985b, p. 1029-1030). The interstitial silicates are thought to have crystallized from trapped intercumulus liquid (Raal, 1965, p. 21; Reynolds, 1985b, p. 1092).

In the magnetitites, densification and conversion into monomineralic ore layers occurs through annealing at elevated subsolidus temperatures. Subsidius cooling results in the exsolution textures exhibited by the titanomagnetite grains. The thick, massive titanomagnetite layers are considered to have formed impermeable layers to upward moving volatiles during later

stages of cooling, so that concentration of volatiles in certain areas resulted in the alteration features, as well as the reaction features at the basal contact of magnetitite layers described earlier.

## 7. CONCLUSIONS

The M and END12 boreholes contain no correlatable horizons. Lithologically and petrographically the M boreholes correlate well with the subzones A and lower B of the upper zone, both in the Potgietersrus limb and in the eastern Bushveld. END12 is anomalous with respect to the lithological succession encountered elsewhere in the Bushveld Complex, although the presence of olivine and apatite indicates it to contain stratigraphically higher horizons than the M boreholes.

Utilizing the compositional variation of the main cumulus minerals, it is considered that the appearance of cumulus apatite marks the base of subzone D. A reasonable correlation of compositional trends with the eastern Bushveld indicates that END12 contains units of upper subzone C and lower subzone D. The uppermost horizons of the upper zone are not present in END12, so that the position of the roof in this area is uncertain. Although this precludes the establishment of the thickness of the upper zone in this part of the Bushveld Complex, this study indicates that the upper zone in the Potgietersrus limb is thicker than previously believed. Nevertheless, the upper zone of the Potgietersrus limb has been shown to be a compacted version of the upper zone as described from the eastern Bushveld. This implies that cooling must have been more rapid in the Potgietersrus limb.

Electronmicroprobe data indicate that plagioclase in the Potgietersrus limb has an unusually high Fe and Ti content, which has been traced to needle-like inclusions of titanomagnetite.

Despite problems encountered in obtaining accurate probe data due to the extreme exsolution displayed by all pyroxenes, the two-pyroxene minimum has been established to occur at compositions of  $\text{Ca}_{40}\text{Mg}_{34}\text{Fe}_{26}$  and  $\text{Mg}_{49}\text{Fe}_{51}$  for the coexisting pyroxenes, which is earlier in the crystallization-history of the intrusion than in the eastern Bushveld. This indicates a lower  $a\text{SiO}_2$  for the Potgietersrus magma, as is also suggested by the abundance of olivine in all rocks from subzones C and D and the absence of

quartz. The lower  $a_{\text{SiO}_2}$  may be due to a lower crystallization temperature. The greater immiscibility gap between the coexisting pyroxenes of the Potgietersrus limb, compared to the eastern Bushveld suggests also slightly lower temperature than for other parts of the Bushveld Complex.

Olivine compositions indicate that the crystallization gap for olivine does not appear to be present in the Potgietersrus area. This indicates a higher  $a_{\text{FeO}}$  for the Potgietersrus magma, than for the rest of the Bushveld Complex. A higher  $a_{\text{FeO}}$  implies a lower  $f_{\text{O}_2}$  during crystallization. A lower  $f_{\text{O}_2}$  is also suggested by the fact that the Fe/Fe+Mg ratio of the Potgietersrus orthopyroxene for coprecipitating plagioclase of specific Na-content is the highest of all data available for the Bushveld Complex. This ratio for the orthopyroxene, as well as the apparent absence of the olivine crystallization gap also corroborates the conclusion made that the Potgietersrus upper zone crystallized at a lower temperature, compared to the eastern portion of the Bushveld Complex.

Compositional trends encountered in the succession studied indicate these rocks to represent the later stages of a fractionally crystallizing magma. The continuation of the Ca-depletion trend of the clinopyroxenes in the Potgietersrus area differs greatly from the trends displayed by the rest of the Bushveld and Skaergaard but is similar to that of the Dufek intrusion.

No arguments can be put forward to discount the conclusion of Reynolds (1985) and Cawthorn *et al.* (1983), that the sequence formed by *in situ* bottom crystallization. The presence of cumulus textures indicate that during their crystallization the rate of chemical diffusion was rapid compared to the rate of crystal growth. The prominence of subsolidus reaction textures indicate that equilibrium seldom existed between cumulus minerals and the intercumulus liquid.

The presence of olivine-apatite-magnetite-rich rocks in the upper portions of borehole END12 is interpreted as evidence that liquid immiscibility occurred at a time when strong fractional

crystallization resulted in the formation of a Fe- and P-rich residual magma, according to the model of Reynolds (1985b).

Monomineralic layers are thought to form from a layer of stagnant magma near the floor of the intrusion. Diffusion played a role in the purification of these layers. *In situ* bottom crystallization of plagioclase would result in the formation of dense Fe-rich liquids that would accumulate on the floor. Periodic increases in the  $fO_2$  of the magma would trigger crystallization of titanomagnetite from this layer and it would be terminated when the density of the stagnant layer decreases sufficiently, through continued magnetite crystallization, to allow mixing with the overlying magma. Annealing probably commenced immediately after crystallization of magnetites, resulting in densification, as expressed by polygonal grain boundaries. Titanomagnetite layers are considered to have formed impermeable layers to upward percolating volatile-rich, as well as immiscible sulphide liquids, resulting in alteration of the silicates and the concentration of sulphides below these layers.

## 8. ACKNOWLEDGEMENTS

Firstly I should very much like to thank my husband, Keith and my parents, without whose constant encouragement and constructive discussion this work would never have reached completion. For financial assistance whilst at the Institute for Geological Research on the Bushveld Complex, I would like to thank my parents and the CSIR.

This project was initiated at the suggestion of Prof. G. von Gruenewaldt. Research commenced at the Institute for Geological Research on the Bushveld Complex at the University of Pretoria and was completed whilst at the Geological Survey of South Africa. I would like to thank my supervisors, Prof. G. von Gruenewaldt and E.B. Förtsch for their guidance and helpful suggestions. Drr. C. Frick and F. Walraven of the Geological Survey are thanked for providing facilities to complete the research and for criticism of early drafts of this thesis. For editing of the manuscript, my husband and parents are thanked. I am deeply indebted to Mr. M.P. Brandt for relentlessly pushing the completion of this work, during the first few months of employment at the NICR (CSIR).

For manufacture of thin sections, needed for the study, Mrr. J. Jacobs and M. Cloete are thanked. Assistance from Mr. G. du Plessis and Miss. H. Horsch during microprobe analyses are much appreciated. Mr. M. Köhler is thanked for the preparation of photographic material.

## 9. REFERENCES

- AMBLER, E.P. and ASHLEY, P.M., 1977. Vermicular orthopyroxene-magnetite symplectites from Wateranga layered mafic intrusion, Queensland, Australia. *Lithos* 10, p. 163-172.
- ARMBRUSTMACHER, T.J. and BANKS, N.G., 1974. Clouded plagioclase in metadolerite dikes Southeastern Bighorn Mountains, Wyoming. *Am. Miner.*, 59, p. 656-665.
- ATKINS, F.B., 1969. Pyroxenes of the Bushveld Intrusion, South Africa., *J. Petrol.*, 10, p. 222-249.
- BENCE, A.E. and ALBEE, A.L., 1968. Empirical correction factors for the electron microanalysis of silicates and oxides. *J. Geol.*, 76., p. 382-403.
- BERNING, J., 1941. The upper zone of the Bushveld Complex, west of Potgietersrust. M.Sc. thesis, Univ. of Pretoria, 40pp. (Unpubl.)
- BOSHOFF, J.C., 1942. The upper zone of the Bushveld Igneous Complex at Tauteshoogte. D.Sc. thesis, Univ. of Pretoria, 70pp. (Unpubl.).
- BOYD, F.R. and BROWN, G.M., 1969. Electron-probe study of pyroxene exsolution. *Carnegie Inst. Wash. Yb.*, 67, p. 83-86.
- BROWN, G.M., 1979. The problem of the diversity of igneous rocks. In: Yoder, H.S. (Editor). *The evolution of the igneous rocks.* Princeton Univ. Press, Princeton, p. 3-14.
- and VINCENT, E.A., 1963. Pyroxenes from the late stages of fractionation of the Skaergaard Intrusion, East Greenland. *J. Petrol.*, 4, p. 175-197.



BUCHANAN, D.L., 1972. The petrography of rocks of the Bushveld Complex Type intersected by boreholes in the Bethal area. M.Sc. thesis, Univ. of Pretoria, 86pp. (Unpubl.).

----- 1975. The petrography of the Bushveld Complex intersected by boreholes in the Bethal area. Trans. geol. Soc. S. Afr., 78, p. 335-348.

-----, 1977. Cryptic variation in minerals from the Bushveld Complex rocks of the Bethal Area. Trans. geol. Soc. S. Afr., 80, p. 49-52.

-----, 1979. A combined transmission electron microscope and electron microprobe study of Bushveld pyroxenes from the Bethal area. J. Petrol., 20, p. 327-354.

BUDDINGTON, A.F., 1939. Adirondack igneous rocks and their metamorphism. Mem. geol. Soc. Am., 7, 354pp.

BURRI, C., PARKER, R.L. and WENK, E., 1967. Die optische Orientierung der Plagioklase. Birkhäuser Verlag, Basel, 334pp.

CAMPBELL, I.H., 1978. Some problems with the cumulus theory. Lithos 11, p. 311-323.

----- and BORLEY, G.D., 1974. The geochemistry of pyroxenes from the Lower Layered Series of the Jimberlana Intrusion, Western Australia. Contrib. Mineral. Petrol., 47, p. 281-297.

----- and NOLAN, J., 1974. Factors effecting the stability field of Ca-poor pyroxene and the origin of the Ca-poor minimum in Ca-rich pyroxenes from tholeiitic intrusions. Contr. Miner. Petrol., 48, 205-219.

CAWTHORN, R.G. and McCARTHY, T.S., 1980. Variations in Cr content of magnetite from the upper zone of the Bushveld Complex - evidence for heterogeneity and convection currents in magma chambers. Earth planet. Sci. Lett., 46, p. 335-343.

----- and DAVIES, G. 1983. Vertical chemical gradients in a single grain of magnetite from the Bushveld Complex, South Africa. *Mineral. Mag.*, 47, p. 27-34.

CHAYES, E., 1956. Petrographic modal analysis, an elementary statistical appraisal. John Wiley and Sons, New York, 113pp.

COX, K.G., BELL, J.D. and PANKHURST, R.J., 1979. The interpretation of igneous rocks. Allen and Unwin, London, 450pp.

DALY, R.A., 1928. Bushveld Igneous Complex of the Transvaal. *Bull. geol. Soc. Am.*, 39, p. 703-768.

DEER, W.A., HOWIE, R.A. and ZUSSMAN, J., 1963. Rock forming minerals., 1-4. William Clowes and Sons, Ltd., London.

-----, 1977. Rock forming minerals: Framework silicates., 4, 2nd Ed., Longman, London.

DEHM, R.M., 1980. Geologische Kartierung, tektonische und petrographische Bearbeitung und geochemische Untersuchung an den Nebensteinsmagnetiten der Subzone C, Obere Zone des Bushveld Komplex nördlich Roosenekal, Eastern Transvaal. Diplomarbeit, Univ. München, 162pp. (Unpubl.).

FLEET, M.E., 1974. Partition of major and minor elements and equilibration in coexisting pyroxenes., *Contr. Miner. Petrol.*, 44, p. 259-274.

GOODE, A.D.T., 1974. Oxidation of natural olivines. *Nature*, 248, p. 500-501.

-----, 1977. Intercumulus igneous layering in the Kalka Layered Intrusion, central Australia. *Geol. Mag.*, 114, p. 215-218.

GROBLER, N.J. and WHITFIELD, G.G., 1970. The olivine-apatite-magnetites and related rocks in the Villa Nora occurrence of the Bushveld Igneous Complex. *Spec. Publ. geol. Soc. S. Afr.*, 1, p. 208-227.

GROENEVELD, D., 1970. The structural features and the petrography of the Bushveld Complex in the vicinity of Stoffberg, eastern Transvaal. Spec. Publ. geol. Soc. S. Afr., 1, p. 36-45.

GRUENEWALDT, G. von, 1966. The geology of the Bushveld Igneous Complex east of the Kruis River Cobalt occurrence, north of Middelburg, Transvaal. M.Sc. thesis, Univ. Pretoria 104pp. (Unpubl.).

-----, 1970. On the phase-change orthopyroxene-pigeonite and the resulting textures in the main and upper zones of the Bushveld Complex in Eastern Transvaal. Spec. Publ. geol. Soc. S. Afr., 1, p. 67-73.

-----, 1971. A petrographical and mineralogical investigation of the rocks of the Bushveld Igneous Complex in the Tauteshoogte-Roossenekal area of the eastern Transvaal. D.Sc. thesis, Univ. Pretoria 228pp. (Unpubl.).

-----, 1973a. The main and upper zones of the Bushveld Complex in the Roossenekal area, eastern Transvaal. Trans. geol. Soc. S. Afr., 76, p. 207-227.

-----, 1973b. The modified differentiation index and the modified crystallization index as parameters of differentiation in layered intrusions. Trans. geol. Soc. S. Afr. 76 (1), p. 53-61.

-----, 1977. The mineral resources of the Bushveld Complex. Miner. Sci. Engng., 9, p. 83-95.

-----, COERTZE, F.J., PLESSIS, M.D. du, FERGUSON, J., HUNTER, D.R., LENTHALL, D.H., VERMAAK, C.F, LEE, C. and WALRAVEN, F., 1980. Bushveld Complex IN: KENT, L.E. (Compiler). Stratigraphy of South Africa. Handbk geol. Surv. S. Afr., 8, Ch. 4.3, p. 223-233.

HAGGERTY, S.E. and BARKER, I., 1967. The alteration of olivine in basaltic and associated lavas. Part I: High Temperature Alteration. Contr. Miner. Petrol., 16, p. 233-257.

HALL, A.L., 1909. The geology of the country east of Potgietersrust, including Marabastad goldfields. A. Rep. geol. Surv. Transvaal for 1908, p. 62-102.

-----, 1932. The Bushveld Igneous Complex of the Central Transvaal. Mem. geol. Surv. S. Afr., 28, 560pp.

HARGRAVES, R.B. and YOUNG, W.M., 1969. Source of stable remanent magnetism in Lambertville Diabase. Am. J. Sci., 267, p. 1161-1177.

HASELTON, J.D. and NASH, W.P., 1975. Ilmenite-orthopyroxene intergrowths from the Moon and the Skaergaard Intrusion. Earth planet. Sci. Lett. 26, p. 287-291.

HATCH, F.H., WELLS, A.K. and WELLS, M.K., 1972. The petrology of the igneous rocks. 13th Ed. Allen and Unwin, London, 551pp.

HENKEL, J., 1981. Geologische Kartierung, petrographische Bearbeitung und geochemische Untersuchungen der Nebensteinsmagnetite der Subzonen A und B, Obere Zone des Bushveld Complex, nördlich Roossenekal, eastern Transvaal, Süd-Afrika. Diplomarbeit, Univ. München, 148pp. (Unpubl.)

HIEMSTRA, S.A. and LIEBENBERG, W.R., 1964. The mineralogy of some vanadium-bearing titaniferous magnetites from the Bushveld Igneous Complex. S. Afr. Govt metall. Lab. Publ., Proj 15/63, 26pp.

HIMMELBERG, G.R. and FORD, A.B., 1976. Pyroxenes of the Dufek Intrusion, Antarctica., J. Petrol. 17, p. 219-243.

HJELMQUIST, S., 1950. The titaniferous iron-ore deposits of Taberg in the south of Sweden: Sveriges Geologiska Undersökning, Arsbok., 43, 55pp.

HULBERT, L., 1983. A petrological investigation of the Rustenburg Layered Suite and associated mineralization south of Potgietersrus. D.Sc. thesis, Univ. Pretoria 511pp. (Unpubl.).

----- and GRUENEWALDT, G. von, 1985. Textural and compositional features of chromite in the lower and critical zones of the Bushveld Complex South of Potgietersrus. *Econ. Geol.*, 80, p. 872-895.

IRVINE, T.N., 1979. Rocks whose composition is determined by crystal accumulation and sorting. In: YODER, H.S. (Editor). *The evolution of the igneous rocks*. Princeton. Univ. Press, Princeton. p. 245-306.

-----, 1980. Magmatic infiltration metasomatism, double-diffusive fractional crystallization and adcumulus growth in the Muskox intrusion and other layered intrusions. In: HARGRAVES, R.B. (Editor), *Physics of magmatic processes*, Princeton Univ. Press, Princeton. p. 325-383

-----, 1982. Terminology for layered intrusions. *J. Petrol.*, 23 (2), p. 127-162.

JACKSON, E.D., 1961. Primary textures and mineral associations in the ultramafic zone of the Stillwater Complex, Montana. *Prof. Pap. geol. Surv. U.S.*, 358, p. 1-106.

KERR, P.F., 1959. *Optical mineralogy*. 3rd Ed. McGraw-Hill Book Co., N.Y., 142pp.

KOLKER, A., 1982. Mineralogy and geochemistry of Fe-Ti oxide and apatite (nelsonite) deposits and evaluation of the liquid immiscibility hypothesis. *Econ. Geol.*, 77, p. 1146-1158.

KUSHIRO, I., 1960. Si-Al relation in clinopyroxenes from igneous rocks. *Am. J. Sci.* 258, 548-554.

KYNASTON, H., and MELLOR, E.T., 1905. On a traverse from Pretoria to Pietersburg, via the Springbok Flats, Nylstroom and Pietpotgietersrust, returning by the Olifants and Elands Rivers. *A. Rept. geol. Surv. Transvaal for 1904*, p. 11-25.

LeBAS, M.J., 1962. The role of aluminium in igneous clinopyroxenes with relation to their parentage. *Am. J. Sci.*, 260, p. 267-288.

LINDSLEY, D.H. and MUNOZ, J.L., 1969. Subsolidus relations along the join hedenbergite-ferrosilite. *Am. J. Sci.*, 267(A), p. 295-324.

MAO H.K. and BELL, P.M., 1972. Luna 20 plagioclase: crystal-field effects and chemical analysis of iron. *Carnegie Inst. Wash. Yb* 72, p. 662-665.

MARAIS, C. L., 1977. A investigation of the pyroxenite marker and the associated rocks in the main zone of the eastern Bushveld Complex. M.Sc. thesis, Univ. Pretoria, 87pp. (Unpubl.).

MARKGRAAF, J., 1976. Pyroxenes of the western Bushveld Complex, South Africa. *Trans. geol. Soc. S. Afr.*, 79 (2), p. 217-224.

McBIRNEY, A.R., 1975. Differentiation of the Skaergaard Intrusion. *Nature*, 253, p. 691-694.

----- and NOYES, R.M., 1979. Crystallization and layering of the Skaergaard Intrusion, *J. Petrol.*, 20 (3), p. 487-554.

MCCARTHY T.S. and CAWTHORN, R.G. 1983. The geochemistry of the vanadiferous magnetite in the Bushveld Complex: Implications for crystallization mechanisms in layered complexes. *Miner. Deposita*, 18, p. 505-518.

McSWEEN, H.Y.Jr and NYSTROM, P.G.Jr, 1979. Mineralogy and petrology of the Dutchmans Creek gabbroic intrusion, South Carolina. *Am. Mineral.*, 64, p. 531-545.

MERWE, M.J. van der, 1976. The Layered Sequence of the Potgietersrus limb of the Bushveld Complex. *Econ. Geol.*, 71, p. 1337-1351.

-----1978. The geology of the basic and ultramafic rocks of the Potgietersrus limb of the Bushveld Complex. Ph.D. thesis, Univ. Witwatersrand, 176pp. (Unpubl.).

MOLENGRAAFF, G.A.F., 1898. A. Rep. geol Surv. Transvaal for 1898, 43pp.

-----, 1901. Géologie de la République Sud-Africaine de Transvaal. Bull. Soc. géol. de France, 4 (1), p. 13-92.

MOLYNEUX, T.G., 1964. The geology and structure of the area in the vicinity of Magnet Heights, Eastern Transvaal, with special reference to the magnetic iron ore. M.Sc. thesis, Univ. Pretoria, 112pp. (Unpubl.).

-----, 1970a. A geological investigation of the Bushveld Complex in Sekhukhuneland and part of the Steelpoort Valley, Eastern Transvaal, with particular reference to the oxide minerals. D.Sc. thesis, Univ. Pretoria, 125pp. (Unpubl.).

-----, 1970b. The geology of the area in the vicinity of Magnet Heights, Eastern Transvaal, with special reference to the magnetic iron ore. Spec. Publ. geol. Soc. S. Afr., 1, p. 228-241

-----, 1972. X-ray data and chemical analyses of some titanomagnetite and ilmenite samples from the Bushveld Complex, South Africa. Mineralog. Mag., 38, p. 863-871.

-----, 1974. A geological investigation of the Bushveld Complex in Sekhukhuneland and part of the Steelpoort Valley. Trans. geol. Soc. S. Afr., 77, p. 329-338.

MOORHOUSE, W.W., 1959. The study of rocks in thin section. Harper and Row, New York, 514pp.

NASLUND, H.R., 1976. Liquid immiscibility in the system  $KAlSi_3O_8$ - $NaAlSi_3O_8$ - $FeO$ - $Fe_2O_3$ - $SiO_2$  and its application to natural magmas. Carnegie Inst. Wash. Yb. 75, p. 592-597.

NIENABER-ROBERTS, C.J., 1985. Identification of inclusions in plagioclase from the Bushveld Complex, using electron microprobe and SEM. (Abstr.) Proc. Electron Microsc. Soc. Southern Africa, 15, p. 49-50.

-----, in press. A note on the needle-like inclusions in plagioclase from the Bushveld Complex. Ann. geol. Surv. S. Afr., 20.

OSORNE, F.F., 1928. Certain magmatic titaniferous iron ores and their origin. Part II. Econ. Geol., 23, p. 895-922.

PHILPOTTS, A.R., 1967. Origin of certain iron-titanium oxide and apatite rocks. Econ. Geol., 62, p. 303-315.

RAAL, F., 1965. The transition between the main and the upper zone of the Bushveld Complex in the Western Transvaal. M.Sc. thesis, Univ. Pretoria, 59pp. (Unpubl.).

RAMDOHR, R., 1969. The ore minerals and their intergrowths. Pergamon Press. N.Y., 1174pp.

REYNOLDS, I.M., 1978. Mineralogical studies of South African titaniferous iron ores: their application to extractive metallurgy. Trans. geol. Soc. S. Afr., 81, p. 233-240.

-----, 1985a. The nature and origin of titaniferous magnetite-rich layers in the upper zone of the Bushveld Complex: a review and synthesis. Econ. Geol., 80, p. 1089-1108.

-----, 1985b. Contrasted mineralogy and textural relationships in the uppermost titaniferous magnetite layers of the Bushveld Complex in the Bierkraal area north of Rustenburg. Econ. Geol., 80, p. 1027-1048.

RIBBE, P.H. and SMITH, J.V., 1966. X-ray-emission microanalysis of rock-forming minerals: IV. Plagioclase feldspars. J. Geol., 74, p. 217-233.



ROBINSON, P., ROSS, M., NORD, G.L. Jr, SMYTH, J.R. and JAFFE, H.W., 1977. Exsolution lamellae in augite and pigeonite: fossil indicators of lattice parameters at high temperature and pressure. *Am. Miner.*, 62, p. 857-873.

ROEDER, 1984. Fluid inclusions. *Reviews in mineralogy*, 12, Mineralog. Soc. Am., 644pp.

RUTHERFORD, M.J. and HERMES, O.D., 1984. Melatroctolite-anorthositic gabbro complex, Cumberland, Rhode Island: Petrology, origin and regional setting. *Bull. geol. Soc. Am.*, 95, p. 844-854.

SINGEWALD, J.J., 1913. The titaniferous iron ores in the United States. *Bull. U.S. Bureau of Mines*, 64, 143pp.

SMITH, J.V., 1974. *Feldspar Minerals*. Springer-Verlag, New York, v. 2, 690pp.

SNYDER, J.L., 1959. Distribution of certain elements in the Duluth complex. *Geochim. Cosmochim. Acta*, 16, p. 243-277.

SPARKS, R.S.J. and HUPPERT, H.E., 1984. Density changes during the fractional crystallization of basaltic magmas: fluid dynamic implications. *Contr. Miner. Petrol.*, 85, p. 300-309.

STANTON, R.I., 1972. *Ore Petrology*. McGraw-Hill, N.Y., 713 pp.

STRECKEISEN, A., 1974. Classification and nomenclature of plutonic rocks. *Geol. Rundsch.*, 63, p. 773-786.

TAYLOR, R.B., 1964. Geology of the Duluth Gabbro Complex, near Duluth, Minnesota. *Bull. Minnesota geol. Surv.*, 44, 62pp.

TOIT, A.L. du, 1918. Plumasite (corundum-aplite) and titaniferous magnetite rocks from Natal: *Trans. geol. Soc. S. Afr.*, 21, p. 53-73.

TRÖGER, W.E., 1959. Optische Bestimmung der gesteinsbildenden Minerale Teil 1. Bestimmungstabellen. Schweizerbart'sche Verlagsbuchhandlung, Stuttgart, 147 pp.

TYSON, R.M, and CHANG, L.Y., 1984. The petrology and sulfide mineralization of the Partridge River Troctolite, Duluth Complex, Minnesota. *Can. Miner.*, 22, p. 23-38.

VANCE, J.A., 1969. On synneusis. *Contr. Miner. Petrol.*, 24, p. 7-29.

VERHOOGEN, J., 1962. Distribution of titanium between silicates and oxides in igneous rocks. *Am. J. Sci.*, 260, p. 211-220.

WAGER, L.R. and BROWN, G.M., 1968. Layered igneous rocks. Oliver and Boyd, Edinburgh and London, 588pp.

-----, BROWN, G.M. and WADSWORTH, W.J., 1960. Types of igneous cumulates. *J. Petrol.*, 1, p. 73-85.

-----, and MITCHELL, R.L., 1951. The distribution of trace elements during strong fractionation of basic magma - a further study of the Skaergaard intrusion, east Greenland. *Geochim. Cosmochim. Acta*, 1, p. 129-208.

WILLEMSE, J., 1969a. The geology of the Bushveld Igneous Complex, the largest repository of magmatic ore deposits in the world. *Econ. Geol., Monogr.* 4, p. 1-22.

-----, 1969b. The vanadiferous magnetic iron ore of the Bushveld Igneous Complex. *Econ. Geol., Monogr.* 4, p. 187-208.

WILSON, J.R., ESBENSEN, K.H., and THY, P., 1981. Igneous petrology of the synorogenic Fogen-Hyllingen Layered Basic Complex, south-central Scandinavian Caledonides. *J. Petrol.*, 22, p. 584-627.

## APPENDIX 1A

## MODAL ANALYSES ON THIN SECTIONS FROM BOREHOLE M5

DEPTH	DESCRIPTION	PLAG	OPX	CPX	OL	ORE	AP	QTZ	BI	HBL	SYMPL	OTHER	n	IC
25,0	Mgt anorthosite	86,8*	3,7	0,1	0,0	5,6	0,0	1,6	1,5	0,4	0,1	0,1	1316	41
26,0	Mgt anorthosite	54,4*	0,3	0,0	0,0	39,9?	0,0	0,0	0,4	0,0	5,0	0,0	1000	33
26,6	Mgt anorthosite	53,6*	0,4	0,0	0,0	40,0?	0,0	0,1	1,6	0,0	4,3	0,0	1258	59
31,0	Mgt anorthosite	78,2*	1,1	0,3	0,0	17,4	0,0	0,0	1,9	0,0	1,1	0,0	1404	54
32,5	Mgt anorthosite	57,5*	1,7	0,0	0,0	36,7	0,0	0,0	1,3	0,1	2,6	0,0	1017	52
33,7	Mgt anorthosite	48,2*	0,0	0,0	0,0	48,8	0,0	0,1	1,2	0,0	1,4	0,2	1275	42
34,6	Mgt anorthosite	47,5*	2,0	0,0	0,0	45,6	0,0	0,0	1,4	0,0	2,3	1,1	1425	51
35,3	Mgt anorthosite	84,7*	0,0	0,0	0,0	10,5*	0,0	0,1	2,1	0,6	0,0	1,1	1157	44
35,7	Mgt anorthosite	79,2*	1,7	1,0	0,0	15,6*	0,0	0,0	0,6	0,0	1,9	0,0	1283	50
36,0	Mgt anorthosite	72,9*	3,5	0,0	0,0	20,5*	0,0	0,0	0,7	0,0	2,4	0,0	1389	73
36,5	Mgt anorthosite	81,1*	4,0	0,4	0,0	10,4*	0,0	0,0	1,7	0,0	2,1	0,2	1466	57
37,7	Mgt leuconorite	49,6*	5,7	0,0	0,0	41,9*	0,0	0,1	0,0	0,0	0,6	2,1	1395	56
38,9	Mgt anorthosite	94,2*	0,0	0,1	0,0	4,8*	0,0	0,0	0,8	0,0	0,0	0,1	1227	86
39,0	Mgt anorthosite	65,2*	0,8	0,0	0,0	32,2*	0,0	0,0	0,6	0,0	0,0	0,0	500	
39,7	Mgt anorthosite	86,9*	1,2	0,0	0,0	5,0*	0,0	0,9	0,1	1,5	0,0	4,3	1283	39
39,9	Anorthosite	94,2*	0,1	2,7	0,0	0,2*	0,2	2,7	0,0	0,0	0,0	0,0	1200	41
40,0	Anorthosite	92,5*	0,8	0,0	0,0	2,2*	0,0	2,0	0,2	0,0	0,0	1,4	1208	44
42,4	Leuconorite	78,1	17,4	0,0	0,0	0,0	0,0	1,6	2,2	0,0	0,0	0,0	1150	38
47,0	Leuconorite	76,7*	18,8*	2,8	0,0	0,0	0,0	0,7	0,3	0,7	0,0	0,0	1284	36
52,0	Leuconorite	81,1*	13,5*	4,0	0,0	0,0	0,0	5,5	0,7	0,2	0,0	0,0	1061	59
56,0	Leucogabbronorite	68,2*	22,9*	8,7	0,0	0,1	0,0	0,0	0,1	0,0	0,0	0,0	1258	36
57,9	Anorthosite	87,6*	1,0	1,1	0,0	0,3	0,0	0,0	2,3	0,0	0,0	0,4	1320	24
58,4	Anorthosite	90,1*	4,2*	1,8	0,0	0,0	0,0	0,8	2,3	1,8	0,0	0,0	1471	61
60,0	Anorthosite	95,5*	0,6	0,7	0,0	0,3	0,0	1,4	0,3	0,1	0,0	1,1	1205	55
60,4	Gabbronorite	59,9*	24,7*	11,3	0,0	0,1	0,0	0,0	0,0	0,0	0,7	3,3	952	29
64,7	Leuconorite	89,1*	6,1*	4,0	0,0	0,2	0,0	6,6	3,3	0,0	0,0	0,0	1299	56
65,8	Gabbronorite	55,2*	37,6*	7,0	0,0	0,0	0,0	0,0	0,0	0,0	0,0	0,0	1094	74
66,5	Leucogabbro	80,8*	1,8*	14,0	0,0	0,0	0,0	7,7	1,8	0,9	0,0	0,0	1544	40
68,2	Anorthosite	89,5*	5,8*	2,1	0,0	0,2	0,0	1,5	0,5	0,3	0,0	0,3	1361	51
72,0	Anorthosite	97,5*	0,0	0,6	0,0	0,0	0,0	6,6	2,2	0,0	0,0	0,0	1200	53
72,5	Mgt anorthosite	59,4*	0,0	4,0	0,0	0,1*	0,0	0,0	0,4	0,1	0,0	0,0	1265	22
83,0	Norite	61,3*	36,2*	1,1	0,0	0,8	0,0	5,5	0,0	0,1	0,0	0,0	1354	35
89,0	Leucogabbronorite	70,2*	16,9*	11,8	0,0	0,1	0,0	0,5	0,1	0,4	0,0	0,0	1347	41
93,4	Leucogabbronorite	76,8*	16,3*	5,6	0,0	1,1	0,0	0,0	0,0	0,0	0,0	0,2	1000	41
96,0	Leucogabbronorite	74,9*	7,7*	15,9	0,0	0,0	0,0	0,0	0,4	0,2	0,0	0,0	1132	32
106,0	Anorthosite	86,4*	4,0*	0,6	0,0	0,7	0,0	3,5	1,1	0,9	0,0	0,0	1398	31
111,0	Leuconorite	83,2*	11,3	0,9	0,0	0,8	0,1	0,9	1,4	0,4	0,0	0,0	1000	
120,6	Mgt anorthosite	74,5*	0,0	0,0	0,0	2,4	0,0	0,2	2,2	0,0	0,8	0,0	1200	52
125,0	Leucogabbro	84,7*	2,4	7,8	0,0	0,6*	0,0	6,6	1,1	0,8	0,0	0,0	1315	30
129,9	Mgt anorthosite	81,3*	0,0	0,0	0,0	5,5*	0,1	4,1	5,9	3,0	0,0	0,0	1494	31
135,5	Mgt anorthosite	72,2*	2,3	0,5	0,0	2,9*	0,0	0,0	0,0	0,0	3,1	0,0	1000	48
139,0	Mgt leuconorite	76,9*	9,3	0,0	3,3	8,1*	0,0	0,0	0,0	0,0	0,0	0,0	1353	
144,4	Anorthosite	88,2*	6,8	0,0	0,0	3,5*	0,1	0,0	0,7	0,0	0,5	0,1	1227	36
148,7	Anorthosite	90,1*	1,7	3,1	0,0	6,6*	2,2	2,2	3,3	0,5	0,0	1,2	1386	13
154,0	Mgt anorthosite	75,5*	3,1	0,3	0,0	1,8*	0,0	0,0	0,0	0,0	3,2	0,0	1278	44
159,8	Anorthosite	93,9*	0,2	0,6	0,0	7,0*	0,3	0,3	5,5	0,0	0,0	0,0	1200	30
163,0	Mgt leucogabbro	76,5*	0,6	14,3*	0,0	7,0	0,0	0,0	1,1	0,1	0,4	0,0	1225	28
165,1	Leucogabbronorite	77,0*	17,6*	3,5	0,0	1,9*	0,0	0,0	0,0	0,0	0,0	0,0	1000	96
170,1	Mgt l.gabbronorite	55,8*	8,6*	16,4*	0,0	1,5*	0,0	0,0	0,0	0,3	0,4	0,0	1164	64
182,0	Mgt gabbronorite	45,0*	20,5*	13,5*	0,0	1,2*	0,0	0,0	1,5	0,7	0,7	0,0	1259	110

\* Cumulus

? Possibly cumulus

n Number of points analysed

IC IC number (Chayes, 1956)

## APPENDIX 1B

## MODAL ANALYSES ON THIN SECTIONS FROM BOREHOLE .M4

DEPTH	DESCRIPTION	PLAG	OPX	CPX	OL	ORE	AP	QTZ	BI	HBL	SYMPL	OTHER	n	IC
25,0	Mgt leuconorite	72,5*	10,3*	2,5	0,0	14,1?	0,0	0,0	0,2	0,0	0,4	0,0	1000	67
26,2	Mgt l.gabbronorite	70,3*	9,6*	4,8*	0,0	13,4	0,0	0,0	1,3	0,0	0,5	0,0	1207	55
29,1	Mgt l.gabbronorite	57,5*	17,3*	5,4*	0,0	19,1*	0,0	0,0	0,1	0,0	0,5	0,0	1554	82
34,5	Mgt anorthosite	65,7*	0,8	0,0	0,0	29,2*	0,0	0,0	0,0	0,0	4,3	0,0	1000	72
39,1	Mgt gabbronorite	54,2*	11,4*	22,3*	0,0	11,5*	0,0	0,0	0,3	0,0	0,3	0,0	1352	57
49,6	Mgt l.gabbronorite	59,9*	5,7*	11,5*	0,0	21,1?	0,0	0,0	0,8	0,0	1,0	0,0	1196	46
57,0	Mgt leucogabbro	69,9*	3,9*	14,7*	0,0	10,5*	0,0	0,0	0,5	0,0	0,4	0,0	1229	62
64,1	Mgt leucogabbro	68,9*	3,5*	17,2	0,0	9,2*	0,0	0,0	0,5	0,0	0,7	0,0	1193	42
66,3	Anorthositic mgtt	20,8*	0,8	0,0	0,0	76,4*	0,0	0,0	1,1	0,0	0,5	0,0	1000	26
69,0	Mgt leucogabbro	71,2*	0,7	14,0	0,0	12,4*	0,0	0,1	1,1	0,0	0,5	0,0	1171	42
74,0	Mgt anorthosite	80,9*	0,1	4,0	0,0	11,7*	0,0	0,1	2,9	0,0	0,2	0,0	1400	40
77,0	Melagabbronorite	17,3	21,8*	60,0*	0,0	0,9	0,0	0,0	0,0	0,0	0,0	0,0	1200	41
85,0	Mgt leucogabbro	67,1*	0,0	9,7	0,0	20,8	0,0	0,0	0,9	0,0	1,4	0,0	1431	39
86,1	Leuconorite	66,9*	26,7*	3,3	0,0	2,6*	0,0	0,0	0,5	0,0	0,0	0,0	1000	200
88,9	Melagabbronorite	20,3*	35,7*	42,1*	1,0	0,2	0,0	0,0	0,7	0,0	0,0	0,0	1000	48
92,0	Mgt l.gnorite	69,9*	8,0*	13,2*	0,0	7,5	0,0	0,0	1,3	0,0	0,0	0,0	1433	55
99,4	Mgt m.gnorite	27,5?	31,9*	33,6*	0,0	6,8	0,0	0,0	0,2	0,0	0,0	0,0	1000	48
108,6	Mgt l.gnorite	66,5?	16,3*	10,0*	0,0	5,4	0,0	0,0	0,9	0,0	0,7	0,2	1000	46
116,2	Mgt norite	40,6*	37,3*	2,7	0,0	17,2	0,0	0,0	1,2	0,0	1,0	0,0	1252	44
121,2	Mgt anorthosite	57,5*	1,1	0,0	0,0	35,5?	0,0	0,1	1,5	0,9	3,3	0,0	1714	39
125,5	Mgt anorthosite	61,5*	3,8	0,5	0,0	27,5?	0,0	0,0	3,8	0,0	2,8	0,0	1266	43
125,6	Mgt anorthosite	53,3*	3,3	0,6	0,0	37,6?	0,0	0,0	0,0	0,0	5,1	0,0	1000	72
130,5	Mgt anorthosite	87,1*	0,6	0,0	0,0	5,8	0,0	0,0	3,6	0,0	0,0	0,0	1303	50
139,0	Mgt anorthosite	83,9*	2,1	0,2	0,0	12,1*	0,0	0,0	1,0	0,0	0,6	0,0	1218	62
145,8	Mgt anorthosite	87,0*	2,0	1,0	0,0	8,4*	0,0	0,6	0,7	0,2	0,0	0,0	1476	74
154,3	Mgt anorthosite	81,1*	0,8	0,1	0,0	16,1*	0,0	0,5	1,0	0,4	0,0	0,0	1383	61
158,0	Anorthositic mgtt	14,0	0,0	0,0	0,0	86,0*	0,0	0,0	0,0	0,0	0,0	0,0	1000	
146,0	Anorthosite	92,3*	2,6	4,9	0,0	0,0	0,0	0,2	0,0	0,0	0,0	0,0	1251	51
168,4	Anorthositic mgtt	10,1*	0,0	0,0	0,0	89,1*	0,0	0,0	0,1	0,0	0,6	0,0	1000	
172,3	L.gabbronorite	72,2*	22,1*	5,7	0,0	0,0	0,0	0,0	0,1	0,0	0,0	0,0	1139	40
181,0	L.gabbronorite	76,3*	17,3*	5,9	0,0	0,2	0,0	0,0	0,2	0,1	0,0	0,0	2958	44

\* Cumulus

? Possibly cumulus

n Number of points analysed

IC IC number (Chayes, 1956)

## APPENDIX 1C

## MODAL ANALYSES ON THIN SECTION; FROM BOREHOLE END12

DEPTH	DESCRIPTION	PLAG	OPX	CPX	OL	ORE	AP	QZ	BI	HBL	SYMPL	OTHER	n	IC
33,5	Mgt l.troctolite	54,4*	0,2	0,0	24,9*	13,0?	5,0*	0,0	2,2	0,3	0,0	0,0	1200	91
35,1	Mgt-b l.troctolite	59,4*	0,0	4,2	24,9*	6,7	3,0*	0,0	1,8	0,0	0,0	0,0	1000	82
41,1	Mgt l.troctolite	54,1*	0,0	1,7	22,9*	13,0?	6,3*	0,0	1,3	0,0	0,0	0,0	1000	109
47,2	Mgt troctolite	39,4*	0,0	0,1	29,7*	18,7*	13,4*	0,0	1,0	0,0	0,0	0,0	895	114
53,3	Mgt troctolite	37,1*	0,0	0,1	29,7*	18,7*	13,4*	0,0	1,0	0,0	0,0	0,0	1250	113
57,9	Mgt troctolite	40,2*	0,0	0,0	30,6*	15,8*	10,3*	0,0	2,9	0,3	0,0	0,0	1188	148
65,5	Mgt troctolite	34,7*	0,1	0,0	32,5*	20,8*	11,8*	0,0	0,1	0,0	0,0	0,0	1000	86
71,6	Mgt troctolite	30,1*	0,0	1,5	26,6*	22,1?	18,8*	0,0	1,8	0,0	0,0	0,0	1052	130
141,7	Olivine gabbro	42,3*	0,0	5,3	43,4*	1,8	5,2*	0,0	1,5	0,4	0,0	0,0	1347	46
142,6	Anorthositic mgtt	20,2*	0,0	0,0	0,1	79,4*	0,0	0,0	0,3	0,0	0,0	0,0	1289	
144,8	Mgt l.troctolite	60,5*	0,0	2,7	17,5*	14,8*	1,6	0,0	2,9	0,0	0,0	0,0	1457	74
149,3	Leucogabbro	78,0*	0,0	13,7	4,2	2,1	1,4	0,0	6,6	0,0	0,0	0,0	1105	71
152,4	Mgt-b ol l.gabbro	63,4*	0,0	15,5	9,4	10,5*	0,5	0,0	6,6	0,0	0,0	0,0	1198	66
163,0	Pl-b mgt dunite	5,2	0,2	0,0	80,6*	12,8*	1,1*	0,0	2,2	0,1	0,0	0,0	1200	152
172,2	Mgt ol leucogabbro	55,3*	0,0	7,4	17,7*	17,3?	1,7*	0,0	6,6	0,0	0,0	0,0	1000	94
173,7	Mgt-b ol l.gabbro	60,3*	0,2	5,9	23,1?	5,4*	1,3*	0,0	3,4	0,3	0,0	0,0	1200	102
179,8	Mgt-b l.troctolite	62,1*	0,0	3,0	24,0	5,3*	4,7*	0,0	4,8	0,1	0,0	0,0	1000	117
184,4	Mgt ol melagabbro	9,3	0,0	10,0	57,2*	21,2*	1,8*	0,0	2,2	0,0	0,0	0,0	800	124
190,5	Mgt dunite	0,2	0,0	0,0	73,3*	22,1*	4,2*	0,0	2,2	0,0	0,0	0,0	936	85
195,0	Mgt troctolite	26,6?	0,0	0,7	46,9*	20,6*	3,9*	0,0	3,3	1,0	0,0	0,0	1000	125
196,6	Mgt m.troctolite	10,7?	1,0	0,0	58,3*	22,6*	5,8*	0,0	9,9	0,8	0,0	0,0	1200	95
202,7	Pl-b mgt dunite	3,6*	0,0	0,5	65,2*	26,5*	4,1*	0,0	1,1	0,0	0,0	0,0	1000	114
204,2	Mgt troctolite	25,4*	0,0	1,5	20,1*	41,6*	11,1*	0,0	1,1	0,0	0,0	0,0	1000	108
207,2	Mgt l.troctolite	51,6*	0,0	3,8*	23,2*	12,1*	8,2*	0,0	1,1	0,0	0,0	0,0	1000	71
217,9	Mgt troctolite	41,6*	0,2	3,1	33,7*	11,4*	10,0*	0,0	0,0	0,0	0,0	0,0	1000	94
228,6	Mgt ol gabbro	47,8*	0,0	5,8*	26,7*	10,6*	8,4*	0,0	2,7	0,0	0,0	0,0	1118	67
234,7	Mgt-b troctolite	54,3*	0,0	1,7	28,3*	8,0*	5,1*	0,0	6,6	0,0	0,0	0,0	1000	71
239,2	Mgt-b ol gnorite	45,5*	2,1	8,5*	22,8*	8,1*	6,5*	0,0	2,2	0,0	0,0	0,0	1000	92
249,9	Mgt-b ol gabbro	48,8*	0,0	5,8*	27,5*	8,2*	7,6*	0,0	2,1	0,0	0,0	0,0	1000	103
260,6	Mgt-b troctolite	58,7*	0,0	3,3	29,4*	7,3*	1,1	0,0	2,2	0,0	0,0	0,0	1216	109
266,7	Mgt anorthosite	80,7*	0,0	4,3	0,8*	12,0*	1,4*	0,0	8,5	0,0	0,0	0,0	1000	
274,3	Mgt m troctolite	10,4	0,0	0,2	60,5*	21,4?	7,0*	0,0	0,0	0,0	0,0	0,0	1000	96
275,8	Mgt troctolite	30,5	0,0	0,0	49,6*	13,5*	5,9*	0,0	5,5	0,0	0,0	0,0	1000	118
289,5	Mgt ol gabbro	47,3*	0,0	5,1	25,8*	11,0*	10,1*	0,0	7,7	0,0	0,0	0,0	1390	81
297,1	Mgt ol gabbro	33,3*	0,0	5,5*	20,3*	15,9*	24,5*	0,0	5,5	0,0	0,0	0,0	1000	88
300,2	Mgt ol leucogabbro	58,5*	0,0	6,0*	12,4*	19,8*	11,8*	0,0	1,1	0,0	0,0	0,0	1000	
310,8	Mgt ol gabbro	37,5*	0,0	7,0*	20,4*	19,0*	14,6*	0,0	8,8	0,0	0,0	0,0	1000	77
313,9	Mgt ol gabbro	37,4*	0,0	5,2*	30,4*	14,6*	12,0*	0,0	4,4	0,0	0,0	0,0	1000	63
320,0	Olivine gabbro	53,1*	10,5	1,8	26,2?	2,9	3,0*	0,0	1,1	0,0	0,0	0,0	1215	77
332,5	Leucotroctolite	83,2*	0,0	0,1	6,5*	4,1*	4,2*	0,0	2,2	0,3	0,0	0,0	1090	109
341,4	Mgt-b ol l.gabbro	61,9*	0,0	8,9	20,2*	7,3*	0,2	0,0	9,9	0,6	0,0	0,0	1000	63
344,4	Mgt-b l.troctolite	63,9*	0,0	1,1	27,1*	6,6*	0,0	0,0	1,4	0,0	0,0	0,0	1269	89
350,5	Mgt l.troctolite	66,5*	0,2	0,9*	9,4	21,8*	0,6	0,0	6,8	0,0	0,0	0,0	1000	73
352,0	Mgt-b l.gabbro	70,5*	0,0	16,2	3,2*	8,3	0,0*	0,0	8,8	0,0	0,0	0,0	1246	95
359,7	Mgt troctolite	29,1?	0,0	0,0	46,1*	15,6*	8,6*	0,0	1,1	0,0	0,5	0,0	1000	53
361,2	Mgt-b l.troctolite	81,1*	0,0	0,1	14,1*	4,7	0,0	0,0	0,0	0,0	0,0	0,0	1323	72
365,8	Mgt ol gabbro	39,8*	0,0	9,9*	27,9	13,3	8,7*	0,0	4,4	0,0	0,0	0,0	1010	75
376,4	L.troct mgtt	21,8*	0,0	0,0	2,9	68,8*	0,0	0,1	4,7	0,0	1,7	0,0	1245	
381,0	Ol l.gabbro	67,7*	4,3	0,8	19,3*	3,3?	1,7	0,0	9,9	0,0	0,0	0,0	1246	56
384,1	Leucotroctolite	64,9*	1,7	0,0	26,4*	2,1	0,0	0,0	5,1	0,0	0,0	0,0	1199	31
387,0	Leucotroctolite	79,1*	0,0	0,5	10,6?	3,7	0,0	0,9	8,8	0,1	0,0	0,0	1282	
396,2	Mgt l.troctolite	52,5*	0,0	0,4	23,5*	22,0	0,5	0,0	5,5	0,0	0,5	0,0	1280	73
400,5	Melagabbro	31,7*	0,5	58,8*	0,0	8,5	0,0	0,0	1,1	0,0	0,4	0,0	1011	43
412,1	Mgt l.troctolite	74,6*	0,0	1,7	11,7*	9,3*	0,0	0,0	2,5	0,0	0,2	0,0	1226	70
422,1	Mgt l.troctolite	78,7*	0,0	1,9	0,1	8,5?	7,2	0,0	3,7	0,0	0,0	0,0	1323	47
429,4	Mgt l.troctolite	57,9*	0,0	0,0	27,1	14,6?	0,1	0,0	3,3	0,0	0,0	0,0	1176	65
430,0	Mgt troctolite	53,8*	0,0	0,8	30,2*	14,8?	0,0	0,0	3,3	0,0	0,1	0,0	1000	62
448,0	Mgt ol l.gabbro	54,3*	0,0	9,5*	15,1*	19,5*	0,2	0,0	1,4	0,0	0,0	0,0	1197	74
460,2	Mgt l.troctolite	52,9*	0,0	0,0	20,4*	26,0?	0,1	0,0	6,6	0,0	0,0	0,0	1179	72
466,3	Mgt dunite	0,5	0,0	0,0	59,0*	30,7*	9,7*	0,0	0,0	0,0	0,0	0,0	1000	59
472,4	Mgt m.troctolite	7,0	0,0	0,0	56,0*	28,0*	8,0*	0,0	6,6	0,4	0,0	0,0	1089	n.d.
483,1	Mgt ol l.gabbro	59,9*	0,0	6,4	19,3*	10,6*	1,8*	0,0	1,8	0,0	0,3	0,0	1431	71
493,7	Dunitic mgtt	0,0	0,0	0,1	46,1*	50,5*	2,9*	0,0	4,4	0,0	0,0	0,0	1565	66
502,9	Mgt dunite	0,7	0,3	0,2	28,5*	44,3*	21,0*	0,0	0,0	0,0	0,0	5,0	1000	97
512,0	Mgt ol gabbro	27,8*	0,0	3,9	42,1*	19,6*	6,0*	0,0	5,5	0,0	0,0	0,0	850	97
518,1	Mgt m.ol gabbro	25,2*	0,1	17,0	36,5*	15,7*	2,7*	0,0	3,3	0,0	0,0	2,5	1190	107
521,2	Pl-b mgt lherzolite	0,3	0,1	5,1	45,8*	37,2*	11,8*	0,1	0,0	0,0	0,0	0,0	1000	113
536,4	Leucotroctolite	80,0*	0,3	1,7	13,8?	2,6	0,0	0,0	1,5	0,0	0,0	0,0	1314	78

5339,4	Mgt-b l.troctolite	73,7*	0,4	0,5	18,5?	6,3	0,0	0,0	0,4	0,0	0,1	0,0	1167	82
545,6	Leucotroctolite	79,0*	1,9	0,6	14,4?	4,0*	0,0	0,1	0,0	0,0	0,0	0,0	500	82
545,7	L.troctolitic mgtt	12,4*	0,3	0,0	4,0*	83,3*	0,0	0,0	0,0	0,0	0,0	0,0	1000	
551,4	Melanoritic mgtt	1,8	3,6*	0,0	2,8	91,2*	0,0	0,6	0,0	0,0	0,0	0,0	1000	
551,6	Mgt-b leuconorite	65,6*	25,5*	1,1	0,1	6,2	0,0	0,0	1,3	0,0	0,0	0,0	1338	67
551,9	Ol gnoritic mgtt	15,4	0,7*	1,9	15,5	65,4*	0,0	0,1	0,8	0,0	0,0	0,0	1000	
552,0	Mgt-b troctolite	60,4*	0,0	0,0	32,6*	5,4*	0,0	0,4	1,1	0,0	0,0	0,0	1207	118
557,8	Mgt melagabbrono	26,4*	33,1*	17,8*	0,0	22,3?	0,0	0,0	0,3	0,0	0,0	0,0	995	128
564,5	Mgt-b l.troctolite	77,8*	0,9	0,4	3,1	9,6	0,0	0,0	0,9	0,0	0,0	0,0	1171	85
566,8	Ol l.gnoritic mgtt	6,6	0,4	0,4	0,4	91,6*	0,6	0,0	0,0	0,0	0,0	0,0	1000	
576,0	M.troctolitic mgtt	4,9	0,1	0,0	26,8*	65,0*	0,0	0,0	3,2	0,0	0,0	0,0	1280	
579,1	Mgt m.troctolite	18,7	0,3	0,5	38,1*	41,9*	0,1	0,0	0,2	0,0	0,2	0,0	1000	76
580,6	Mgt-b ol l.gnorite	76,3*	4,6	0,9	6,9*	9,7*	0,0	0,0	0,6	0,0	0,0	0,0	1253	32
582,1	Mgt ol m.gnorite	16,7?	1,6	2,0*	25,2*	33,2*	0,0	0,0	0,3	0,0	0,1	0,0	1015	60
585,5	Mgt-b anorthosite	91,6*	0,0	2,9	0,0	4,9	0,0	0,0	0,5	0,0	0,0	0,0	1154	61
591,3	Mgt ol l.gabbrono	73,7*	4,8	3,6	6,8	10,0	0,0	0,0	1,1	0,0	0,0	0,0	1165	
595,9	Mgt m.troctolite	22,4?	0,0	0,0	63,3*	13,0*	0,2	0,0	1,0	0,0	0,1	0,0	1000	34
598,9	Mgt troctolite	48,0*	0,0	0,0	35,5*	14,8*	0,3	0,0	0,6	0,0	0,8	0,0	1000	61
601,9	Mgt-b anorthosite	91,8	0,2	0,2	0,0	5,9	0,0	0,0	1,2	0,0	0,0	0,0	1378	84
609,6	Anorthosite	96,7	0,5	1,5	0,0	0,2	0,0	0,9	0,3	0,0	0,0	0,0	1258	63
617,2	Mgt-b anorthosite	86,0*	2,7	0,0	1,7	5,6	0,0	0,0	0,0	0,0	0,0	3,0	1151	81
624,2	Mgt anorthosite	80,0*	1,1	0,3	0,2	15,8?	0,0	0,0	2,5	0,0	0,0	0,0	1237	89
629,1	Mgt-b anorthosite	86,2*	3,1	2,4	0,0	6,6	0,0	0,0	1,7	0,0	0,0	0,0	1200	88
630,0	Anorthosite	93,3*	0,0	1,4	0,0	3,9	0,5	0,0	0,8	0,0	0,0	0,0	1266	69
638,5	Mgt ol l.norite	54,8*	14,4*	2,5	10,6	14,5*	0,0	0,0	3,0	0,0	0,0	0,0	1083	93
646,1	Mgt ol l.gnorite	61,2*	10,2?	4,4	11,9?	11,6*	0,0	0,0	0,4	0,0	0,0	0,0	1322	100
656,8	Mgt ol l.gnorite	65,6*	0,7*	14,0*	10,4	8,8?	0,0	0,0	0,2	0,0	0,0	0,0	688	19
666,0	Mgt ol l.gnorite	60,1*	2,1?	16,5*	7,9?	12,2*	0,0	0,0	0,9	0,0	0,0	0,0	1000	86
667,5	Mgt ol l.gnorite	57,5*	5,9*	15,2*	6,4?	12,9?	0,0	0,0	1,4	0,0	0,0	0,0	1177	55

\* Cumulus  
 ? Possibly cumulus  
 n Number of points analysed  
 IC IC number (Chayes, 1956)

## APPENDIX 2

## PLAGIOCLASE COMPOSITIONS, OBTAINED USING EXTINCTION ANGLES (Mol% An)

BOREHOLE	DEPTH	1	2	3	4	AV	PROBE
M4	25,0	63,3	60,0	60,3	-	61,2	58,2
	49,6	-	-	-	58,4	58,4	58,7
	57,0	60,0	64,0	58,0	-	60,7	-
	85,0	61,8	-	60,2	-	61,0	-
	116,2	63,3	-	60,9	-	62,1	-
	139,0	61,3	-	62,8	-	62,1	59,9
	146,0	-	-	-	-	-	60,7
	164,2	61,8	-	60,3	55,6	59,2	59,3
	172,3	60,3	62,0	57,8	-	60,0	-
	M5	25,0	60,0	59,0	60,0	-	59,7
35,5		61,0	-	60,6	-	60,8	-
65,8		65,2	60,7	62,3	-	62,7	62,9
96,0		62,4	-	-	-	62,4	-
125,0		64,0	62,8	64,0	-	63,6	-
154,0		57,8	-	56,4	-	-	-
170,0		-	-	-	-	47,4	-
182,0		55,0	-	53,4	-	54,2	55,28
END12	70,1	53,0	-	51,9	51,1	52,0	51,54
	141,7	49,9	-	48,4	-	49,2	46,99
	289,6	50,8	-	50,3	-	50,6	-
	332,5	53,3	-	52,3	-	52,8	-
	341,0	-	-	-	44,3	44,3	-
	365,8	50,7	-	52,1	-	51,4	-
	387,0	-	-	-	56,5	56,5	-
	400,5	48,8	-	48,2	-	48,5	55,6
	429,0	-	-	-	-	-	49,7
	460,0	59,1	-	58,4	-	58,8	55,4
	483,1	55,3	-	55,0	-	55,2	-
	518,2	53,0	-	50,5	-	51,8	-
	522,0	63,4	-	61,3	-	62,4	-
	580,0	56,3	-	54,4	55,0	55,2	-
	609,6	55,0	-	53,9	-	54,5	-
638,6	54,0	-	52,9	-	53,5	-	
667,0	56,8	54,0	55,2	-	55,3	-	

- 1 Kerr (1959, p. 261)
- 2 ---- (1959, p. 258)
- 3 Tröger (1959, p. 102)
- 4 Burri *et al.* (1967, Plate XI)

APPENDIX 3

MICROPROBE ANALYSES OF PLAGIOCLASES

DEPTH	BOREHOLES M5 AND M4 COMBINED*														BOREHOLE END12																			
	25,0	49,6	74,0	92,0	130,5	139,0	146,0	149,2	155,2	161,9	164,2	190,0	230,2	263,2	306,2	33,5	70,1	141,7	152,4	190,5	228,6	300,2	320,0	352,0	387,0	400,5	429,5	460,2	512,0	551,0	591,3	630,0	667,5	
SiO <sub>2</sub>	50,21	53,37	53,04	52,98	54,21	52,47	52,05	53,18	52,12	52,84	52,13	52,25	53,21	53,35	53,29	54,48	55,39	56,86	55,42	57,85	57,52	53,67	57,22	53,27	53,03	50,86	50,40	51,68	51,66	49,48	52,12	49,69	54,17	
Al <sub>2</sub> O <sub>3</sub>	31,98	27,87	29,31	28,12	27,68	29,08	29,51	29,44	29,77	29,33	29,32	28,90	29,91	28,96	29,21	27,97	27,93	27,36	29,01	27,44	25,88	28,28	28,42	20,88	28,05	29,16	29,66	27,96	28,82	31,07	29,34	29,63	28,63	
TiO <sub>2</sub>	0,13	0,15	0,15	0,15	0,17	0,13	0,16	0,15	0,21	0,17	0,17	0,14	0,15	0,17	0,14	0,18	0,16	0,16	0,15	0,13	0,15	0,18	0,10	0,18	0,16	0,19	0,15	0,14	0,18	0,18	0,12	0,11	0,16	
MgO	0,11	0,09	0,10	0,09	0,08	0,09	0,08	0,12	0,08	0,10	0,10	0,11	0,10	0,10	0,19	0,06	0,09	0,08	0,08	0,08	0,10	0,08	0,10	0,12	0,07	0,07	0,07	0,08	0,09	0,11	0,09	0,02	0,02	
FeO	0,45	0,37	0,44	0,43	0,38	0,31	0,42	0,47	0,33	0,49	0,45	0,33	0,37	0,34	0,90	0,29	0,26	0,22	0,22	0,17	0,35	0,29	0,17	0,44	0,16	0,18	0,32	0,24	0,29	0,24	0,27	0,26	0,26	
MnO	0,09	0,11	0,11	0,08	0,11	0,12	0,10	0,09	0,09	0,14	0,11	0,11	0,11	0,12	0,07	0,13	0,10	0,13	0,07	0,07	0,11	0,14	0,07	0,11	0,11	0,13	0,13	0,08	0,10	0,11	0,11	0,11	0,14	0,14
Cr <sub>2</sub> O <sub>3</sub>	0,15	0,13	0,14	0,10	0,21	0,21	0,12	0,09	0,11	0,17	0,14	0,24	0,16	0,25	0,12	0,19	0,14	0,14	0,12	0,12	0,10	0,11	0,09	0,20	0,05	0,14	0,15	0,12	0,21	0,18	0,12	0,14	0,14	
NiO	0,31	0,21	0,28	0,24	0,24	0,21	0,19	0,28	0,25	0,25	0,22	0,22	0,25	0,25	0,28	0,19	0,20	0,20	0,28	0,26	0,28	0,25	0,28	0,36	0,22	0,27	0,23	0,27	0,23	0,25	0,23	0,26	0,22	
CaO	11,74	12,96	11,77	11,29	12,15	12,02	11,79	11,90	11,87	11,70	11,50	12,82	11,84	12,45	10,98	9,72	9,48	9,44	9,68	8,28	9,26	10,94	8,47	16,26	11,04	12,47	11,09	13,31	10,29	11,31	11,42	12,55	10,99	
Na <sub>2</sub> O	4,35	4,87	3,75	4,44	4,42	4,16	3,98	4,44	4,04	4,12	3,98	4,04	3,93	4,72	5,04	4,60	5,63	5,00	5,79	5,17	5,51	5,07	6,85	5,35	5,17	5,60	5,51	6,24	4,81	5,22	5,15	4,70		
K <sub>2</sub> O	0,46	0,25	0,39	0,48	0,38	0,45	0,35	0,29	0,33	0,30	0,36	0,31	0,31	0,38	0,42	0,49	0,40	0,43	0,10	0,36	0,69	0,37	0,52	0,52	0,50	0,90	0,64	0,87	0,82	0,19	0,67	0,49		
Total	99,98	100,38	99,48	98,40	100,03	99,15	98,75	100,45	99,20	99,44	98,65	99,41	100,48	100,30	100,19	98,67	98,84	100,62	100,46	100,29	99,28	100,14	100,36	99,19	98,78	99,11	98,74	100,03	98,93	98,54	99,53	98,66	99,92	

STRUCTURAL FORMULAE ON THE BASIS OF 32 OXYGEN ATOMS

Si	9,167	9,711	9,664	9,773	9,849	9,619	9,569	9,621	9,539	9,635	9,593	9,577	9,605	9,669	9,666	9,959	10,066	10,168	9,932	10,306	10,395	9,763	10,141	10,071	9,762	9,411	9,362	9,518	9,555	9,189	9,547	9,265	9,818
Al	6,881	5,977	6,295	6,113	5,927	6,334	6,395	6,278	6,423	6,309	6,360	6,244	6,362	6,185	6,245	6,026	5,982	5,765	6,127	5,762	5,513	6,064	6,142	4,652	6,087	6,360	6,494	6,069	6,283	6,801	6,334	6,512	6,116
Ti	0,018	0,021	0,021	0,021	0,024	0,022	0,022	0,021	0,029	0,023	0,023	0,020	0,021	0,024	0,019	0,024	0,022	0,022	0,020	0,018	0,020	0,024	0,018	0,025	0,025	0,022	0,027	0,021	0,020	0,025	0,017	0,016	0,022
Mg	0,029	0,024	0,028	0,025	0,021	0,033	0,022	0,033	0,022	0,027	0,027	0,030	0,027	0,027	0,050	0,016	0,023	0,022	0,022	0,020	0,027	0,023	0,061	0,033	0,018	0,018	0,020	0,020	0,021	0,026	0,030	0,026	0,006
Fe	0,069	0,056	0,067	0,066	0,057	0,047	0,064	0,071	0,051	0,075	0,069	0,050	0,056	0,052	0,136	0,044	0,040	0,033	0,032	0,026	0,053	0,044	0,159	0,070	0,025	0,028	0,050	0,036	0,046	0,037	0,042	0,040	0,040
Mn	0,014	0,018	0,017	0,013	0,016	0,018	0,015	0,014	0,013	0,015	0,022	0,017	0,017	0,018	0,011	0,020	0,015	0,028	0,010	0,010	0,017	0,021	0,022	0,017	0,021	0,021	0,021	0,013	0,016	0,017	0,017	0,017	0,021
Cr	0,021	0,019	0,020	0,015	0,031	0,031	0,017	0,013	0,015	0,024	0,021	0,034	0,023	0,021	0,018	0,027	0,020	0,020	0,017	0,016	0,014	0,016	0,015	0,030	0,007	0,020	0,022	0,018	0,030	0,027	0,038	0,021	0,020
Ni	0,045	0,030	0,041	0,035	0,035	0,031	0,028	0,041	0,037	0,036	0,032	0,032	0,040	0,037	0,040	0,028	0,029	0,029	0,041	0,037	0,041	0,036	0,042	0,054	0,033	0,041	0,034	0,041	0,035	0,038	0,034	0,040	0,032
Ca	2,297	2,527	2,297	2,231	2,365	2,331	2,322	2,308	2,328	2,289	2,268	2,518	2,289	2,436	2,134	1,903	1,845	1,809	1,858	1,581	1,794	2,132	1,177	3,293	2,178	2,471	2,207	2,627	2,040	2,250	2,251	2,506	2,133
Na	1,539	1,718	1,325	1,588	1,557	1,478	1,419	1,558	1,433	1,414	1,471	1,413	1,415	1,383	1,660	1,786	1,622	1,950	1,736	1,999	1,811	1,943	1,628	2,511	1,910	1,854	2,018	1,966	2,240	1,731	1,854	1,861	1,651
K	0,108	0,057	0,090	0,113	0,088	0,036	0,082	0,067	0,077	0,069	0,084	0,073	0,072	0,088	0,066	0,098	0,113	0,091	0,099	0,023	0,084	0,160	0,345	0,125	0,121	0,118	0,212	0,149	0,205	0,195	0,213	0,160	0,113
Total	20,188	20,158	19,865	19,993	19,970	20,002	19,955	20,025	19,967	19,916	19,970	20,008	19,927	19,940	20,045	19,931	19,777	19,937	19,894	19,798	19,769	20,226	19,750	20,881	20,183	20,364	20,467	20,478	20,491	20,336	20,244	20,464	19,972

ATOMIC PER CENT

Na	39,02	39,93	35,70	40,39	38,83	37,47	37,12	39,61	37,34	37,49	38,48	35,29	37,47	35,40	43,01	47,16	45,31	50,65	47,01	55,48	49,09	45,88	51,68	42,35	45,38	41,73	45,48	41,46	49,94	41,45	44,06	41,11	42,37
Ca	58,24	58,74	61,88	56,74	58,98	59,85	60,74	58,68	60,66	60,68	59,33	62,89	60,62	62,35	55,28	50,25	51,54	46,99	50,31	43,88	48,63	45,34	37,37	55,54	45,75	55,62	49,74	55,40	45,48	53,88	53,26	55,36	54,73
K	2,74	1,32	2,42	2,87	2,19	2,69	2,14	1,70	2,01	1,83	2,20	1,82	1,91	2,25	1,71	2,59	3,16	2,36	2,68	0,64	2,28	3,78	10,95	2,11	2,87	4,78	3,14	4,57	4,67	2,69	3,53	2,90	

\* Depth in M5 + 124,2m = position of M5 sample in the sequence, based on depth of the main magnetite layer in M4.



## APPENDIX 4

## MICROPROBE ANALYSES OF ORTHOPYROXENES

NO: DEPTH:	BOREHOLES AND M4 COMBINED*														BOREHOLE END12											
	17 25,0	16 49,6	15 74,0	14 92,0	Bulk B14 92,0	12 130,5	11 139,0	10 146,0	9 149,2	8 5,2	5 190,0	3 263,2	2 268,2	1 306,2	Bulk B1 306,2	Bulk B32 160,0	B32 160,0	27 320,	26 352,0	25 387,0	24 400,5	22 551,0	Bulk B22 551,0	Bulk B21 557,8	20 591,3	18 667,5
SiO <sub>2</sub>	52,07	51,43	50,37	50,68	52,51	50,70	51,70	50,75	52,88	,00	51,20	51,67	51,09	52,49	52,72	49,49	49,07	50,89	50,23	48,24	48,95	50,62	50,94	51,19	53,60	50,42
Al <sub>2</sub> O <sub>3</sub>	0,99	0,94	0,69	0,90	0,77	0,60	0,94	1,02	0,86	,99	0,82	1,02	0,89	0,89	0,83	0,63	0,42	0,67	0,60	0,54	0,56	0,65	0,79	0,59	1,06	0,69
TiO <sub>2</sub>	0,26	0,29	0,34	0,38	0,24	0,33	0,41	0,27	0,21	,40	0,40	0,32	0,33	0,30	0,18	0,29	0,31	0,37	0,38	0,36	0,27	0,26	0,19	0,15	0,31	0,30
MgO	19,60	20,69	17,49	18,72	18,65	16,31	21,17	19,36	15,59	,67	20,28	19,63	17,63	20,32	19,27	11,82	12,71	14,20	14,31	13,12	12,78	15,08	14,36	15,44	15,35	16,31
FeO	24,12	23,71	27,62	26,01	24,64	29,05	23,95	25,48	27,79	,34	24,15	25,38	23,85	23,85	20,82	34,09	35,09	31,68	30,99	33,83	33,58	30,18	26,17	28,03	26,81	26,67
MnO	0,58	0,63	0,56	0,59	0,45	0,84	0,38	0,64	0,73	,66	0,64	0,39	0,51	0,34	0,38	0,95	0,73	0,81	0,68	0,83	0,55	0,84	0,50	0,55	0,58	1,12
Cr <sub>2</sub> O <sub>3</sub>	0,07	0,11	0,17	0,14	0,00	0,20	0,15	0,14	0,16	,13	0,18	0,24	0,09	0,07	0,00	0,17	0,00	0,13	0,09	0,10	0,15	0,11	0,01	0,01	0,14	0,00
NiO	0,20	0,19	0,23	0,34	n.d.	0,23	0,28	0,29	0,29	,32	0,24	0,22	0,26	0,30	n.d.	0,28	n.d.	0,20	0,24	0,25	0,27	0,24	n.d.	n.d.	0,35	1,97
CaO	1,06	1,46	1,21	1,31	3,71	1,48	1,01	0,84	0,73	,98	1,36	0,94	2,92	0,76	n.d.	1,26	n.d.	0,20	1,11	1,32	1,49	1,18	6,36	3,91	1,35	1,80
Na <sub>2</sub> O	0,09	0,10	0,10	0,09	0,05	0,08	0,00	0,10	0,11	,11	0,06	0,05	0,09	0,10	0,03	0,12	0,00	0,18	0,07	0,10	0,10	0,09	0,02	0,01	0,10	0,14
K <sub>2</sub> O	0,05	0,05	0,06	0,05	0,01	0,08	0,00	0,07	0,05	,05	0,05	0,05	0,06	0,06	0,02	0,07	0,02	0,03	0,07	0,09	0,08	0,06	0,09	0,01	0,07	0,07
Total	99,09	99,60	98,84	99,21	101,03	99,90	99,99	98,96	99,40	,65	99,38	99,13	99,25	99,48	99,55	99,17	99,36	100,27	98,77	98,78	98,78	99,31	99,43	99,89	99,72	99,49

## STRUCTURAL FORMULAE ON THE BASIS OF 6 OXYGEN ATOMS

Si	1,981	1,951	1,964	1,954	1,975	1,970	1,949	1,954	2,034	949	1,953	1,973	1,968	1,983	1,984	1,987	1,969	1,989	1,989	1,950	1,970	1,986	1,982	1,976	2,043	1,961
Al	0,045	0,042	0,032	0,041	0,034	0,028	0,042	0,046	0,039	044	0,037	0,046	0,040	0,040	0,041	0,030	0,020	0,031	0,028	0,026	0,027	0,030	0,036	0,027	0,048	0,044
Ti	0,007	0,008	0,010	0,011	0,007	0,010	0,012	0,008	0,006	011	0,012	0,009	0,010	0,009	0,005	0,009	0,009	0,011	0,011	0,011	0,008	0,008	0,006	0,005	0,009	0,009
Mg	1,112	1,170	1,016	1,075	1,045	0,945	1,189	1,111	0,894	121	1,153	1,084	1,012	1,145	1,079	0,708	0,700	0,827	0,845	0,791	0,767	0,882	0,833	0,900	0,872	0,946
Fe	0,768	0,752	0,900	0,839	0,775	0,944	0,755	0,820	0,894	810	0,770	0,810	0,818	0,754	0,647	1,145	1,177	1,035	1,026	1,144	1,131	0,990	0,851	0,916	0,855	0,868
Mn	0,019	0,020	0,018	0,019	0,014	0,027	0,012	0,021	0,024	021	0,021	0,013	0,017	0,011	0,012	0,032	0,025	0,027	0,023	0,029	0,019	0,028	0,017	0,018	0,019	0,037
Cr	0,002	0,003	0,005	0,004	0,000	0,006	0,004	0,004	0,005	004	0,005	0,007	0,003	0,003	0,002	0,005	0,000	0,004	0,003	0,003	0,005	0,003	0,000	0,001	0,004	0,000
Ni	0,006	0,006	0,007	0,010	n.d.	0,007	0,009	0,009	0,009	010	0,007	0,007	0,008	0,009	n.d.	0,009	n.d.	0,006	0,008	0,008	0,009	0,008	n.d.	n.d.	0,011	0,062
Ca	0,043	0,059	0,051	0,054	0,150	0,062	0,041	0,035	0,030	040	0,052	0,038	0,121	0,031	0,220	0,054	0,043	0,047	0,047	0,057	0,064	0,049	0,265	0,164	0,055	0,075
Na	0,007	0,007	0,008	0,007	0,004	0,006	0,006	0,007	0,008	008	0,004	0,004	0,007	0,007	0,003	0,009	0,000	0,013	0,006	0,008	0,008	0,007	0,001	0,004	0,007	0,011
K	0,002	0,002	0,003	0,003	0,001	0,004	0,003	0,004	0,002	003	0,003	0,002	0,003	0,003	0,001	0,003	0,001	0,002	0,004	0,005	0,004	0,003	0,005	0,000	0,004	0,003
Total	3,992	4,020	4,014	4,017	4,005	4,009	4,022	4,019	3,945	021	4,017	3,993	4,007	4,345	3,992	3,991	4,004	3,992	3,990	4,032	4,012	3,994	3,998	4,011	3,927	4,016

## ATOMIC PER CENT

Mg	57,26	58,47	51,18	54,10	52,67	47,78	59,54	55,91	48,53	,27	57,77	55,73	51,42	58,99	55,11	36,51	35,99	42,72	43,53	39,14	38,72	45,25	42,37	45,03	48,42	49,12
Fe**	40,52	38,58	46,25	43,18	39,77	49,09	38,41	42,33	49,84	,72	39,63	42,31	42,43	39,41	33,66	60,70	61,80	54,86	54,04	58,04	58,05	52,23	44,15	46,77	48,53	46,99
Ca	2,21	2,95	2,57	2,72	7,56	3,13	2,05	1,76	1,63	,01	2,61	1,95	6,15	1,60	11,24	2,78	2,21	2,43	2,42	2,82	3,23	2,51	13,48	8,20	3,05	3,89

\* Depth in M5 + 124,2m = depth of M5 sample in the sequence, based on a depth of the main magnetite layer in M4.

\*\* Fe + Mn

APPENDIX 5

MICROPROBE ANALYSES OF CLINOPYROXENES

		BOREHOLES M5 AND M4, COMBINED*														BOREHOLE END12																				
NO:	**	17	17	16	14	Bulk	**	11	7	6	5	4	3	**	2	1	***	1	B1	34	33	32	Bulk	Bulk	30	29	28	27	26	Bulk	Bulk	23	22	B22	B21	20
DEPTH:		25,0	25,0	49,6	92,0	92,0	116,2	139,0	164,2	173,2	190,0	2	263,2	268,2	306,2	306,2	306,2	141,7	152,4	160,0	160,6	184,4	228,6	249,9	260,6	320,0	352,0	387,	400,5	512,0	551,0	551,0	557,8	630,0		
SiO <sub>2</sub>	51,23	49,81	50,89	50,47	51,68	50,29	50,12	49,76	49,12	50,97	19	50,83	50,51	51,49	51,95	51,92	50,37	49,48	50,45	50,62	48,62	52,67	49,73	53,23	52,92	50,62	52,83	51,56	48,37	51,88	50,67	50,50	50,00			
Al <sub>2</sub> O <sub>3</sub>	1,66	1,95	1,50	1,86	1,89	1,71	2,20	1,51	2,19	2,04	0,08	2,33	1,56	2,06	1,64	1,60	1,03	1,79	1,25	1,13	1,32	1,75	1,56	1,57	1,37	2,57	1,28	1,60	1,13	1,21	1,38	1,44	0,98			
TiO <sub>2</sub>	0,47	0,63	0,46	0,76	0,58	0,59	0,72	0,43	0,84	0,66	0,72	0,71	0,47	0,61	0,39	0,37	0,35	0,57	0,42	0,22	0,47	0,40	0,65	0,61	0,44	0,46	0,50	0,82	0,39	0,42	0,27	0,35	0,43			
MgO	12,82	13,11	12,69	12,41	12,98	13,51	12,74	10,78	12,68	12,67	46	12,27	12,54	13,72	13,85	14,04	9,11	9,22	9,55	9,58	8,97	9,52	9,36	9,92	11,78	9,15	9,33	10,61	11,00	11,19	11,04	11,80	11,92			
FeO	9,98	10,78	10,83	11,56	12,01	10,51	10,39	14,13	12,15	10,11	65	11,28	11,51	11,14	10,34	10,81	16,36	16,21	17,01	17,75	22,24	15,64	16,75	16,23	19,77	14,97	15,28	14,69	17,94	14,69	15,54	15,58	16,32			
MnO	0,42	0,38	0,24	0,29	0,27	0,36	0,38	0,60	0,42	0,35	26	11,28	11,51	11,14	10,34	10,81	0,71	0,33	0,59	0,42	0,52	0,43	0,59	0,51	0,41	0,45	0,52	0,51	0,66	0,41	0,34	0,35	0,36			
Cr <sub>2</sub> O <sub>3</sub>	0,14	0,18	0,11	0,17	0,00	0,12	0,16	0,14	0,21	0,26	17	0,37	0,76	0,36	0,28	0,25	0,16	0,12	0,20	0,01	0,01	0,08	0,11	0,11	0,13	0,13	0,18	0,20	0,34	0,29	0,28	n.d.	0,30			
NiO	0,23	0,33	0,17	0,29	n.d.	0,29	0,30	0,29	0,31	0,25	34	0,17	0,15	0,18	0,02	0,00	0,21	0,38	0,23	n.d.	n.d.	0,26	0,26	0,29	0,27	0,18	0,20	0,34	0,29	0,28	n.d.	0,30				
CaO	21,90	20,97	21,34	21,55	20,30	21,18	21,66	20,33	21,97	21,00	18	21,23	20,81	20,01	21,50	20,32	20,40	20,68	19,72	19,60	17,34	19,44	19,27	15,88	12,35	20,46	20,42	19,10	19,40	19,27	19,93	18,90	18,83			
Na <sub>2</sub> O	0,32	0,25	0,30	0,31	0,22	0,33	0,30	0,28	0,32	0,30	30	0,28	0,08	0,30	0,29	0,18	0,20	0,22	0,25	0,14	0,11	0,24	0,28	0,29	0,22	0,24	0,32	0,34	0,31	0,24	0,13	0,12	0,19			
K <sub>2</sub> O	0,06	0,07	0,05	0,06	0,03	0,05	0,05	0,06	0,04	0,07	0,06	0,05	0,03	0,07	n.d.	0,01	0,07	0,07	0,08	0,02	0,01	0,06	0,08	0,08	0,05	0,07	0,06	0,08	0,06	0,06	0,02	0,00	0,07			
Total	99,23	98,46	98,58	99,73	99,96	98,94	99,02	98,51	100,25	98,68	141	99,72	100,24	100,28	99,50	98,97	99,07	99,75	99,49	99,61	100,49	98,64	98,69	99,71	99,30	100,86	99,80	99,76	99,79	99,33	99,06	98,84				

STRUCTURAL FORMULAE ON THE BASIS OF 6 OXYGEN ATOMS																																				
	Si	Al	Ti	Mg	Fe	Mn	Cr	Ni	Ca	Na	K	Total	Si	Al	Ti	Mg	Fe	Mn	Cr	Ni	Ca	Na	K	Total	Si	Al	Ti	Mg	Fe	Mn	Cr	Ni	Ca	Na	K	Total
Si	1,944	1,914	1,948	1,921	1,948	1,920	1,913	1,940	1,875	1,941	32	1,927	1,938	1,933	1,945	1,955	1,970	1,935	1,959	1,970	1,918	1,999	1,951	2,039	2,020	1,953	2,002	1,971	1,898	1,981	1,956	1,941	1,95			
Al	0,074	0,088	0,068	0,084	0,084	0,077	0,099	0,069	0,098	0,092	93	0,104	0,071	0,091	0,072	0,071	0,048	0,082	0,057	0,052	0,062	0,078	0,072	0,071	0,062	0,117	0,057	0,072	0,052	0,054	0,063	0,066	0,05			
Ti	0,013	0,018	0,013	0,022	0,016	0,017	0,021	0,013	0,024	0,019	21	0,020	0,011	0,017	0,011	0,011	0,010	0,017	0,012	0,007	0,014	0,011	0,019	0,013	0,013	0,013	0,014	0,017	0,012	0,011	0,008	0,011	0,01			
Mg	0,725	0,751	0,724	0,704	0,730	0,759	0,725	0,726	0,722	0,719	01	0,693	0,717	0,768	0,773	0,788	0,531	0,538	0,553	0,556	0,534	0,539	0,547	0,566	0,670	0,526	0,527	0,604	0,644	0,637	0,646	0,695	0,64			
Fe	0,317	0,347	0,347	0,368	0,379	0,335	0,332	0,461	0,388	0,322	99	0,358	0,371	0,768	0,773	0,788	0,531	0,538	0,553	0,556	0,534	0,539	0,547	0,566	0,670	0,526	0,527	0,604	0,644	0,637	0,646	0,695	0,64			
Mn	0,014	0,012	0,008	0,009	0,009	0,012	0,012	0,020	0,013	0,011	08	0,012	0,025	0,011	0,009	0,998	0,024	0,011	0,019	0,014	0,018	0,014	0,020	0,017	0,013	0,015	0,017	0,017	0,013	0,011	0,011	0,011	0,01			
Cr	0,004	0,005	0,005	0,005	0,000	0,004	0,005	0,004	0,006	0,008	05	0,005	0,005	0,001	0,001	0,000	0,005	0,004	0,006	0,000	n.d.	0,008	0,003	0,003	0,003	0,004	0,004	0,004	0,006	0,004	0,000	0,001	0,00			
Ni	0,007	0,010	0,005	0,009	n.d.	0,009	0,009	0,009	0,009	0,007	10	0,006	0,010	0,009	0,001	0,820	0,005	0,004	0,006	0,000	n.d.	0,008	0,008	0,009	0,008	0,008	0,005	0,006	0,009	0,009	n.d.	n.d.	0,79			
Ca	0,891	0,863	0,875	0,879	0,821	0,866	0,886	0,857	0,899	0,857	16	0,862	0,856	0,805	0,862	0,820	0,855	0,867	0,820	0,817	0,743	0,791	0,810	0,810	0,810	0,846	0,829	0,782	0,816	0,778	0,824	0,789	0,01			
Na	0,024	0,019	0,022	0,023	0,016	0,025	0,022	0,021	0,023	0,024	22	0,021	0,006	0,022	0,021	0,013	0,016	0,017	0,019	0,010	0,009	0,017	0,021	0,021	0,016	0,018	0,023	0,026	0,024	0,018	0,010	0,009	0,00			
K	0,003	0,004	0,003	0,003	0,001	0,002	0,003	0,003	0,002	0,003	03	0,003	0,003	0,003	0,003	0,001	0,004	0,003	0,004	0,008	0,000	0,003	0,004	0,004	0,004	0,002	0,003	0,003	0,003	0,003	0,001	0,000	0,00			
Total	4,016	4,031	4,016	4,027	4,004	4,036	4,027	4,023	4,059	4,003	10	4,011	4,016	4,014	4,019	4,006	4,004	4,016	4,008	4,012	4,041	3,958	4,004	3,917	3,944	3,983	3,966	3,983	4,074	3,988	4,021	4,030	4,00			

ATOMIC PER CENT																																				
	Mg	Fe****	Ca	Mg	Fe****	Ca	Mg	Fe****	Ca	Mg	Fe****	Ca	Mg	Fe****	Ca	Mg	Fe****	Ca	Mg	Fe****	Ca	Mg	Fe****	Ca	Mg	Fe****	Ca	Mg	Fe****	Ca	Mg	Fe****	Ca	Mg	Fe****	Ca
Mg	37,24	38,06	37,05	35,92	37,65	38,80	37,08	31,87	35,71	37,66	43	36,00	36,41	39,71	39,28	40,45	27,30	27,65	28,45	28,30	26,22	29,29	28,40	32,25	36,83	28,13	28,38	32,26	31,10	33,40	32,58	34,38	30,92			
Fe****	17,00	18,20	18,17	19,23	19,55	17,51	17,60	24,49	19,83	17,44	15	19,22	20,11	18,67	16,92	17,86	28,74	27,80	29,37	30,13	37,35	27,72	29,54	30,60	35,40	26,63	26,97	25,96	29,50	25,28	25,87	26,03	26,57			
Ca	45,76	43,74	44,78	44,85	42,34	43,69	45,32	43,64	44,46	44,89	41	44,78	43,47	41,62	43,80	42,09	43,96	44,55	42,18	41,58	36,44	42,99	42,06	37,15	27,76	45,24	44,64	41,77	39,40	41,32	41,55	39,59	38,16			

\* Depth of M5 + 124.2m = position of M5 sample in sequence, based on depth main magnetite layer in M4.  
 \*\* Analyses of clinopyroxene lamellae in inverted pigeonite.  
 \*\*\* Analyses obtained at Rhodes University.  
 \*\*\*\* Fe + Mn

## MICROPROBE ANALYSES OF OLIVINES

BOREHOLE M5*			BOREHOLE END12																	
DEPTH:	****		33,5	70,1	125,4	160,0	Bulk 160,0	190,5	228,6	260,6	300,2	352,0	387,0	429,5	460,2	472,4	512,0	521,2	598,9	667,5
SiO <sub>2</sub>	37,15	35,05	30,71	31,00	31,06	32,81	32,15	31,98	31,73	31,45	31,55	31,60	30,59	30,29	31,62	32,34	33,05	30,83	33,81	33,06
Al <sub>2</sub> O <sub>3</sub>	0,23	0,17	0,23	0,37	0,33	0,26	0,03	0,34	0,29	0,34	0,35	0,35	0,29	0,29	0,29	0,27	0,24	0,40	0,22	0,26
TiO <sub>2</sub>	0,15	0,20	0,19	0,19	0,16	0,21	0,00	0,15	0,13	0,27	0,16	0,15	0,16	0,15	0,15	0,18	0,18	0,15	0,16	0,21
MgO	29,94	25,53	6,37	7,63	8,39	9,95	9,17	11,54	11,01	11,57	10,69	10,09	11,62	13,68	15,08	16,06	15,64	15,81	17,22	17,26
FeO	31,71	37,45	59,81	57,57	57,58	54,19	57,77	54,48	53,95	54,24	55,04	56,12	54,01	52,61	51,21	49,42	49,44	50,04	46,87	47,66
MnO	0,49	0,56	1,17	1,03	0,82	1,09	0,90	0,95	1,04	1,23	0,96	0,86	0,89	0,86	0,85	0,53	0,91	0,92	0,88	0,86
Cr <sub>2</sub> O <sub>3</sub>	0,11	0,20	0,16	0,09	0,12	0,21	0,00	0,12	0,18	0,13	0,18	0,15	0,18	0,14	0,15	0,12	0,27	0,16	0,14	0,26
NiO	0,36	0,29	0,25	0,29	0,43	0,25	n.d.	0,33	0,28	0,39	0,30	0,33	0,46	0,28	0,32	0,27	0,30	0,35	0,26	0,26
CaO	0,08	0,12	0,16	0,19	0,12	0,13	0,02	0,32	0,10	0,13	0,16	0,17	0,12	0,12	0,18	0,19	0,26	0,23	0,18	0,13
Na <sub>2</sub> O	0,09	0,09	0,09	0,17	0,13	0,14	0,00	0,18	0,18	0,18	0,19	0,17	0,19	0,16	0,13	0,15	0,12	0,15	0,08	0,08
K <sub>2</sub> O	0,05	0,06	0,09	0,06	0,06	0,08	0,02	0,07	0,07	0,07	0,06	0,08	0,08	0,06	0,09	0,10	0,09	0,07	0,08	0,09
Total	100,36	99,72	99,23	98,59	99,20	99,32	100,06	100,46	98,96	100,00	99,64	100,07	98,59	98,65	100,07	99,63	100,50	99,11	99,90	100,13

## STRUCTURAL FORMULAE ON THE BASIS OF 4 OXYGEN ATOMS

Si	1,010	0,992	0,996	0,999	0,993	1,023	1,012	0,989	0,996	0,980	0,989	0,991	0,970	0,953	0,967	0,981	0,992	0,951	1,005	0,987
Al	0,007	0,006	0,009	0,014	0,012	0,010	0,001	0,012	0,011	0,013	0,013	0,013	0,011	0,011	0,010	0,010	0,009	0,014	0,008	0,009
Ti	0,003	0,004	0,005	0,005	0,004	0,005	0,000	0,004	0,003	0,006	0,004	0,003	0,004	0,004	0,003	0,004	0,004	0,003	0,004	0,005
Mg	1,213	1,078	0,308	0,367	0,400	0,463	0,430	0,532	0,515	0,537	0,500	0,472	0,549	0,641	0,687	0,726	0,700	0,727	0,763	0,768
Fe	0,721	0,887	1,623	1,552	1,540	1,414	1,520	1,409	1,417	1,413	1,443	1,472	1,432	1,384	1,310	1,253	1,241	1,291	1,165	1,190
Mn	0,011	0,013	0,032	0,028	0,022	0,029	0,024	0,025	0,028	0,032	0,025	0,023	0,024	0,023	0,022	0,014	0,023	0,024	0,022	0,022
Cr	0,002	0,005	0,004	0,002	0,003	0,005	0,000	0,003	0,005	0,003	0,004	0,004	0,004	0,003	0,004	0,003	0,006	0,004	0,003	0,006
Ni	0,008	0,007	0,007	0,007	0,011	0,006	n.d.	0,008	0,007	0,010	0,008	0,008	0,012	0,007	0,008	0,007	0,007	0,009	0,006	0,006
Ca	0,002	0,004	0,005	0,007	0,004	0,004	0,001	0,011	0,003	0,004	0,005	0,006	0,004	0,004	0,006	0,006	0,008	0,008	0,006	0,004
Na	0,005	0,005	0,006	0,010	0,008	0,008	0,000	0,011	0,011	0,011	0,012	0,010	0,012	0,010	0,008	0,009	0,007	0,009	0,005	0,005
K	0,002	0,002	0,004	0,003	0,002	0,003	0,001	0,003	0,003	0,003	0,002	0,003	0,003	0,002	0,003	0,004	0,003	0,003	0,003	0,003
Total	2,984	3,003	2,999	2,994	2,999	2,970	2,989	3,007	2,999	3,012	3,005	3,005	3,025	3,042	3,028	3,017	3,000	3,043	2,990	3,005

## ATOMIC PER CENT

Mg	62,72	54,86	15,95	19,12	20,62	24,67	22,05	27,4	26,66	27,54	25,73	24,28	27,71	31,65	34,40	36,69	36,06	36,03	39,57	39,22
Fe**	37,28	45,14	84,05	80,88	79,38	75,33	77,95	72,6	73,34	72,46	74,27	75,72	72,29	68,35	65,60	63,31	63,94	63,97	60,43	60,78

\* Depth of M5 + 124,2m = position of M5 sample in sequence, based on depth of main magnetite layer in M4.

\*\* Fe + Mn

\*\*\*\* Olivine formed by reaction between ore and inverted pigeonite.

## APPENDIX 7

## CALCULATIONS USED TO OBTAIN PLOTTED MINERAL COMPOSITIONS

PLOTTED VALUE FIG. or APX.		CALCULATION*
An	Fig. 32	$100\text{Ca}/(\text{Ca}+\text{Na})$
Fs	Fig. 32	$100(\text{Fe}+\text{Mn})/(\text{Fe}+\text{Mn}+\text{Mg})$
Fa	Fig. 32	$100(\text{Fe}+\text{Mn})/(\text{Fe}+\text{Mn}+\text{Mg})$
Fe	Fig. 33, 34; Apx. 4, 5	$100(\text{Fe}+\text{Mn})/(\text{Fe}+\text{Mn}+\text{Mg}+\text{Ca})$
Mg	Fig. 33	$100\text{Mg}/(\text{Fe}+\text{Mn}+\text{Mg}+\text{Ca})$
Ca	Fig. 33	$100\text{Ca}/(\text{Fe}+\text{Mn}+\text{Mg}+\text{Ca})$
Na	Apx. 3	$100\text{Na}/(\text{Na}+\text{Ca}+\text{K})$
Ca	Apx. 3	$100\text{Ca}/(\text{Na}+\text{Ca}+\text{K})$
K	Apx. 3	$100\text{Ca}/(\text{Na}+\text{Ca}+\text{K})$
Fe	Apx. 6	$100(\text{Fe}+)/(\text{Fe}+\text{Mg})$
Mg	Apx. 6	$100\text{Mg}/(\text{Fe}+\text{Mg})$

\* All values from structural formulae.

## APPENDIX 8

## COMPARATIVE NOMENCLATURE

## BOREHOLE M5

DEPTH	DESCRIPTION	CUMULATE
25,0	Mgt anorthosite	pC
26,0	Mgt anorthosite	p(m)C
26,6	Mgt anorthosite	p(m)C
27,0	Magnetitite	mC
31,0	Mgt anorthosite	pC
32,5	Mgt anorthosite	pC
33,7	Mgt anorthosite	pC
34,6	Mgt anorthosite	
35,3	Mgt anorthosite	pmC
35,7	Mgt anorthosite	pmC
36,0	Mgt anorthosite	p(m)C
36,5	Mgt anorthosite	pmC
37,7	Mgt leuconorite	pmC
38,9	Mgt anorthosite	pmC
39,0	Mgt anorthosite	pmC
39,7	Mgt anorthosite	pC
39,9	Anorthosite	pC
40,0	Anorthosite	pC
42,4	Leuconorite	
47,0	Leuconorite	piC
52,0	Leuconorite	piC
56,0	Leucogabbronorite	piC
56,5	Magnetitite	mC
57,9	Anorthosite	pC
58,4	Anorthosite	piC
60,0	Anorthosite	pC
60,4	Gabbronorite	piC
64,7	Leuconorite	piC
65,8	Gabbronorite	piC
66,5	Leucogabbro	piC
68,2	Anorthosite	piC

72,0	Anorthosite	pC
72,5	Mgt anorthosite	pmC
83,0	Norite	piC
89,0	Leucogabbronorite	piC
93,4	Leucogabbronorite	piC
96,0	Leucogabbronorite	piC
106,0	Anorthosite	piC
111,0	Leuconorite	pC
120,6	Mgt anorthosite	pC
125,0	Leucogabbro	pmC
129,9	Mgt anorthosite	pmC
135,5	Mgt anorthosite	pmC
139,0	Mgt leuconorite	pmoC
144,4	Anorthosite	pmC
148,7	Anorthosite	pC
154,0	Mgt anorthosite	pmC
159,8	Anorthosite	pC
163,0	Mgt leucogabbro	pcC
165,1	Leucogabbronorite	pimC
170,1	Mgt leucogabbronorite	pciC
182,0	Mgt gabbronorite	pimcC

## BOREHOLE M4

DEPTH	DESCRIPTION	CUMULUS
25,0	Mgt norite	pmiC
26,2	Mgt leucogabbronorite	picC
29,1	Mgt leucogabbronorite	pmicC
34,5	Mgt anorthosite	pmC
39,1	Mgt gabbronorite	pcmiC
46,9	Mgt leucogabbronorite	p(m)ciC
57,0	Mgt leucogabbro	pcmiC
64,1	Mgt leucogabbro	pmC
66,3	Anorthositic mgtt	pmC
69,0	Mgt leucogabbro	pmC
74,0	Mgt anorthosite	pmC
77,0	Melagabbronorite	ciC
85,0	Mgt leucogabbro	pC
86,1	Leuconorite	pimC
88,9	Melagabbronorite	ci(p)C
92,0	Mgt leucogabbronorite	pciC
99,4	Mgt melagabbronorite	cipC
108,6	Mgt leucogabbronorite	picC
116,2	Mgt norite	piC
121,2	Mgt anorthosite	p(m)C
125,5	Mgt anorthosite	p(m)C
125,6	Mgt anorthosite	pC
130,5	Mgt anorthosite	pC
139,0	Mgt anorthosite	pmC
145,8	Mgt anorthosite	pmC
154,3	Mgt anorthosite	pmC
158,0	Anorthositic mgtt	mC
164,0	Anorthosite	pC
168,4	Anorthositic mgtt	mpC
172,3	Leucogabbronorite	piC
181,0	Leucogabbronorite	piC

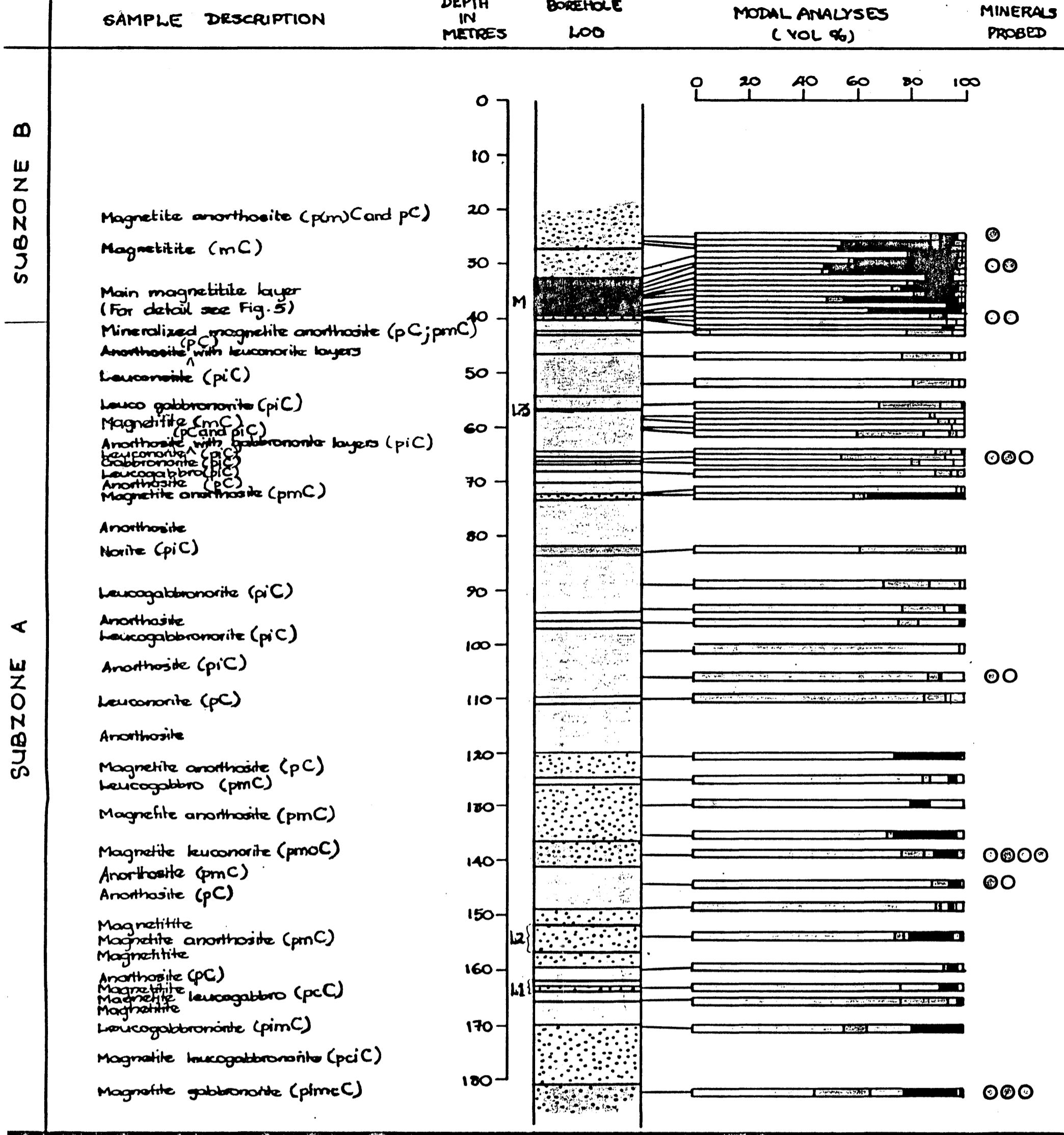
## BOREHOLE END12

DEPTH	DESCRIPTION	CUMULUS
33,5	Mgt leucotroctolite	poaC
35,1	Mgt leucotroctolite	poaC
41,1	Mgt leucotroctolite	poaC
47,2	Mgt troctolite	pomaC
53,3	Mgt troctolite	pomaC
57,9	Mgt troctolite	pomaC
65,5	Mgt troctolite	pomaC
70,1	Mgt leucotroctolite	pomaC
71,6	Mgt troctolite	po(m)aC
141,7	Olivine gabbro	opaC
142,6	Anorthositic mgtt	mpC
144,8	Mgt leucotroctolite	pomC
149,3	Leucogabbro	pC
152,4	Mgt ol leucogabbro	pmC
163,0	Pl-bearing mgt dunite	omaC
172,2	Mgt olivine leucogabbro	po(m)aC
173,7	Mgt olivine leucogabbro	p(o)maC
179,8	Mgt leucotroctolite	pmaC
184,4	Mgt olivine melagabbro	o(m)caC
188,4	Magnetitite	
190,5	Mgt dunite	omaC
195,0	Mgt troctolite	o(p)maC
196,6	Mgt melatroctolite	om(p)a
202,7	Pl-bearing mgt dunite	omapC
204,2	Mgt troctolite	(m)poaC
207,2	Mgt leucotroctolite	pomacC
217,9	Mgt troctolite	pomaC
228,6	Mgt olivine gabbro	pomacC
234,7	Mgt troctolite	pomaC
239,2	Mgt olivine gnorite	pocmaC
249,9	Mgt olivine gabbro	pomacC
260,6	Mgt troctolite	pomC
266,7	Mgt anorthosite	pmaoC
274,3	Mgt melatroctolite	o(m)aC
275,8	Mgt troctolite	omaC



289,5	Mgt olivine gabbro	pomaC
297,1	Mgt olivine gabbro	paomcC
300,2	Mgt olivine leucogabbro	poamcC
310,8	Mgt olivine gabbro	pomacC
313,9	Mgt olivine gabbro	pomaC
320,0	Olivine gabbro	p(o)aC
332,5	Leucotroctolite	poamC
341,4	Mgt olivine leucogabbro	pomC
344,4	Mgt leucotroctolite	pomC
350,5	Mgt leucotroctolite	pmcC
352,0	Mgt leucogabbro	p(m)oaC
359,7	Mgt troctolite	o(p)maC
361,2	Mgt leucotroctolite	pC
365,8	Mgt olivine gabbro	pcaC
376,4	L.troct mgtt	mpC
381,0	Olivine leucogabbro	po(m)C
384,1	Leucotroctolite	poC
387,0	Leucotroctolite	p(o)C
396,2	Mgt leucotroctolite	poC
400,5	Melagabbro	cpC
412,1	Mgt leucotroctolite	pomC
422,1	Mgt leucotroctolite	p(m)C
429,4	Mgt leucotroctolite	p(m)C
430,0	Mgt troctolite	po(m)C
448,0	Mgt olivine leucogabbro	pmocC
460,2	Mgt leucotroctolite	p(m)oC
466,3	Mgt dunite	omaC
472,4	Mgt melatroctolite	omaC
483,1	Mgt olivine leucogabbro	pomcaC
493,7	Dunitic mgtt	moaC
502,9	Mgt dunite	moaC
512,0	Mgt olivine gabbro	opmacC
518,1	Mgt mela olivine gabbro	opcmaC
521,2	Pl-bearing mgt lherzolite	omacC
536,4	Leucotroctolite	p(o)C
539,4	Mgt leucotroctolite	p(o)C
545,6	Leucotroctolite	p(o)mC
545,7	L.troctolitic mgtt	mpoC
551,4	Melanoritic mgtt	mC
551,6	Mgt leuconorite	piC

551,9	Olivine gabbronoritic mgtt	mC
552,0	Mgt troctolite	pomC
557,8	Mgt melagabbrono	ipmcC
564,5	Mgt leucotroctolite	pmC
566,8	Olivine l.gnoritic mgtt	mC
574,5	Magnetitite	mC
576,0	M.troctolitic mgtt	moC
579,1	Mgt melatroctolite	moC
580,6	Mgt olivine leucogabbronorite	pmoC
582,1	Mgt olivine melagabbronorite	moc(p)C
585,5	Mgt anorthosite	pC
591,3	Mgt olivine leucogabbronorite	pC
595,9	Mgt melatroctolite	om(p)C
598,9	Mgt troctolite	pomC
601,9	Mgt anorthosite	pC
609,6	Anorthosite	pC
617,2	Mgt anorthosite	pC
624,2	Mgt arorthosite	p(m)C
629,1	Mgt anorthosite	pC
630,0	Anorthosite	pC
638,5	Mgt olivine leuconorite	pmiC
646,1	Mgt olivine leucogabbronorite	p(o)m(i)C
656,8	Mgt olivine leucogabbronorite	pc(m)C
666,0	Mgt olivine leucogabbronorite	pcm(oi)C
667,5	Mgt olivine leucogabbronorite	pc(mo)iC

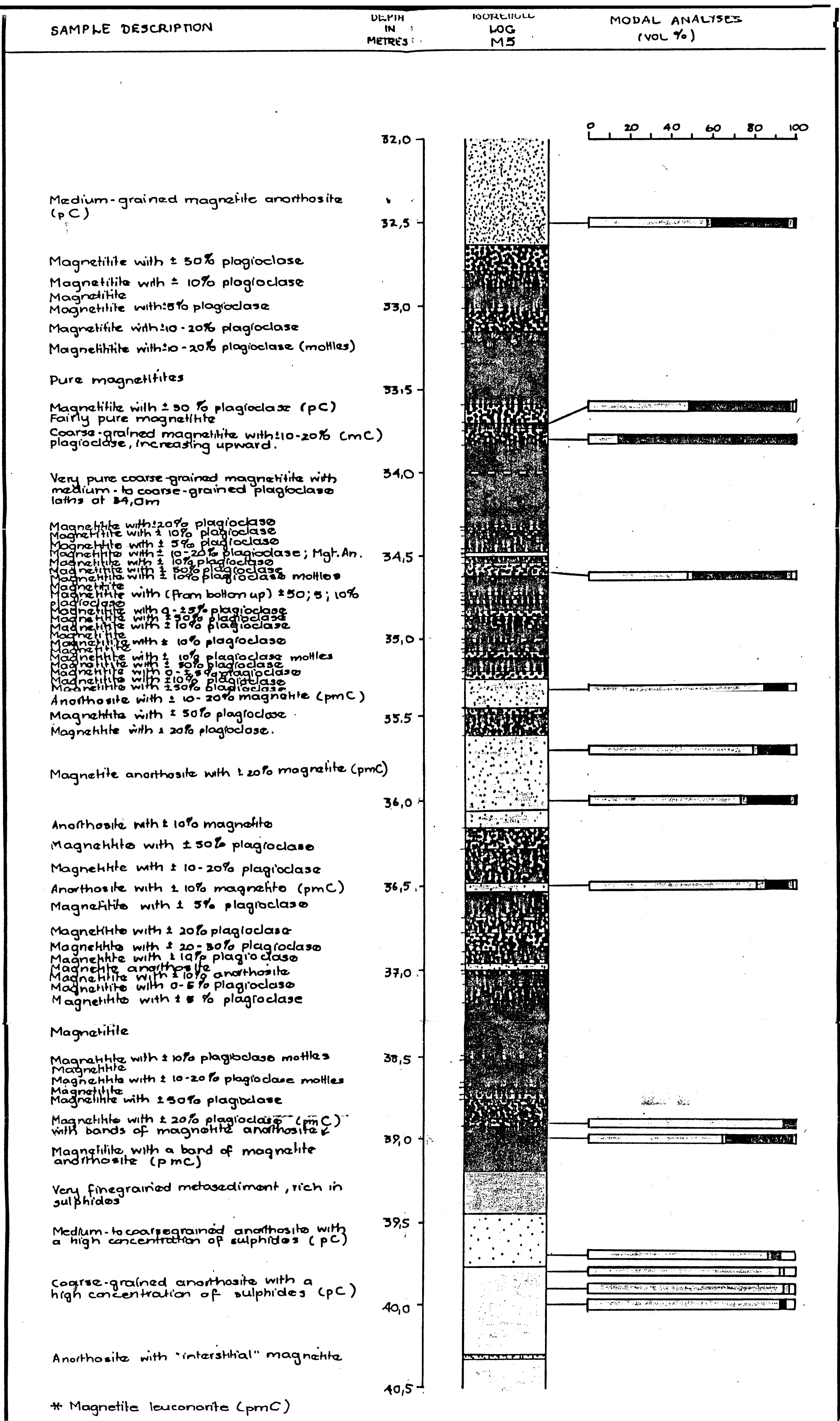


LEGEND

ROCK TYPES	VOL % MINERALS	MINERALS PROBED
Anorthosite	Plagioclase	○
Gabbro	Orthopyroxene	⊙
Gabbro norite	Clinopyroxene	○
Norite	Olivine	○
Magnetite	Ore	
	Symplectite	
	Other minerals	

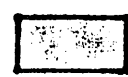
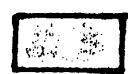

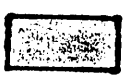
In all cases lighter colouring represents leuco-varieties, and magnetite in excess of 5%

Fig. 1. Detailed borehole log for M5, with modal analyses and sample-points for microprobe analyses.

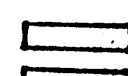
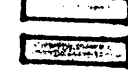
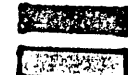
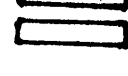




LEGEND

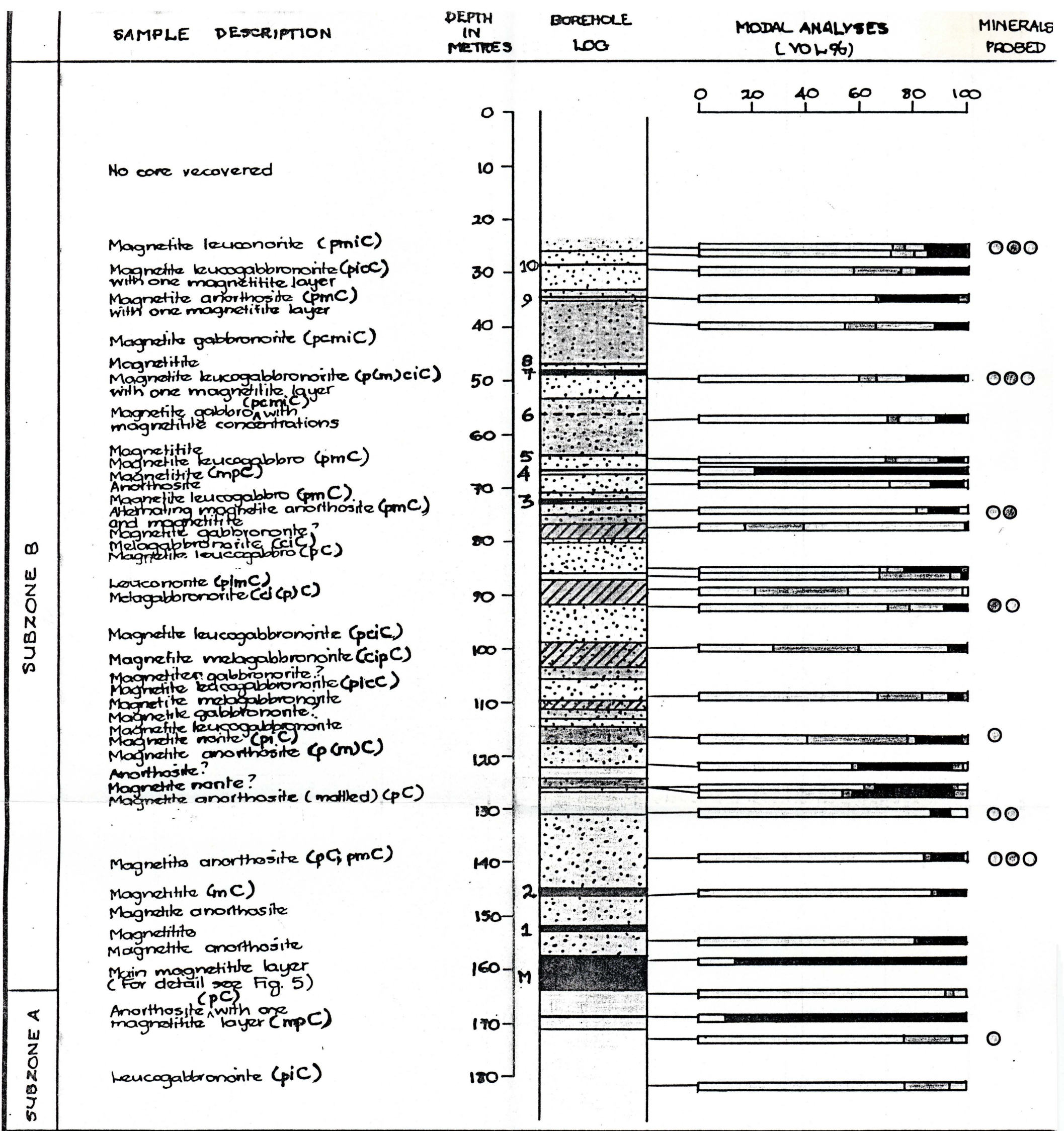
ROCKTYPES

-  Anorthosite
-  Leuconorite
-  Magnetitite
-  Metasediment

VOLUME PER CENT MINERALS

-  Plagioclase
-  Clinopyroxene
-  Orthopyroxene
-  Magnetite
-  Symplectite
-  Other minerals

Folder 2 Detailed log of the main magnetitite layer on Commanodrift, compiled from borehole logs of M5 and M4 (using depths in M5).

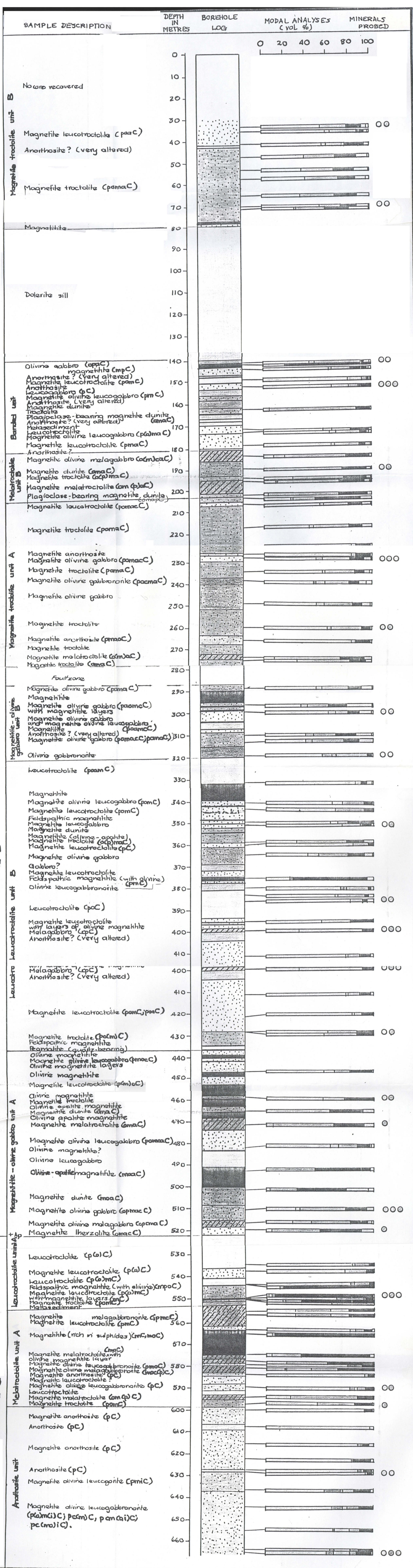


**LEGEND**

- | ROCKTYPES |              | VOL. % MINERALS |                | MINERALS PROBED |   |
|-----------|--------------|-----------------|----------------|-----------------|---|
|           | Anorthosite  |                 | Plagioclase    |                 | ○ |
|           | Gabbro       |                 | Orthopyroxene  |                 | ○ |
|           | Gabbronorite |                 | Clinopyroxene  |                 | ○ |
|           | Norite       |                 | Ore            |                 |   |
|           | Magnetite    |                 | Symplectite    |                 |   |
|           |              |                 | Other minerals |                 |   |

In all cases lighter colouring represents leuco-varieties; /// mela-; :::: magnetite in excess of 5%

Folder 3 Detailed borehole log for M4, with modal analyses and sample-points for microprobe analyses.

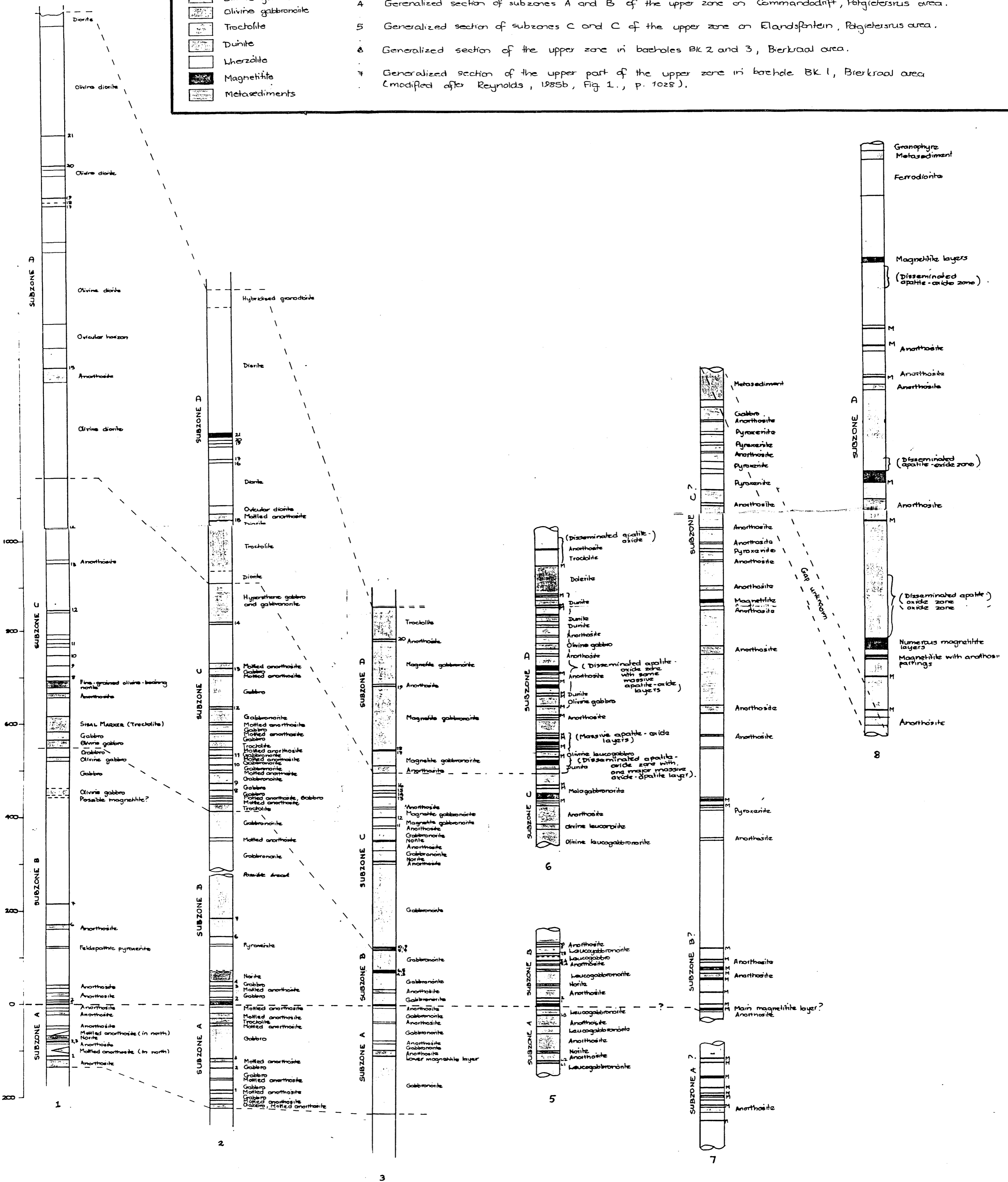


**ROCKTYPES**

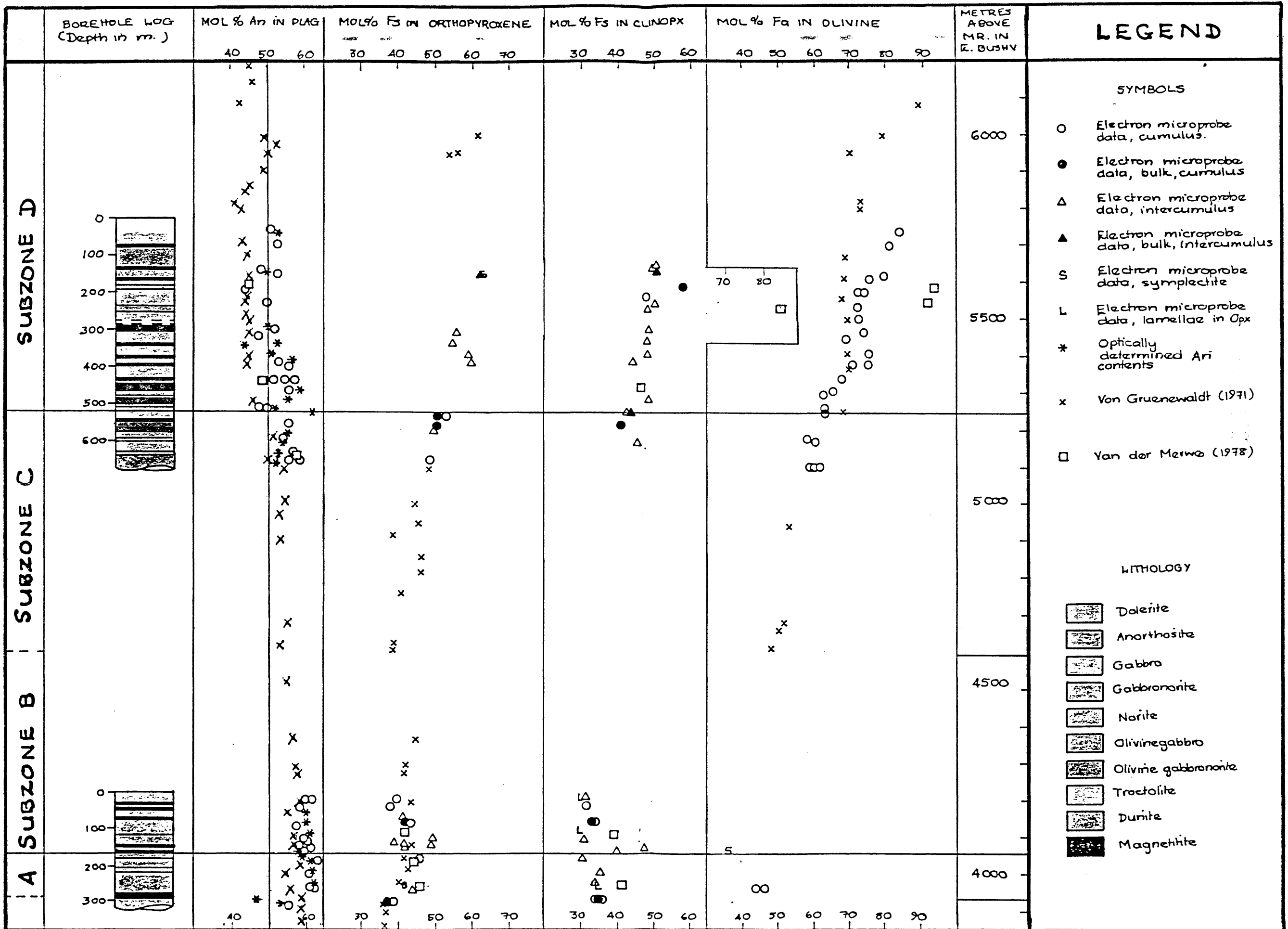
- Dolerite
- Anorthosite
- Gabbro
- Gabbroanorthite
- Norite
- Olivine gabbro
- Olivine gabbroanorthite
- Troctolite
- Dunite
- Wherzölit
- Magnetitite
- Metasediments

**STRATIGRAPHY**

- 1 Columnar section of the upper zone in the Roossenekal area (Van Gruenewaldt, 1971, Folder III).
- 2 Stratigraphic column of the upper zone in the Steelpoort Valley and in Sekhukhuleni (Malynex, 1970, Plate III).
- 3 Generalized section of the upper zone in the Potgietersrus area (Van der Merwe, 1978, Folder 2).
- 4 Generalized section of subzones A and B of the upper zone on Commandodrift, Potgietersrus area.
- 5 Generalized section of subzones C and C of the upper zone on Elandsfontein, Potgietersrus area.
- 6 Generalized section of the upper zone in boreholes BK 2 and 3, Bierkraal area.
- 7 Generalized section of the upper part of the upper zone in borehole BK 1, Bierkraal area (modified after Reynolds, 1985b, Fig 1., p. 1028).



older 5. Correlation between boreholes MS, M4 and EN12 with the stratigraphy of the upper zone from various parts of the upper zone



Folder 6 Compositional variation of plagioclase, orthopyroxene and clinopyroxene and olivine with height, compared to similar data from other parts of the Bushveld Complex.